National Park Service
U.S. Department of the Interior

Natural Resource Stewardship and Science

Historical and Projected Climate Change for Grand Canyon National Park and Surrounding Areas

Natural Resource Report NPS/NRSS/CCRP/NRR—2024/2615

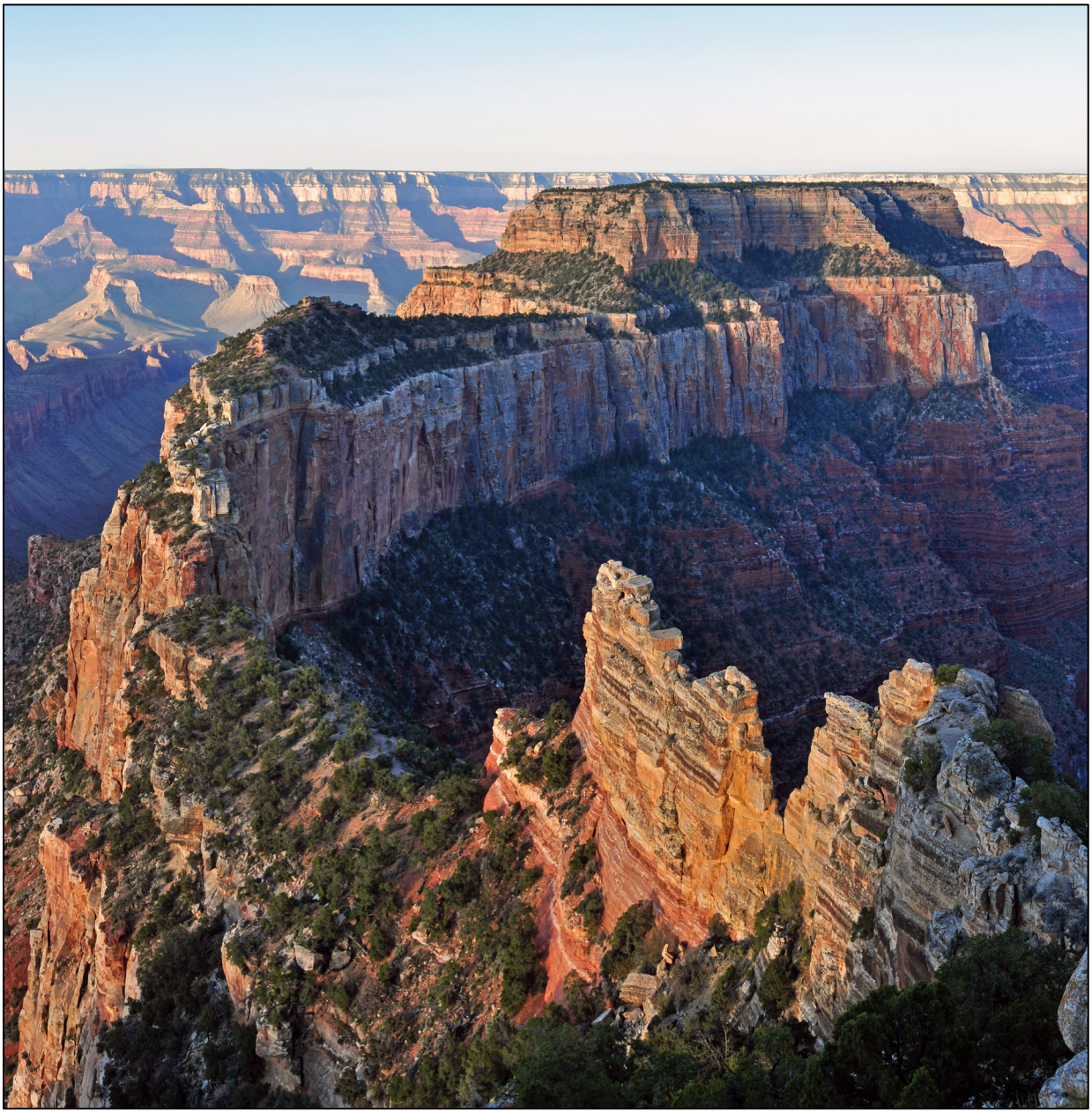

ON THIS PAGE
Sunrise from Cape Royal.
NPS / M. QUINN

ON THE COVER
Winter storm at Grand Canyon, 2021.
NPS

Historical and Projected Climate Change for Grand Canyon National Park and Surrounding Areas

Natural Resource Report NPS/NRSS/CCRP/NRR—2024/2615

David J. Lawrence,[1] Mike Tercek,[2] Amber Runyon,[1] Jeneva Wright[1]

[1] National Park Service
Fort Collins, CO

[2] Walking Shadow Ecology
Gardiner, MT

January 2024

U.S. Department of the Interior
National Park Service
Natural Resource Stewardship and Science
Fort Collins, Colorado

The National Park Service, Natural Resource Stewardship and Science office in Fort Collins, Colorado, publishes a range of reports that address natural resource topics. These reports are of interest and applicability to a broad audience in the National Park Service and others in natural resource management, including scientists, conservation and environmental constituencies, and the public.

The Natural Resource Report Series is used to disseminate comprehensive information and analysis about natural resources and related topics concerning lands managed by the National Park Service. The series supports the advancement of science, informed decision-making, and the achievement of the National Park Service mission. The series also provides a forum for presenting more lengthy results that may not be accepted by publications with page limitations.

All manuscripts in the series receive the appropriate level of peer review to ensure that the information is scientifically credible and technically accurate.

Views, statements, findings, conclusions, recommendations, and data in this report do not necessarily reflect views and policies of the National Park Service, U.S. Department of the Interior. Mention of trade names or commercial products does not constitute endorsement or recommendation for use by the U.S. Government.

This report is available in digital format from the Natural Resource Publications Management website. If you have difficulty accessing information in this publication, particularly if using assistive technology, please email irma@nps.gov.

Please cite this publication as:

Lawrence, D. J., M. Tercek, A. Runyon, and J. Wright. 2024. Historical and projected climate change for Grand Canyon National Park and surrounding areas. Natural Resource Report NPS/NRSS/CCRP/NRR—2024/2615. National Park Service, Fort Collins, Colorado. https://doi.org/10.36967/2301726

NPS 113/192072, January 2024

Contents

Contents (continued)

Figures

Page

Figures (continued)

Page

Executive Summary

Globally, anthropogenic climate change is one of the greatest threats to resources in protected areas. This report examines historical and projected climate change across the Greater Grand Canyon Landscape (GGCL), including Grand Canyon National Park. Grand Canyon National Park warmed significantly from 1895–2020 (annual mean increase of 1.89° F/century), with temperatures increasing at a faster rate from 1970–2020 (6.31° F/century). Warming occurred at all elevations and seasons across the GGCL, but rates differed spatially. Average annual total precipitation within Grand Canyon National Park did not change significantly over either period examined (1895–2020; 1970–2020).

A variety of changes in the region of Grand Canyon National Park have been detected and attributed, at least in part, to anthropogenic climate change, including reduced soil moisture (and associated drought), reduced Colorado River flow, doubling of the area burned by wildfire across the western United States, reduced regeneration of low-elevation ponderosa pine and Douglas-fir as well as pinyon pine and juniper populations, northward shifts in many bird species distributions and declines of bird species occupancy in the Mojave Desert, and reduced bumble bee species richness and abundance (key pollinators).

To help managers understand and plan around a range of plausible future climates, we present two plausible but contrasting climate futures for the Greater Grand Canyon Landscape, characterized at mid-century (2040–2069) and late-century (2070–2099). Examining multiple plausible futures avoids over-optimizing management strategies for a single projected future that may not occur.

Overarching patterns that emerged from both climate futures include additional warming (average, as well as extreme temperatures), seasonal increases in extreme precipitation events, fewer freezing days and days with snow, and higher moisture deficit (a correlate with landscape dryness, conditions conducive to fire, and vegetation stress). The selected climate futures differed in terms of 1) the degree of warming, 2) whether winter precipitation increases or decreases, 3) whether annual precipitation increases or stays similar, 4) whether drought conditions increase or decrease, and 5) whether runoff increases or decreases. Runoff is projected to occur earlier under both climate futures and is projected to exhibit a more episodic pattern.

Based on a literature review, projected changes to the physical, ecological, and cultural resource domains of the region resulting from anthropogenic climate change include:

- Increasing drought risk and aridification
- Reduced Colorado River flow
- Reduced groundwater infiltration
- Decreasing runoff (from snow or rain) in the spring, summer, and fall, and increasing runoff in the winter
- Increasing occurrence of large fires

- Increasing invasive grasses in the Mojave Desert ecosystems west of the park, providing more fuel for wildfire
- Exacerbated post-fire erosion and sediment in Grand Canyon watersheds
- Increased episodes of drought-induced tree mortality
- Upslope shifts of the elevational zones of pinyon-juniper woodland, ponderosa pine forest, and spruce-fir forest, as well as increases in non-forest areas and aboveground biomass declines
- Reduced abundance of riparian vegetation that tolerates water inundation
- Increasing invasive plant distribution and abundance, favoring their establishment and productivity
- Colonization of the GGCL by some bird species and extirpation of others
- Increasing non-native fish populations relative to native fishes
- Declining butterfly populations
- Increasing temperatures will increase visitation, especially during winter and shoulder seasons
- Exacerbation of existing threats to archeological resources, cultural landscapes, and historic structures, as well as emergent vulnerabilities related to climate change

One goal of this work is to support the Resource Stewardship Strategy (RSS) process that Grand Canyon National Park plans to undertake. We anticipate that connecting the climate changes described here to the climate sensitivities of resources within the park will play a critical role in setting goals and strategies during development of the RSS, as well as proactively adapting to anticipated changes.

Acknowledgments

Thanks to Patrick Gonzalez for the original version of the sections “Observed changes in the region attributed to anthropogenic climate change” and “Projected future risks”. Thanks to Garrett Knowlton, Brian Healy, Sarah Haas, Matt Engbring, Garrison Loope, Gregory Holm, Miranda Terwilliger, Hannah Chambless, Brandon Holton, Dave Worthington, Tom Olliff, Joel Reynolds, Cordie Diggins, Kaylin Thomas, Matt Holly, and Grand Canyon National Park leadership for their support in producing and reviewing this work.

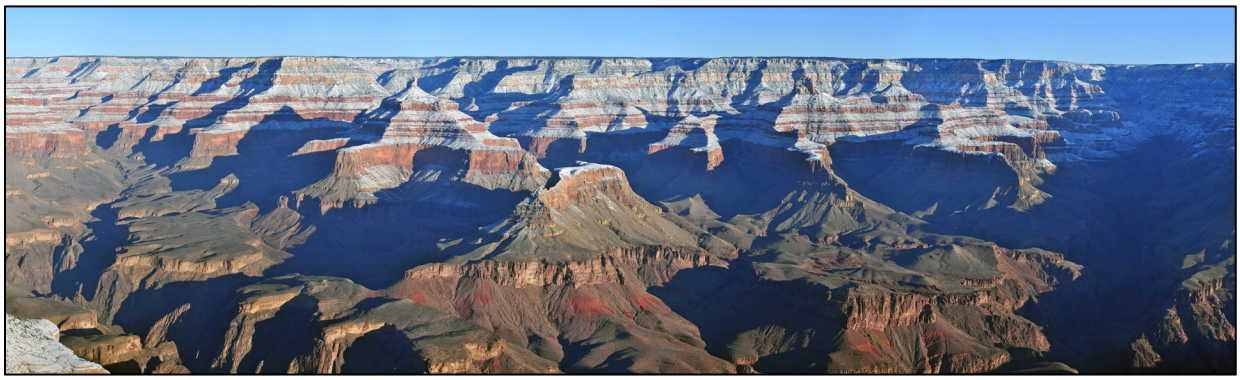

Winter view from Yavapai Point on the South Rim of the Grand Canyon. NPS / M.QUINN

Introduction

Anthropogenic climate change is driving major changes to landscapes across the globe (IPCC, 2014a). Changes in climate will affect most resources managed by the National Park Service (i.e., natural and cultural resources, visitor experience, operations and infrastructure). Understanding how climate may change for a given area is essential to understanding what resources are vulnerable to that change and where, when, and how they are vulnerable. This information is the basis of developing adaptation strategies to address climate change impacts. One intent of this work is to support the Resource Stewardship Strategy (RSS) process that Grand Canyon National Park (GRCA) plans to undertake. We anticipate climate change considerations (and related vulnerabilities) will play a critical role in the goal setting and strategy development that is part of the RSS process.

The climate science community recognizes that future climate is uncertain, but global climate models, driven by different degrees of anthropogenic forcing (i.e., different greenhouse gas emission pathways), provide projections of climate change for a given region. Here we evaluate projections of two contrasting 'climate futures' for the Greater Grand Canyon Landscape (GGCL; Figure 1). The spatial extent of this work is consistent with that defined in the GGCL Assessment (Stortz et al., 2018), intended to include processes that occur outside of the park that affect conditions within the park. Managers can examine contrasting climate futures to understand the range of how the climate may change and plan around that range (NPS, 2021). This exploration allows managers to establish climate-informed goals and strategies to achieve those goals, including using the Resist-Accept-Direct framework for climate change adaptation (Schuurman et al., 2022). This approach avoids over-optimizing management strategies for a single projected future that may not come to fruition (Lawrence et al., 2021). The methods section below summarizes the details and rationale of the climate futures examined for the GGCL.

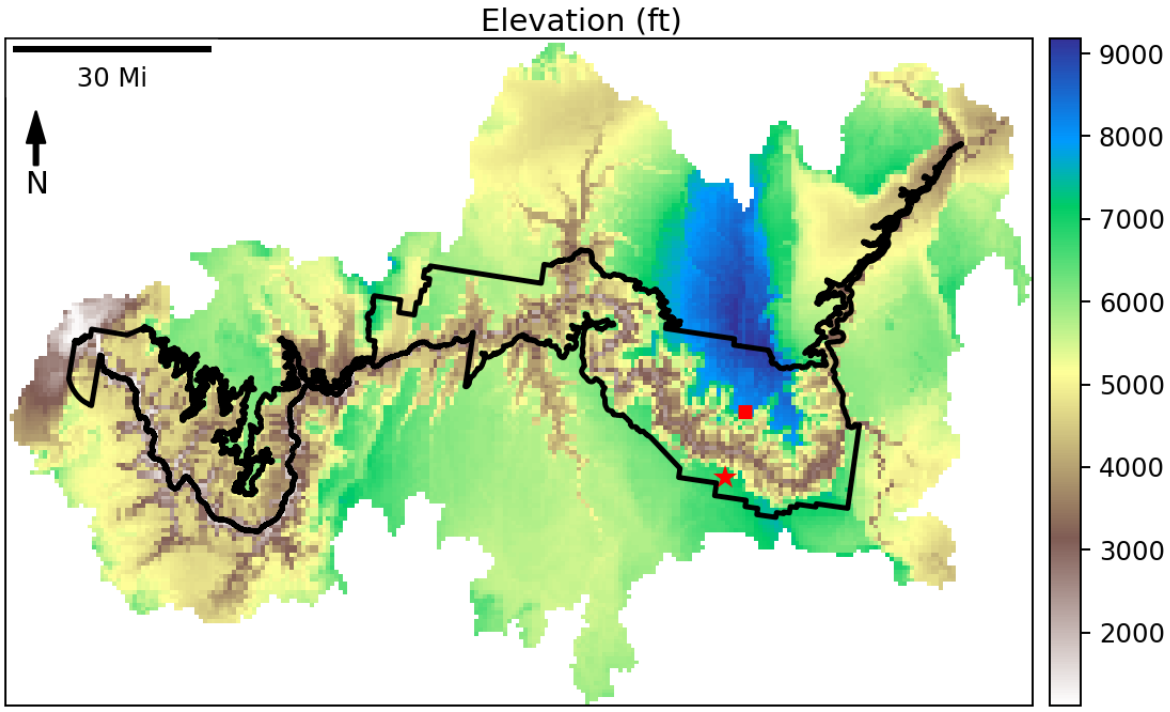

Figure 1. The Greater Grand Canyon Landscape (GGCL), with elevation (feet) indicated via a color ramp. Grand Canyon National Park is delineated by the black polygon. The red star is Grand Canyon Village. The red square is the North Rim Campground.

Methods

Spatial extent of analysis

Unless otherwise specified, all summaries refer to spatial averages across the GGCL (Figure 1). The GGCL comprises 5 million acres (2,023,428 hectares; 7,812 square miles), is located in the Colorado Plateau Physiographic Province, and contains vegetation types ranging from hot, low-elevation desert to cool, high-elevation spruce-fir forest (Stortz et al., 2018). The elevation range of the GGCL is depicted in Figure 1.

Historical climate

We evaluated historical (1895–2020) temperature and precipitation trends using the NOAA monthly U.S. Climate Gridded dataset (NClimGrid; Vose et al., 2014), which represents climate conditions for the continental U.S. as a 5 km gridded surface. We investigated spatial and temporal patterns of historical temperature and precipitation by selecting grid cells that overlaid the GGCL.

Future climate (temperature and precipitation)

We evaluated future climate projections from a series of global climate models (GCMs) derived from the Coupled Model Intercomparison Project Phase 5 archive (CMIP5; Taylor et al., 2012) and statistically downscaled to a 4 km grid using the Multivariate Adaptive Constructed Analog method (MACA; Abatzoglou and Brown, 2012). MACA is a downscaling method that uses daily projections of GCMs, bias corrects the projections based on local or regional observations and creates a high-resolution grid by finding the closest fit analogs from an archive of observations. MACA downscaling was performed for twenty GCMs. We applied those model projections to the GGCL to represent the range of possible climate change outcomes as well as to characterize the uncertainty associated with different GCM representations of the climate system. Models were not screened for regional performance, given challenges in doing so (Barsugli et al., 2013; Dixon et al., 2016). Two future representative concentration pathways (RCPs) were retained for each of the 20 GCMs (RCP 4.5 and RCP 8.5), for a total of 40 projections of the future climate. RCP 4.5 represents a middle-of-the-road scenario and assumes atmospheric CO2 stabilizes through time by using a range of strategies and technologies to reduce future emissions. RCP 8.5 represents a business-as-usual scenario, with human emissions of CO2 increasing through time (IPCC, 2014b). We define a 'projection' as a GCM driven by a given RCP (e.g., Meteorological Research Institute [MRI]-CGCM3 RCP 8.5). For the purposes of this report, climate futures are derived directly from individual projections.

We focused on two time periods for the future projection analysis—a mid-century period centered on 2055 (2040–2069) and a late century period centered on 2085 (2070–2099). These periods were compared to a baseline reference period of 1981–2010, derived from gridMET data (Abatzoglou, 2013). gridMET is the observational training dataset used to bias correct and downscale the MACA projections, therefore no additional bias corrections are required when comparing the historical gridMET data set with the future projections. Using gridMET as the historical reference dataset for future projections is more accurate than using the NClimGrid historical data (which would require bias correction).

To evaluate the range of climate futures relevant to management, we plotted all projections according to two axes—the change in annual average temperature and the change in winter (December, January, February; DJF) precipitation in mid-century, relative to the baseline reference period (Figure 2). Projections of annual temperature change allow us to characterize futures with different degrees of heat, drought, and evapotranspiration, while projections of change in winter precipitation allow us to characterize futures with differences in snow delivery, snow-based recharge, and ultimately runoff, as these were interpreted to be important drivers of the ecology of the ecosystem (and as a result, key drivers of climate change vulnerability on the landscape). Together, different degrees of change in temperature and winter precipitation result in different degrees of changes in climatic water deficit (a key driver of tree mortality, conditions conducive to fire, vegetation biome shifts, and runoff on the landscape; see below).

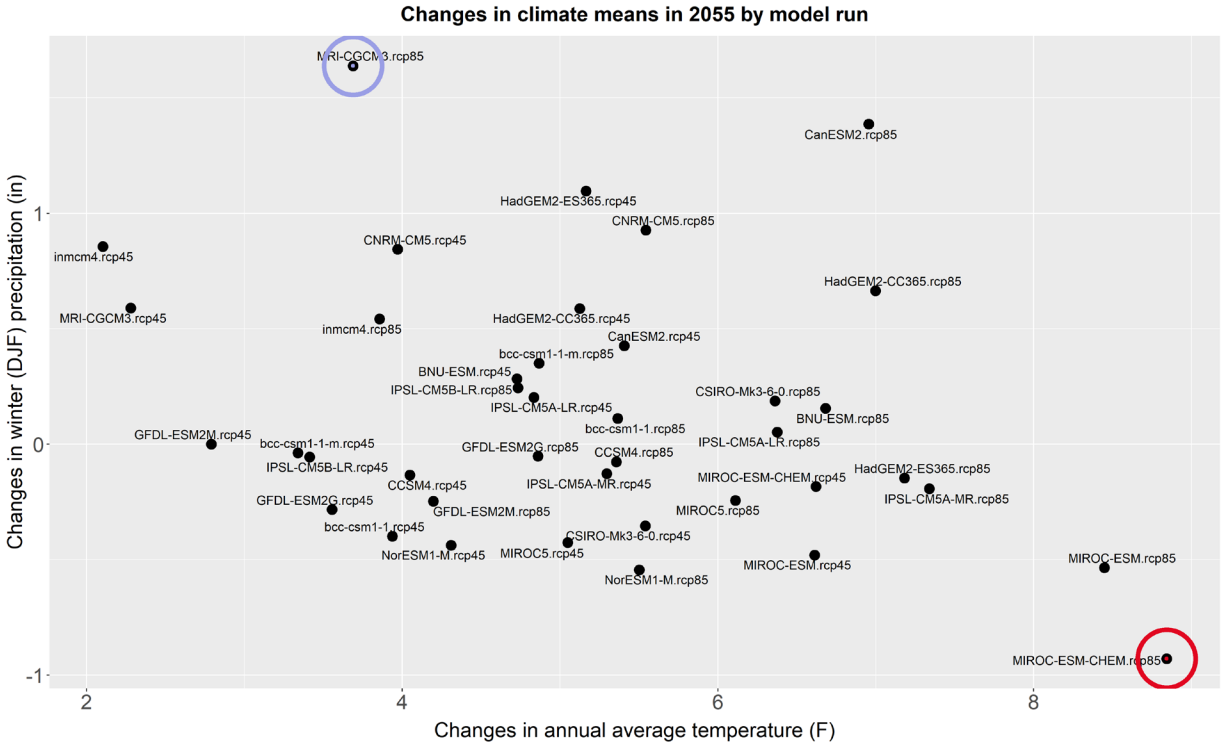

Figure 2. Change in annual average temperature and change in total winter precipitation (sum of December, January, February precipitation; DJF) across the GGCL for the period centered on 2055 (2040–2069), relative to the historical period 1981–2010. The projections selected as climate futures for this report (MRI-CGCM3 RCP 8.5 and MIROC-ESM-CHEM RCP 8.5) are circled.

Projections differed in (1) the magnitude of warming (all project warming) and (2) the direction of change in winter precipitation (i.e., some projections indicate more winter precipitation than historical, others project less; Figure 2). Annual average is projected to increase from 2.1 to 8.8° F at mid-century relative to the baseline period (1981–2010; Figure 2). Winter precipitation decreased in 43% of projections (by as much as – 0.9 inches) and increased in 57% of projections (up to + 1.6 inches, Figure 2), compared to the baseline period.

Because the "correct" modelled future is unknowable, we focus on two plausible and divergent climate futures that capture the range of potential changes in these key climate metrics (Lawrence et al., 2021; Star et al., 2016): 1) The Meteorological Research Institute [MRI]-CGCM3 RCP 8.5 (abbreviated MRI hereafter) climate future has modest mid-century warming, and the greatest increase in winter (DJF) precipitation; and 2) The Model for Interdisciplinary Research on Climate [MIROC]-ESM-CHEM RCP 8.5 (abbreviated MIROC hereafter) climate future has the greatest annual warming and the greatest decline in winter precipitation.

Water Balance

We used a water balance model to evaluate the interactive effects of temperature and precipitation on climate metrics such as snow delivery, climatic water deficit (a measure of landscape dryness), and changes in runoff (for details see Tercek et al., 2021; Thoma et al., 2020). The water balance model was run using the MRI and MIROC climate futures.

Standardized Precipitation Evaporation Index

The Standardized Precipitation Evaporation Index (SPEI) provides another metric to assess changing drought conditions (for details see Appendix 2 of Runyon et al., 2021; Vicente-Serrano et al., 2010). A zero value for SPEI indicates average moisture balance, positive values signify above-average wetness, and negative values represent drier than average conditions. A drought event begins when SPEI falls below −0.5 and lasts until SPEI returns above the threshold. We projected three drought attributes into the future: drought duration, drought severity and the drought-free interval.

Fire

Projections of change in fire regime were beyond the scope of this report, but some inference is available based on changes in moisture deficit (which is often positively correlated with conditions conducive to fire; see below).

Elevation

Because the GGCL spans a broad elevation gradient, we present many of the results for this climate exposure analysis according to elevation. Figure 1 provides context for subsequent figures that delineate climate projections according to elevation.

Historical climate and trends

Temperature

Grand Canyon National Park is warming (Figure 3). Statistically significant warming trends were found over the period of record (1895–2020) for all temperature metrics (Tmax – 2.34° F/century, $p<0.0001$; Tmean – 1.89° F/century, $p<0.0001$; Tmin – 1.44° F/century, $p<0.0001$). The rate of warming increased over the more recent historical period (1970–2020) for all temperature metrics (Figure 3; Tmax – 6.95° F/century, $p<0.0001$; Tmean – 6.31° F/century, $p<0.0001$; Tmin – 5.66° F/century, $p<0.0001$).

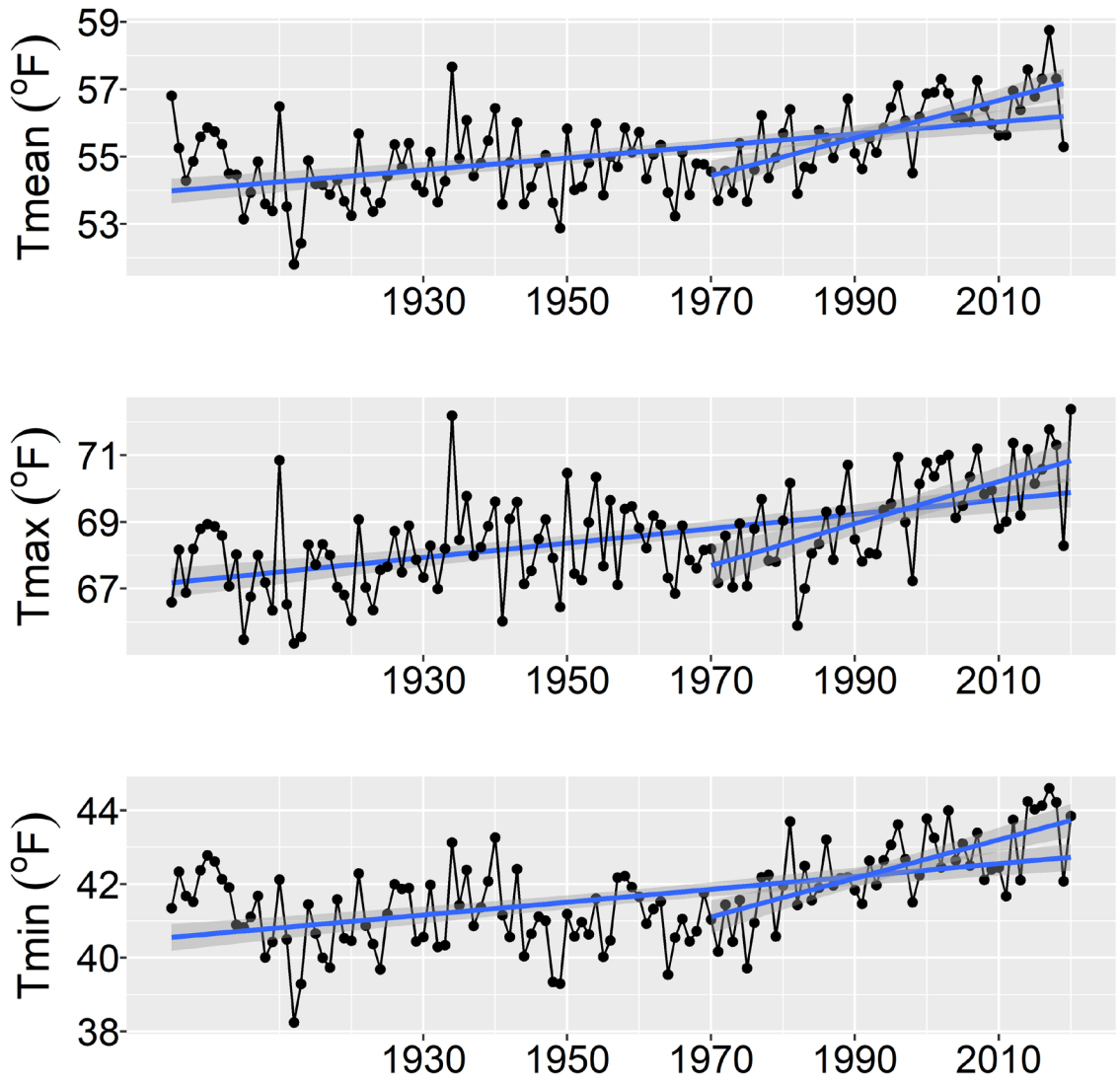

Figure 3. Average annual maximum, minimum, and mean temperatures (°F) increased within the Grand Canyon National Park boundary from 1895–2020. Statistically significant linear regressions (blue lines) across the current period (1970–2020) and the entire time period. Data derived from the NOAA nClimGrid data set.

Warming trends are not spatially uniform in the study area (Figure 4) with some regions exhibiting faster increases in temperature than others. For all temperature metrics (Tmean, Tmax, Tmin), the north central part of the landscape (including Bulrush Wash, Grama Canyon-Kanab Creek, and Hack Canyon watersheds; see Figure 12 from Stortz et al., 2018) exhibited the greatest warming over the 1895–2020 period. For context, the historical mean, maximum, and minimum temperature across the GGCL is provided in Supplemental Figure A1 (see Appendix A).

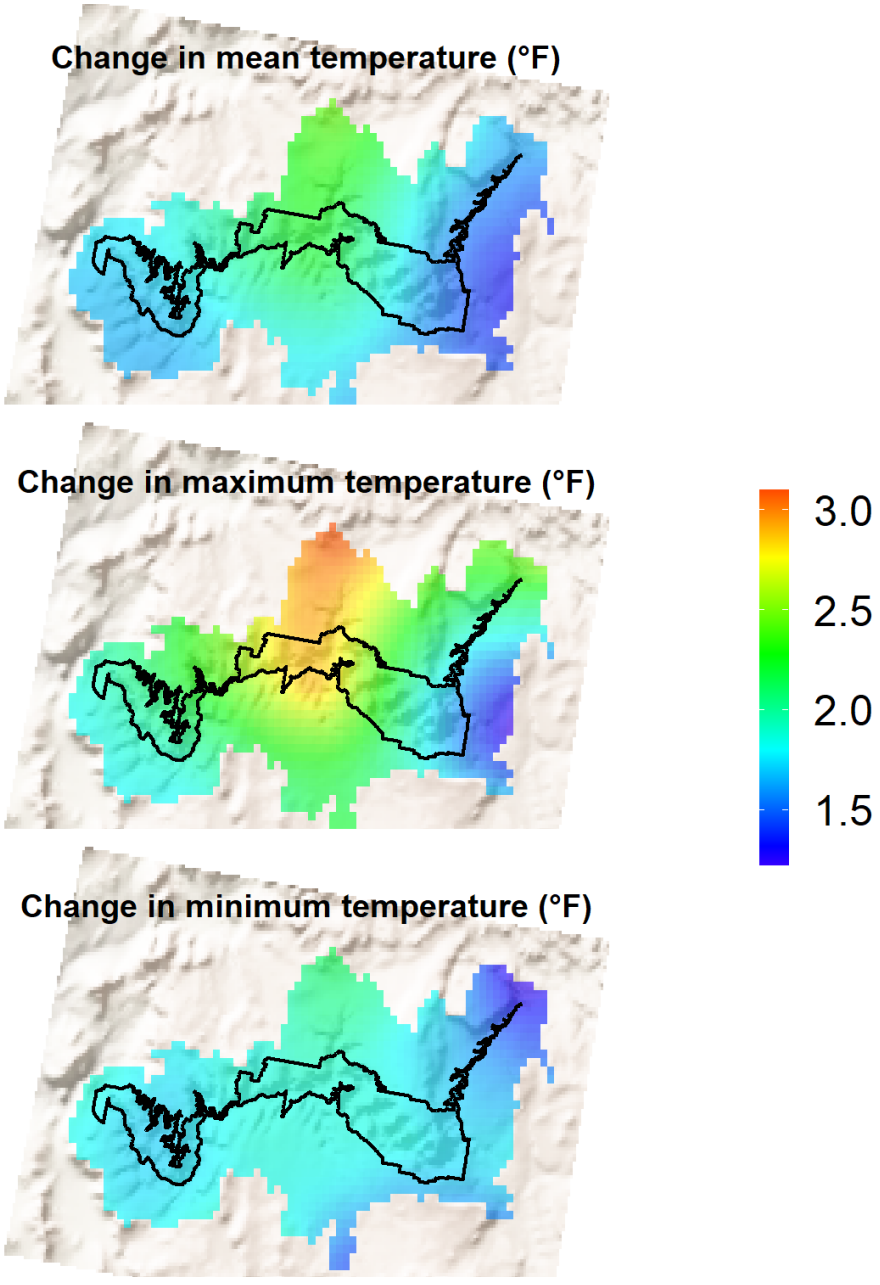

Figure 4. Cell-specific linear regression slope (degrees (°F) per century) depicting warming of mean, maximum, and minimum temperature across the GGCL from 1895–2020. Statistically significant (p-value < 0.05) cells are highlighted. Data are derived from the NOAA nClimGrid data set and presented in 5 km-by-5 km cells and ranged from 1895–2020.

Warming from 1895–2020 occurred at all elevations and seasons (Supplemental Figure A2). The fastest rate of warming for mean temperature occurred at mid and high elevations in the winter (Supplemental Figure A2). The fastest rates of warming for maximum temperature also occurred at mid and high elevations in the winter, while the slowest rates of warming occurred in the fall (Supplemental Figure A2). Minimum temperatures experienced the highest rate of increase at mid and high elevations in the winter, as well as at lower elevations in the summer and fall (Supplemental Figure A2). The slowest rate of minimum temperature increases were observed in the spring across all elevations.

Precipitation

The high elevation Kaibab Plateau receives the greatest precipitation across the landscape (Figure 5). Annual average precipitation within Grand Canyon National Park did not change significantly over either period examined (1895–2020; 1970–2020; Figure 6). Similarly, no statistically significant change in precipitation was observed across the landscape based on a spatial analysis of individual grid cells (data not shown). Although not statistically significant, precipitation had small declining trends in the spring, summer, and winter at the highest elevation, in the summer and winter at mid-elevations, and summer at low elevation (Supplemental Figure A3). Small (non-statistically significant) increasing trends in precipitation occurred in the fall for all elevations.

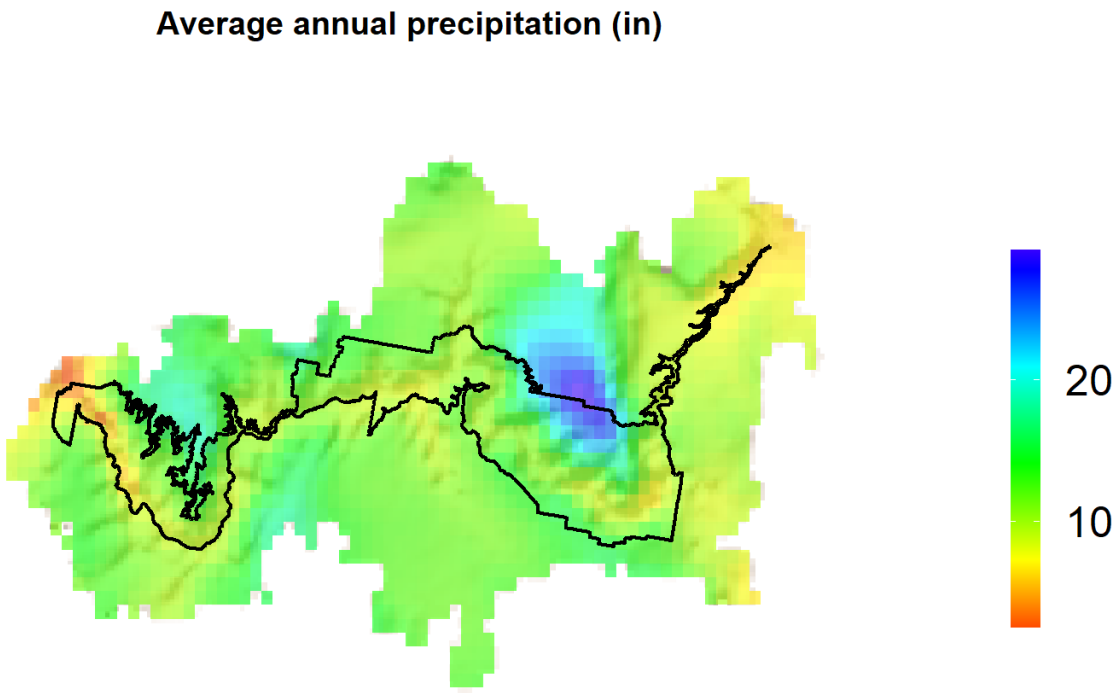

Figure 5. Average annual total precipitation (inches) in 5 km-by-5 km cells from 1895–2020. Derived from the NOAA nClimGrid data set.

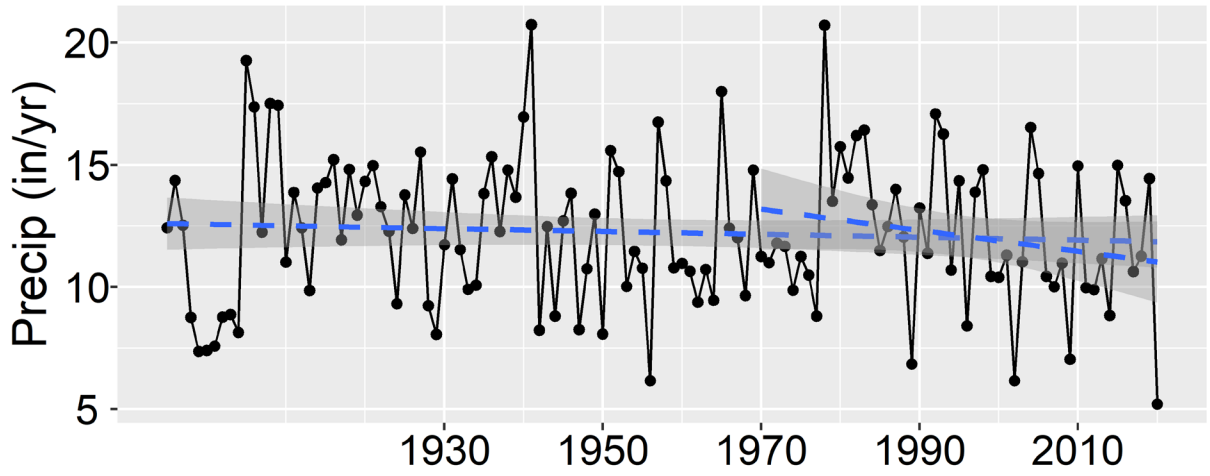

Figure 6. Average annual total precipitation (inches) within the Grand Canyon National Park boundary from 1895–2020. Blue regression lines are from 1970–2020 and the entire time period. Dashed lines represent non-significant trends (p>0.05). Derived from the NOAA nClimGrid data set.

Observed changes in the region attributed to anthropogenic climate change

Greenhouse gas emissions from cars, power plants, deforestation and other human sources have caused climate change globally (IPCC, 2021) and in Grand Canyon National Park (Gonzalez et al., 2018). Anthropogenic climate change increased annual average temperature across the GGCL (see Figure 3, 4 above).

A variety of changes in the region of Grand Canyon National Park have been detected and attributed, at least in part, to anthropogenic climate change following the definitions of detection and attribution of the Intergovernmental Panel on Climate Change (IPCC, 2014a). Many are briefly summarized below.

Drought

From 2000 to 2018, the increased heat and aridity from anthropogenic climate change has caused half the severity of a southwest North American drought, as defined by a deficit of soil moisture compared to the long-term average (Williams et al., 2020). The drought has reduced soil moisture for the southwestern U.S. as a whole to its lowest levels since the 1500s.

Reduced Colorado River flow

Between 1906 and 2018, the naturalized flow of the Colorado River at Lees Ferry, the upstream end of Grand Canyon National Park, decreased 20% (Hoerling et al., 2019), with half of that reduction resulting from long-term climate change. The analysis removed anthropogenic influences such as diversions and reservoirs, so that this statistically significant decline in naturalized flow represents a shift in the underlying climate conditions for the upper Colorado River Basin. Flow has continued to decline in the 21st century resulting in the worst hydrological drought since observations began in 1906 (Udall and Overpeck, 2017; Xiao et al., 2018). The increased heat of anthropogenic climate change has caused one-sixth to one-half of the drought, through reduced snowpack and increased evapotranspiration (Hoerling et al., 2019; Milly and Dunne, 2020; Udall and Overpeck, 2017; Xiao et al., 2018). The remaining fraction of the hydrological drought derives from a low period in precipitation, which has been linked to natural variability in Pacific sea surface temperatures (Delworth et al., 2015; Lehner et al., 2018; Udall and Overpeck, 2017). Continued drought through 2022, magnified by warming-induced reductions in runoff efficiency (i.e., snow water returned to the atmosphere versus flowing to the river; Woodhouse and Pederson, 2018), further exacerbated water management challenges for the 40 million inhabitants of the southwestern United States and northwestern Mexico that depend on the Colorado River as a water supply (Wheeler et al., 2022).

In the winter of 2023 snowpack across the Colorado River watershed is well above average. Based on near-term projections developed by the National Weather Service Colorado Basin River Forecast Center for the Bureau of Reclamation (BOR, 2023) in March 2023, reservoir storage is expected to increase by the end of water year 2023 to 21.27 million acre feet (maf; 37 percent of total system capacity). At the beginning of water year 2023, total system storage in the basin was 19.54 maf (33 percent of 58.48 maf total capacity). The actual end of water year 2023 storage may vary from this

near-term projection due to uncertainty in this season's runoff and reservoir inflow. It is unknown if this trend will continue or reflects year-to-year variability.

Wildfire

Wildfire is a natural and necessary part of most forest and woodland ecosystems in the southwestern U.S. Uncontrolled, fast spreading, high severity, high intensity wildfire, however, can kill people, destroy houses, destroy high value natural and cultural resources, damage ecosystems, as well as release large amounts of carbon dioxide, which contributes to climate change.

From 1984 to 2015, anthropogenic climate change doubled the area burned by wildfire across the western U.S. above what would have burned due to non-climate change factors (Abatzoglou and Williams, 2016). The higher temperatures of anthropogenic climate change have increased the aridity of soil and vegetation and increased the length of fire seasons. Much of the non-climate change fraction of the wildfire increase derives from a low period in summer precipitation, which naturally shows high year-to-year variation in the southwestern U.S. (Holden et al., 2018). Across national parks and protected areas of Canada and the U.S., climate factors explained the majority of burned area from 1984 to 2014, with climate factors (temperature, precipitation, relative humidity, evapotranspiration) outweighing local human factors (population density, roads, and built area) (Mansuy et al., 2019).

While government policies in some areas have suppressed almost all fires, even natural ones, Grand Canyon National Park has a long history of supporting natural ignitions for resource benefit. In addition, Grand Canyon National Park has treated a majority of its landscape with multiple entries of wildfire and prescribed fire.

Tree regeneration decline and tree mortality

From 1979 to 2015, in plots burned by high severity wildfire in northern Arizona and across the western U.S, the increasing heat and aridity of anthropogenic climate change reduced post-fire regeneration of low-elevation ponderosa pine (*Pinus ponderosa*) and Douglas-fir (*Pseudotsuga menziesii*) by half (Davis et al., 2019). Heat and aridity crossed critical thresholds for the survival of seedlings.

van Mantgem et al. (2009) found a statistically significant doubling of tree mortality between 1955 and 2007 by tracking of trees in permanent old-growth conifer forest plots across the western U.S., including a plot in northern Arizona. Their analyses of climate change and non-climate factors found that drought, wildfire, and bark beetle infestations, due to the increased temperatures of anthropogenic climate change, have caused the increased tree mortality. The increased heat of climate change has led to the most extensive bark beetle outbreak in North America in a century, causing extensive tree mortality (Raffa et al., 2008).

Pinyon pine and juniper populations are declining with increasing aridity and temperature (e.g., a 50% decline of populations was observed in the warmest and driest conditions); mortality and lack of recruitment both play a key role in these declines (Shriver et al., 2022). Rodman et al. (2022) found

that pinyon-juniper cover declined from 2000 to 2020 in central Arizona (converting to non-forest), which corresponded to a period of extreme drought and regional tree die-off.

Animal range shifts

Analyses of Audubon Christmas Bird Count data across the lower 48 U.S. states, including count circles in northern Arizona, detected a 30 km ± 17 km northward shift of the winter center of abundance of a set of 254 bird species from 1975 to 2004, attributable more to anthropogenic climate change than other factors (La Sorte and Thompson, 2007). Additional analyses found northward shifts across the lower 48 US states from 1975 to 2011 of winter distributions of six raptor species: American kestrel (*Falco sparverius*), golden eagle (*Aquila chrysaetos*), northern harrier (*Circus cyaneus*), prairie falcon (*Falco mexicanus*), red-tailed hawk (*Buteo jamaicensis*), and rough-legged hawk (*Buteo lagopus*) (Paprocki et al., 2014).

Range expansions of elk on the North and South Rims, as well as javelina on the South Rim, and hog-nosed skunks and coatis below the rim in Grand Canyon National Park have also occurred (Cuarón et al., 2016; Holton et al., 2021). Climate change may serve as a contributing driver of some or all of these expansions, but none have been formally attributed to climate change.

Mojave Desert bird species decline

Field surveys from 2013 to 2016 at 61 sites in the Mojave Desert, west of Grand Canyon National Park, counted birds at sites originally surveyed from 1908 to 1968 (Iknayan and Beissinger, 2018). The research detected an average loss of 43% of bird species. Analyses of potential causal factors, including climate, fire, and grazing, attributed the loss to increased aridity caused by anthropogenic climate change. Some of the species that declined included the canyon wren (*Catherpes mexicanus*), Costa's hummingbird (*Calypte costae*), Lawrence's goldfinch (*Spinus lawrencei*), western bluebird (*Sialia mexicana*), and the white-throated swift (*Aeronautes saxatalis*). Only one species showed a statistically significant increase in occupancy, the common raven (*Corvus corax*).

Bumble bee species decline

Climate change has reduced bumble bee species richness and abundance across North America, with declines of 10% to 20% in northern Arizona, from 1901 to 2014 (Soroye et al., 2020). Temperature increases and precipitation changes outweigh effects of local land use change (Soroye et al., 2020). These species can serve as key pollinators.

View down the Colorado River from Nankoweap in Marble Canyon, Grand Canyon National Park.
NPS / M.QUINN

Future climate projections

Temperature

Both climate futures project warming across the GGCL, but warming is greater under the MIROC climate future (Figure 7, Supplemental Figure A4).

Temperatures are projected to increase most during summer and fall seasons under the MRI climate future during both mid- and late-century periods (Supplemental Figure A5). For the MIROC climate future, seasonal temperatures are projected to increase more in spring and summer during the mid-century period, and during the summer and fall during the late-century period. Temperature increases were greatest at higher elevations under the MIROC climate future, but this pattern was not found under the MRI climate future.

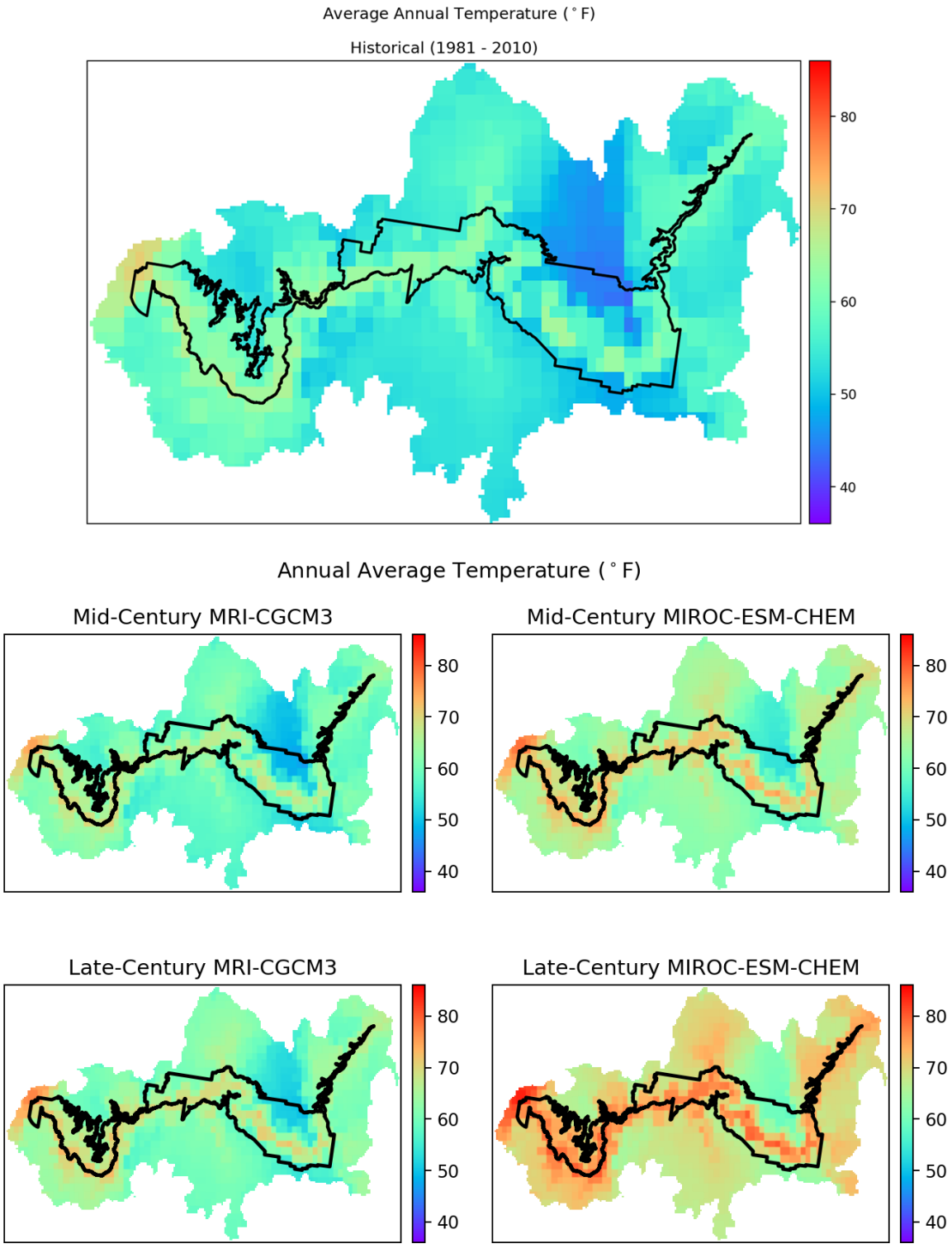

Figure 7. Annual mean temperature under the historical climate (1981–2010), and mid-(2055) and late-(2085) century MRI and MIROC climate futures across the GGCL. The color scale is consistent across panels to ease comparison across climate futures and time periods.

Figure 8 shows the time series of the annual average of daily maximum and minimum temperatures at North Rim Campground (36.2135, −112.0581; 8200 ft elevation), for the historical reference period (1981–2020) and extending out to 2100 for the two climate futures. Data for North Rim Campground is shown given it is a familiar area for park staff. The MIROC climate future is considerably warmer than the MRI climate future, though both indicate significant warming increasing over the period 2040–2100 relative to the baseline period.

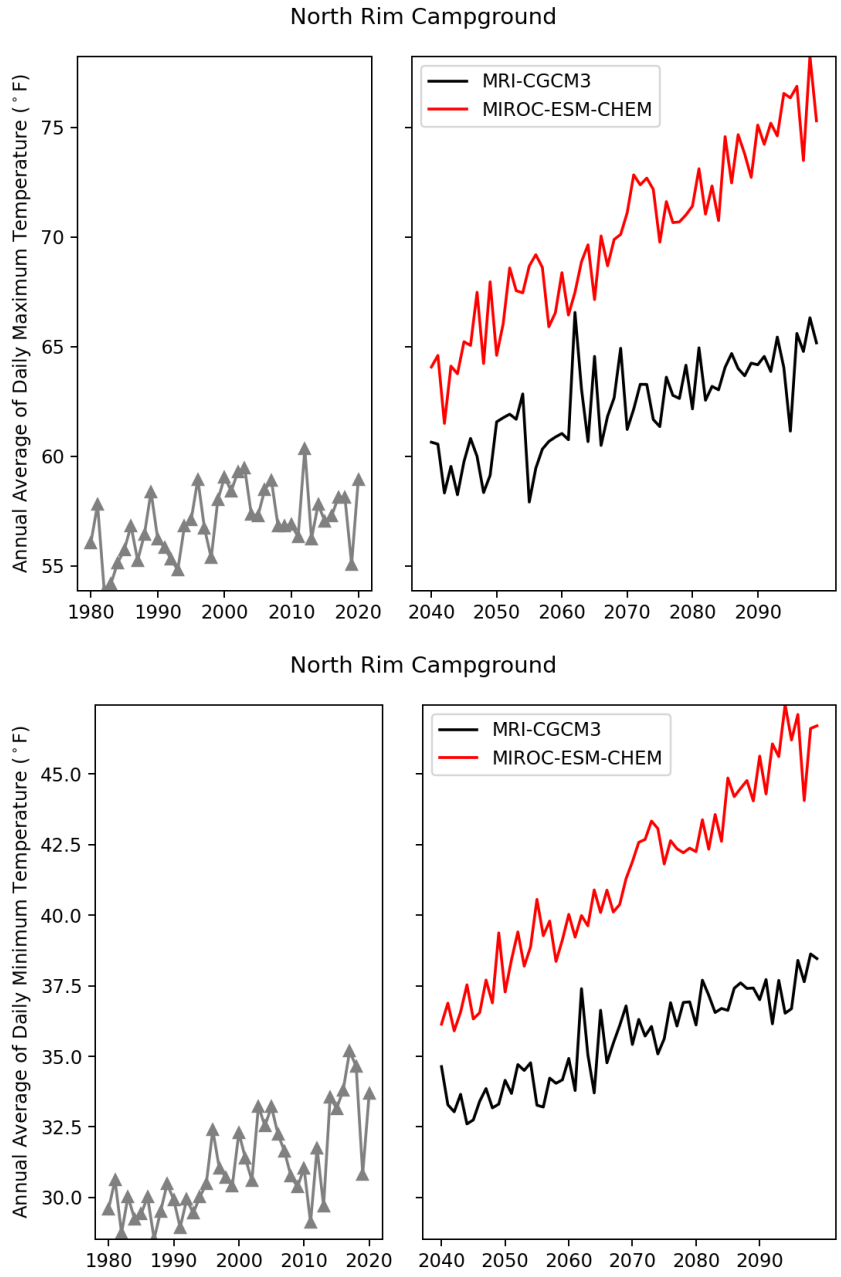

Figure 8. Annual average of daily maximum temperature (upper panel) and minimum temperature (lower panel) at the North Rim Campground for the historical period 1981–2020 and for 2040–2100 under MRI and MIROC climate futures.

Extremely warm temperature conditions, defined as days per year with temperatures above the 99th percentile (85.4° F) of the reference baseline period (1981–2010), are projected to increase significantly under both climate futures (Figure 9). Under the MRI climate future the number of extremely warm days increases from ~18 days per year in 2045 to ~50 days per year by 2100. Under the MIROC climate future the number of extremely warm days increases from ~42 days per year in 2045 to ~140 days per year by 2100. The historical period had 4 days per year with conditions above 85.4° F.

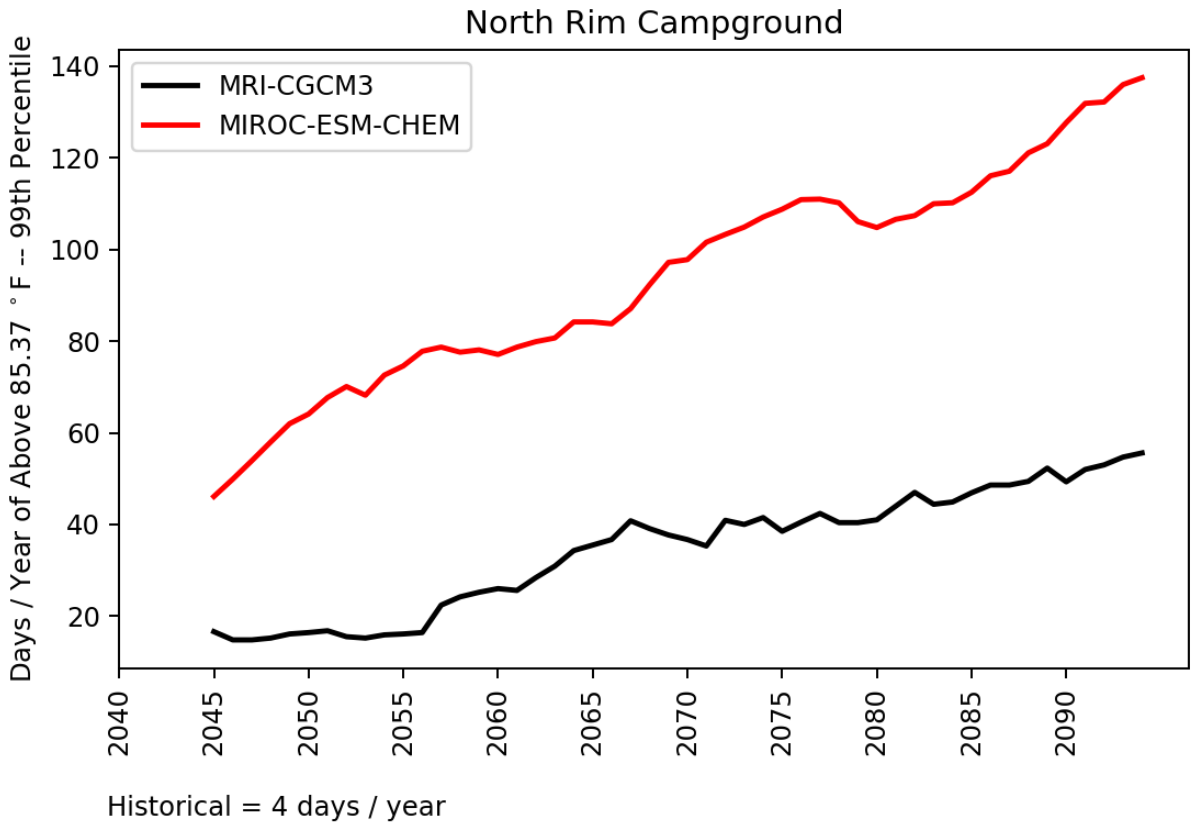

Figure 9. Days per year with maximum temperatures above the 99th percentile temperature (85.4° F), based on a 10-year moving average at North Rim Campground over the period 2045–2100 under the MRI and MIROC climate futures.

The number of days per year below freezing (32° F) are also projected to decline significantly under the MIROC climate future (Figure 10). During the historical reference period (1981–2010) there were 198 days per year below freezing, compared to ~160 days per year in 2045 and ~80 days per year in 2100 under the MIROC climate future. The number of days per year below freezing declined slightly under the MRI climate future, to ~180 days per year in 2100.

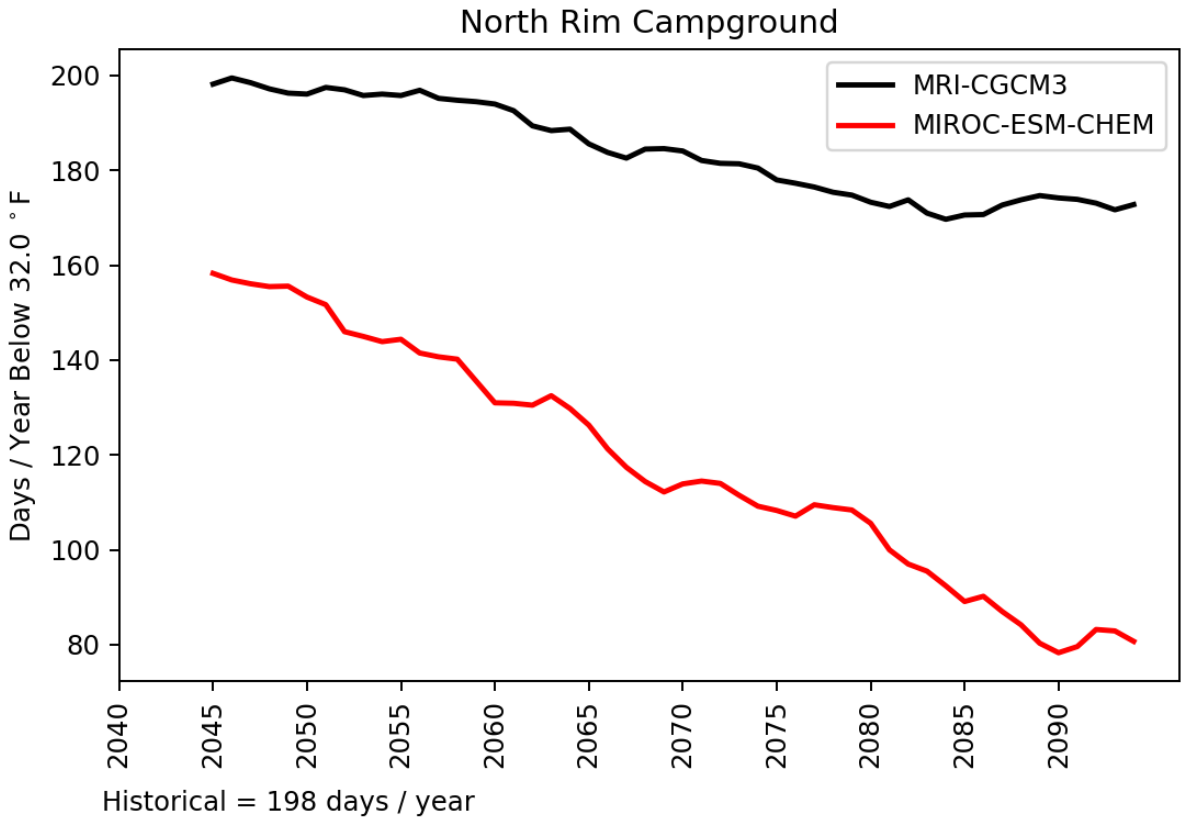

Figure 10. Days per year with minimum temperatures below freezing (32° F), based on a 10-year moving average, at North Rim Campground over the period 2045–2100 under the MRI and MIROC climate futures.

Precipitation

The spatial distribution of average total annual precipitation projections for mid- and late-century periods are shown in Figure 11, with the historical precipitation for 1981–2010 provided for reference (also see Supplemental Figure A6). Under the MRI climate future the greatest relative increases in precipitation during mid-century were on the Kaibab Plateau and in the northwestern-most part of the landscape. By late-century, that climate future projects increased precipitation across the entire landscape. Under the MIROC climate future, relative declines in total annual precipitation were greatest on the Kaibab Plateau and the western part of the GGCL.

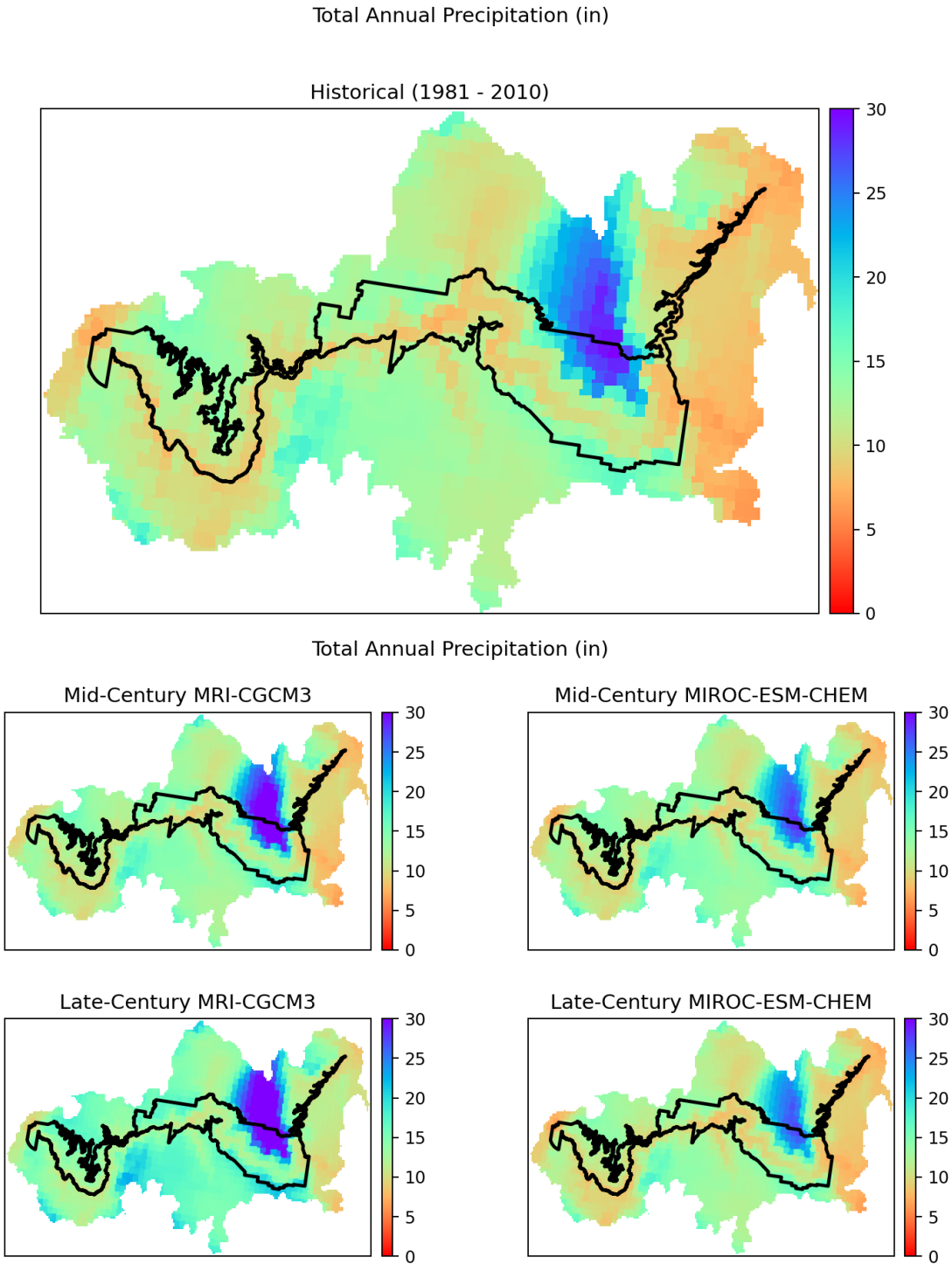

Figure 11. Average total annual precipitation under the historical climate (1981–2010), and mid- and late-century MRI and MIROC climate futures across the GGCL.

Under the MRI climate future, annual precipitation increases at all elevations in the mid- and late-century periods (Supplemental Figure A7, Figure A8). At mid-century, precipitation under this

climate future increased in the spring, and especially the winter, and declined in the summer and fall at all elevations. By late-century, this climate future projects increasing precipitation at all elevations in the spring, and especially the summer and winter, with relatively small declines in the fall.

Under the MIROC climate future, annual precipitation increases slightly during the mid-century and declined slightly at high elevations by late-century (Supplemental Figure A7, Figure A8). During mid-century for this climate future, spring and especially winter precipitation declined at all elevations, and increased during the summer and fall across elevations. By late century, this climate future projects declines in precipitation at all elevations during the spring and winter, while precipitation increases in the summer and fall across elevations.

The two discussed climate futures were selected to bracket the broad range of projected winter precipitation in the CMIP5 archive resulting in one climate future representing wetter winter conditions (MRI) and another (MIROC) representing drier winter conditions. These two climate futures do not similarly bracket the large range of summer precipitation projections. By chance, both of the selected climate futures project an increase in summer precipitation associated with the North American Monsoon. Unfortunately, summer precipitation in the region, even more so than for winter precipitation, has proven difficult to model and there is no current consensus as to whether it will increase or decline over the 21st century (Pascale et al., 2019).

Historical total precipitation trends at the North Rim Campground, and under MRI and MIROC climate futures, are shown in Figure 12. The MRI and MIROC climate futures indicate an increase in extreme precipitation events (defined here as days per year with precipitation greater than the 99th percentile) at the North Rim Campground for all seasons, relative to the historical period for both the mid- and late-century periods (Figure 13). Seasonal increases in days per year with extreme precipitation are most pronounced for the MRI climate future. Annually, the MIROC climate future project a similar number of extreme precipitation events compared to the historical reference period.

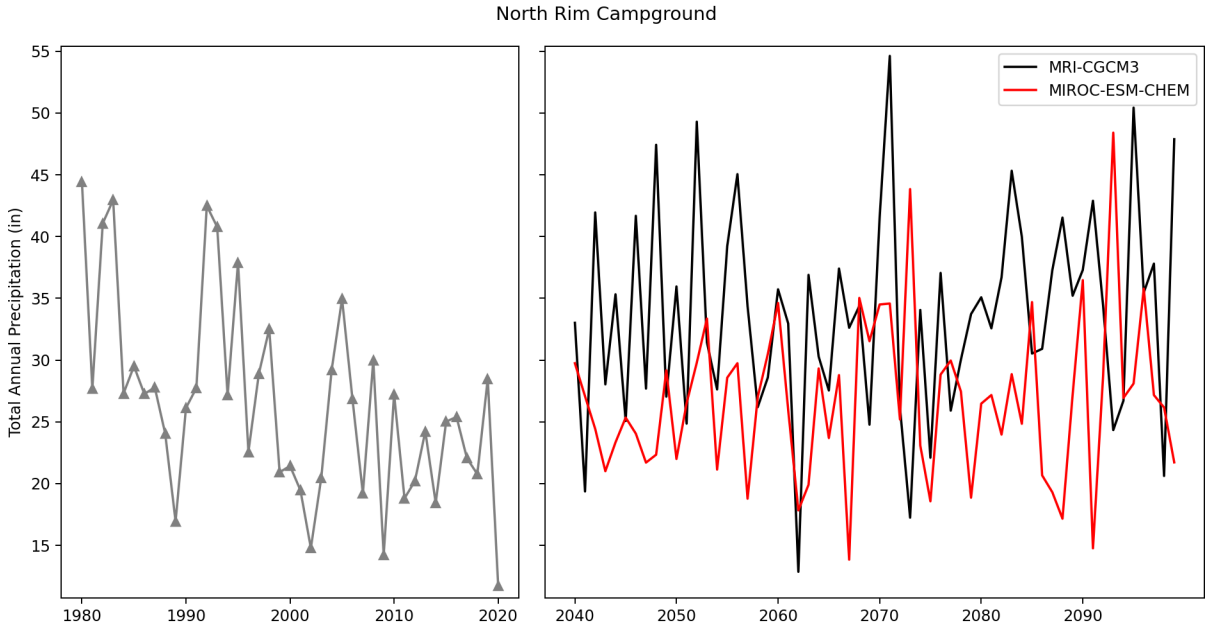

Figure 12. Total annual precipitation at the North Rim Campground for the historical period 1981–2020 and 2040–2100 under the MRI and MIROC climate futures.

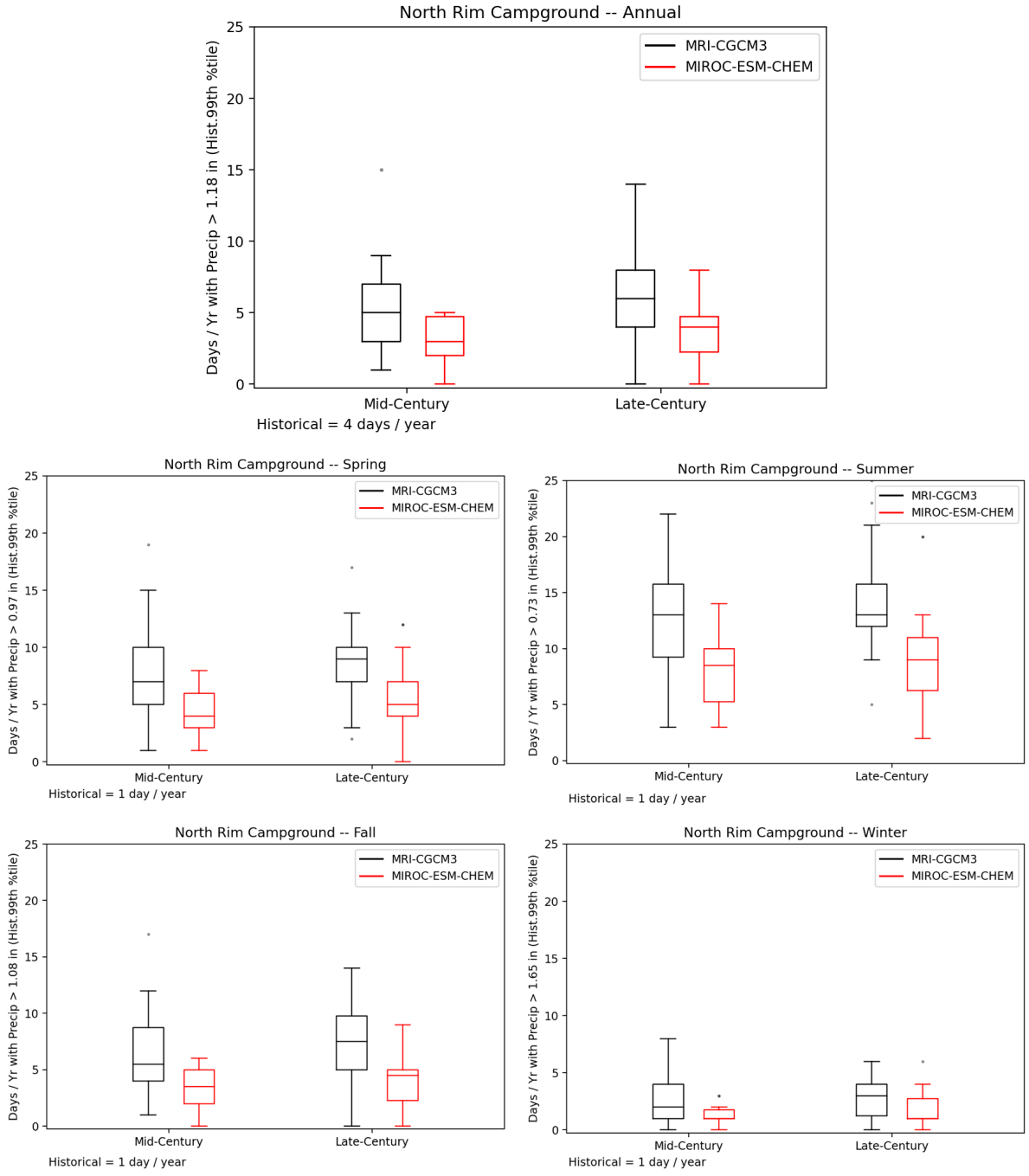

Figure 13. Days per year with precipitation greater than the 99th percentile at North Rim Campground annually and seasonally for the MRI and MIROC climate futures at mid- and late-century. The center line of box plot indicates the median value (50th percentile), while the box contains the 25th to 75th percentiles of the data. The whiskers mark the 5th and 95th percentiles, and values beyond the upper and lower bounds (dots on plot) are potential outliers.

Snow dynamics

The number of days with snow per year (i.e., days where the snow water equivalent is greater than 0) declines under both climate futures examined, with increasing declines from mid- to late-century (Figure 14). The MIROC climate future indicates a significantly greater loss of snow days per year compared to the MRI climate future that exhibits more modest warming.

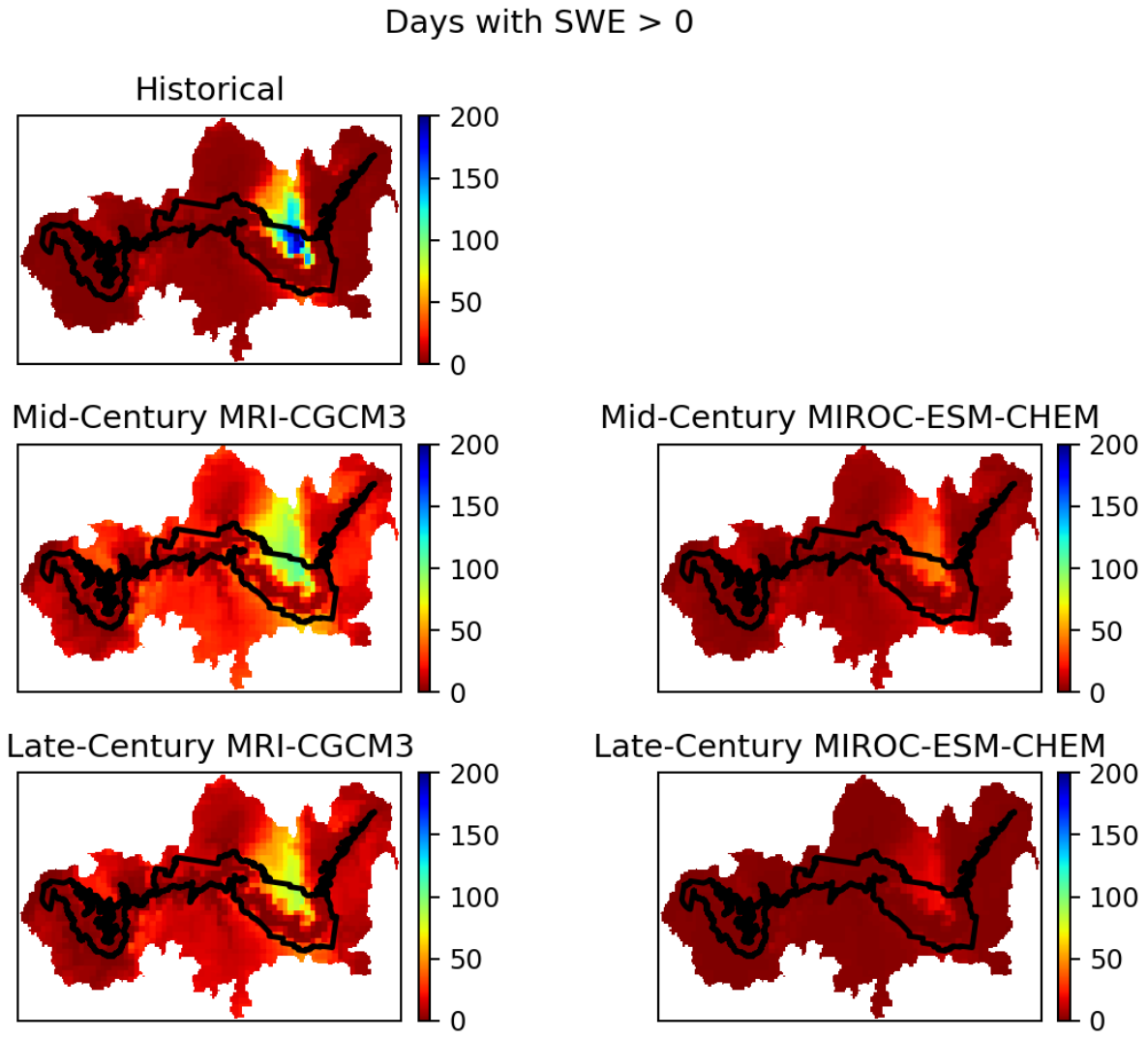

Figure 14. The number of days per year with snow water equivalent (SWE) greater than 0 during the historical period, as well as for mid- and late-century for the MRI and MIROC climate futures across the GGCL.

At mid-century, the number of days with snow at the highest elevations per year declined 24% (58.7 days relative to 77.7 days per year historically) under the MRI climate future and 71% under the MIROC climate future (Supplemental Figure A9). By late century under the MIROC climate future there is almost a total loss of snow at the mid and low elevations, which do not receive as much

precipitation as the higher elevation areas of the GGCL. The loss of days with snow cover at lower elevations, especially for the MIROC climate future, is apparent in Figure 15.

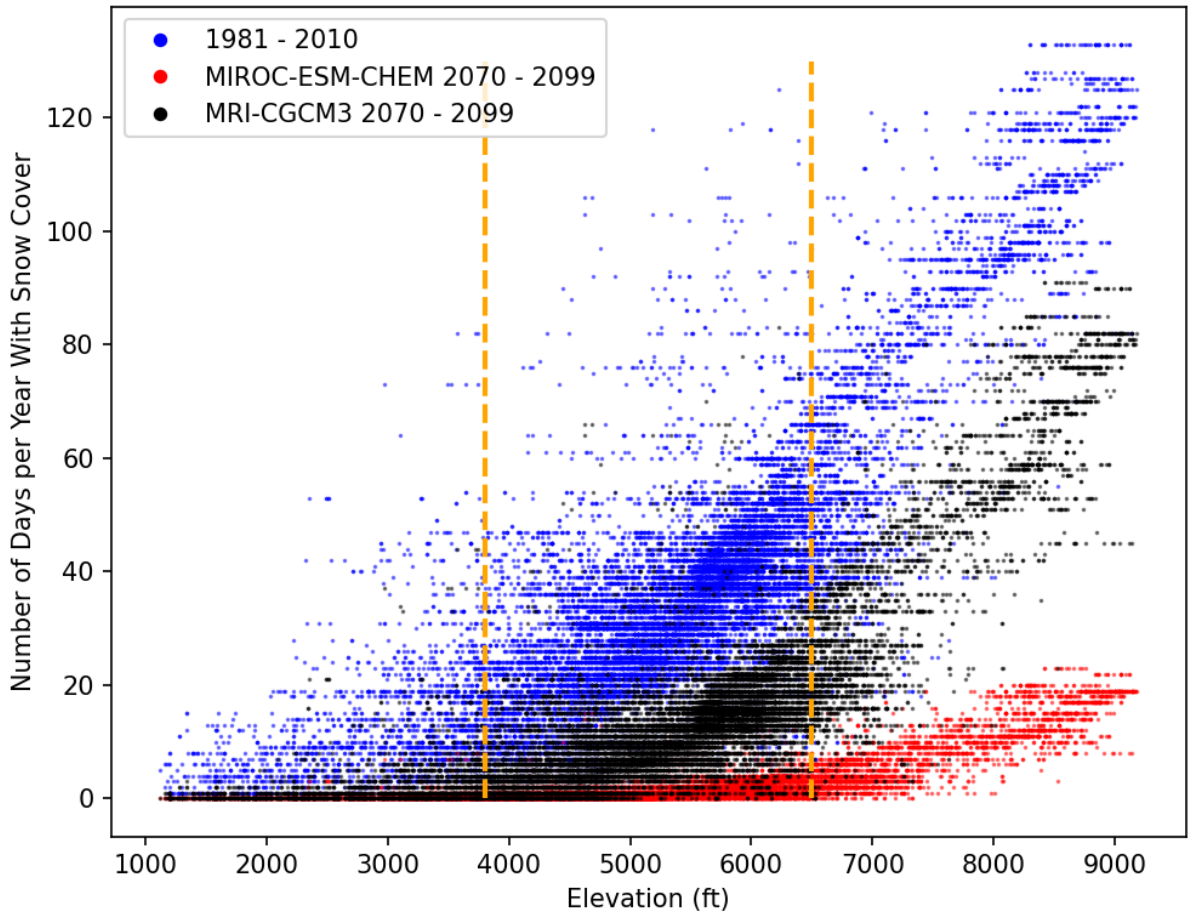

Figure 15. Number of days per year with snow cover by elevation across the GGCL for the historical reference period (1981–2010) and the late century period (2070–2099) for the MRI and MIROC climate futures. Each point is a grid cell from the GGCL. Vertical lines demarcate the elevation bands used throughout the report.

Historically, the high elevation Kaibab Plateau was the only area of the GGCL that accumulates a large snowpack (Figure 16). Under both climate futures snow as proportion of total precipitation declines on the Kaibab Plateau, with the greatest loss under the MIROC climate future (Figure 16).

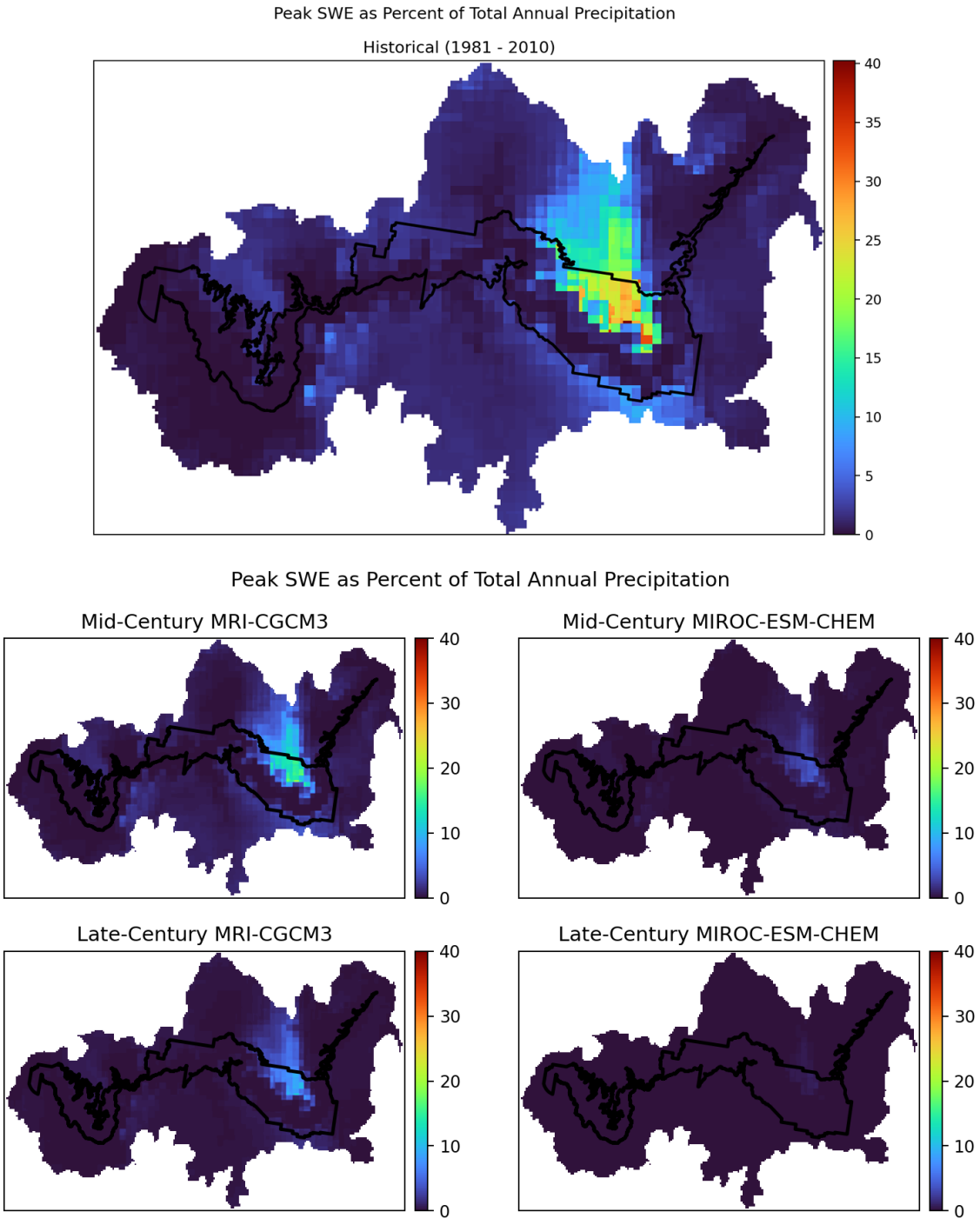

Figure 16. Peak snow water equivalent as a percent of the total annual precipitation for the historical reference period and mid- and late-century for the MRI and MIROC climate futures across the GGCL.

At the North Rim Campground seasonal snow accumulation (Figure 17), the number of days with snow per year (Figure 18), and peak snow water equivalent (Figure 18) declines significantly under

both climate futures. Under the hotter MIROC climate future there is little snow accumulation by mid-century and almost no snow accumulation by late century (Figure 17).

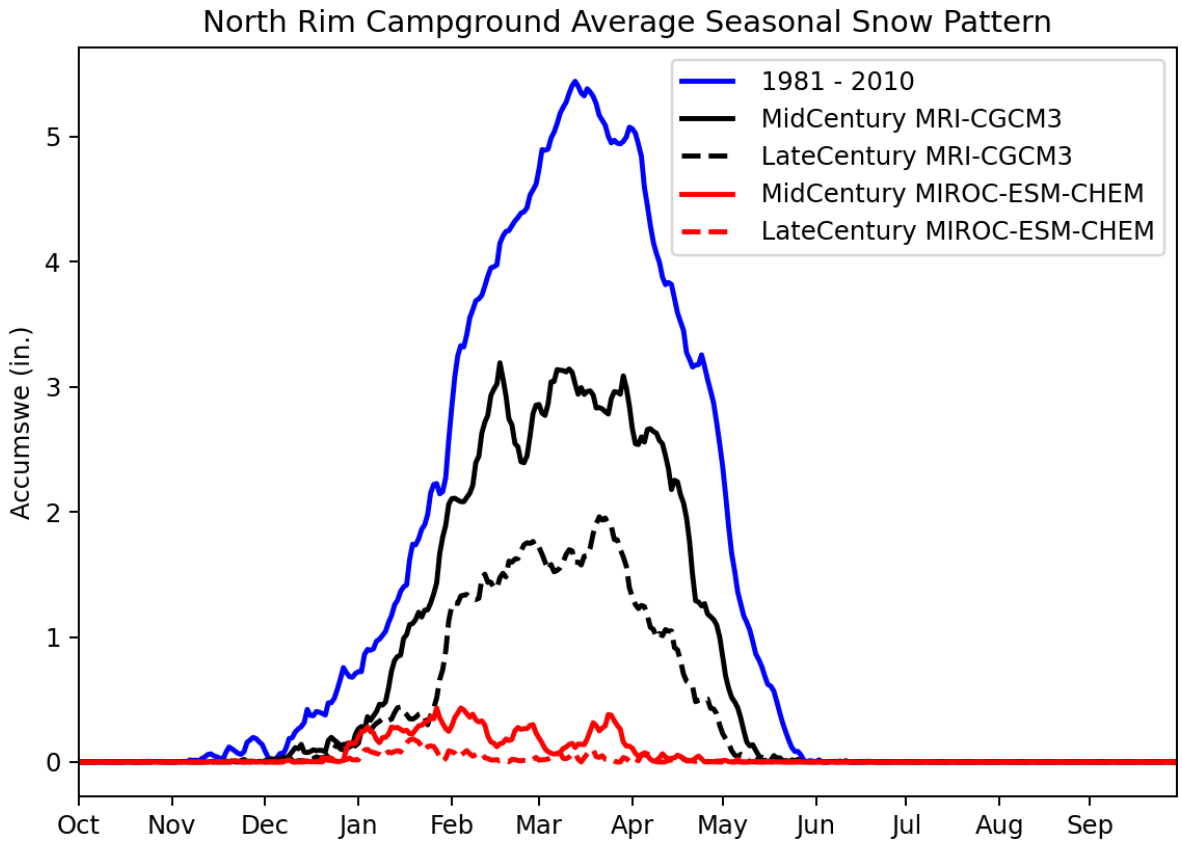

Figure 17. The seasonal snow pattern (Accumswe—accumulated snow water equivalent, inches) at the North Rim Campground, for the historical reference period and mid- and late-century for the MRI and MIROC climate futures.

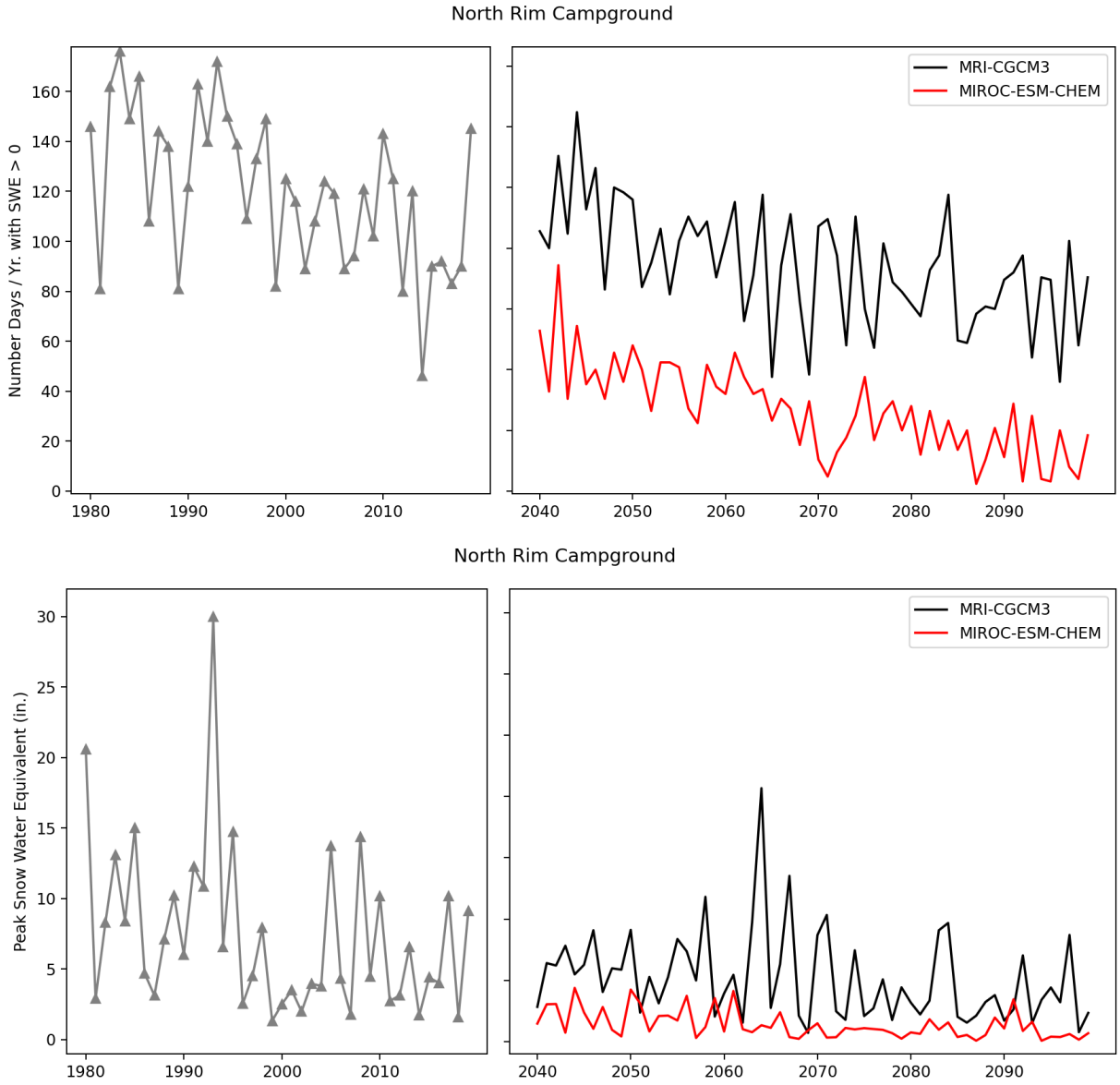

Figure 18. The number of days per year with snow water equivalent (SWE) greater than 0 (top panel) and the peak snow water equivalent (bottom panel) during the historical period, as well as for 2040–2100 for the MRI and MIROC climate futures at the North Rim Campground.

Moisture deficit dynamics

Moisture deficit, the difference between potential evapotranspiration and actual evapotranspiration (D = PET-AET), indicates the amount of additional water plants would use if it were available. It is often used as an indicator of landscape dryness, and increasing deficit correlates with increased fire occurrence and plant stress (Thoma et al., 2020). Moisture deficit is determined using a water balance model (see methods), which accounts for the interactive effects of temperature and precipitation.

Historically, the Kaibab Plateau has the lowest annual moisture deficit, while the northwestern part of the GGCL has the highest deficit (Figure 19). Relative annual moisture deficit is projected to increase by mid- and late-century under the MIROC climate future, with the greatest increases (measured as percent of historical deficit) on the high elevation Kaibab Plateau (Figure 20, Figure 21). Annual deficit also increases under the MRI climate future (Figure 20, Figure 21), but less than the hotter (MIROC) climate future.

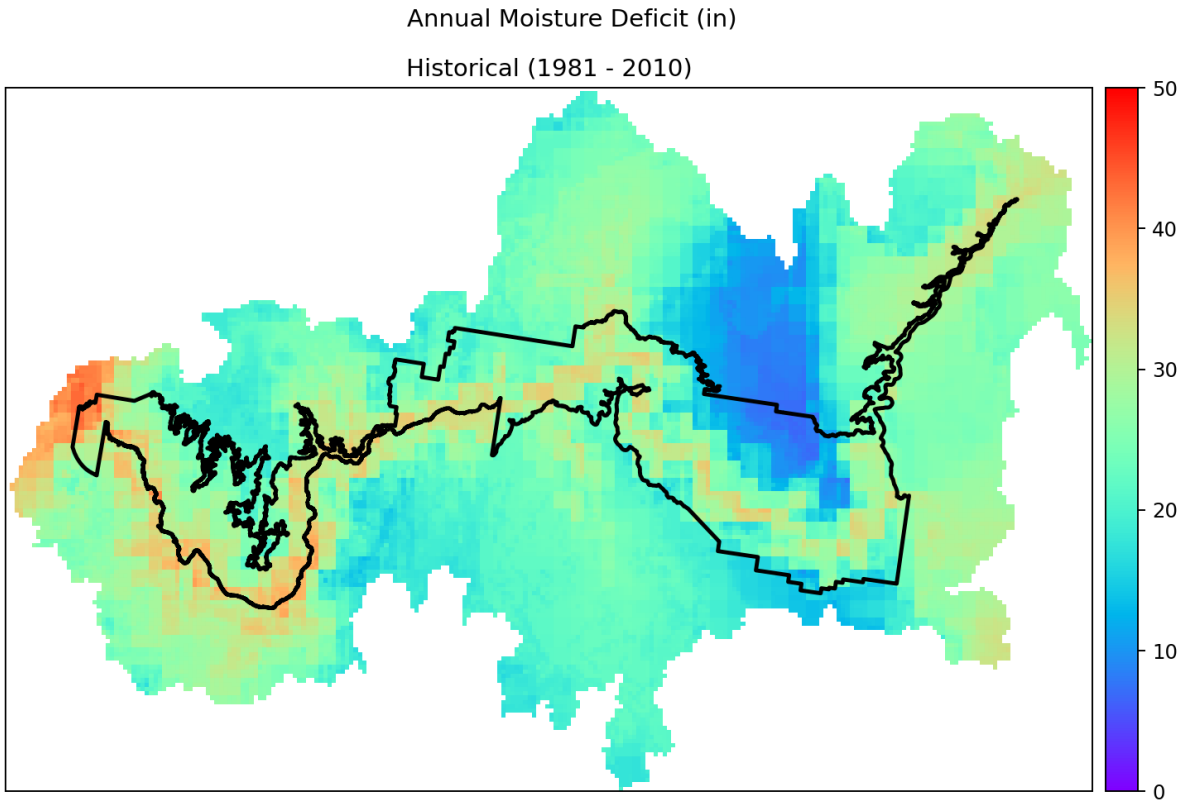

Figure 19. Historical total annual moisture deficit (inches) for the GGCL. Deficit (PET-AET), indicates the amount of additional water plants would use if it were available, and provides a measure of landscape dryness.

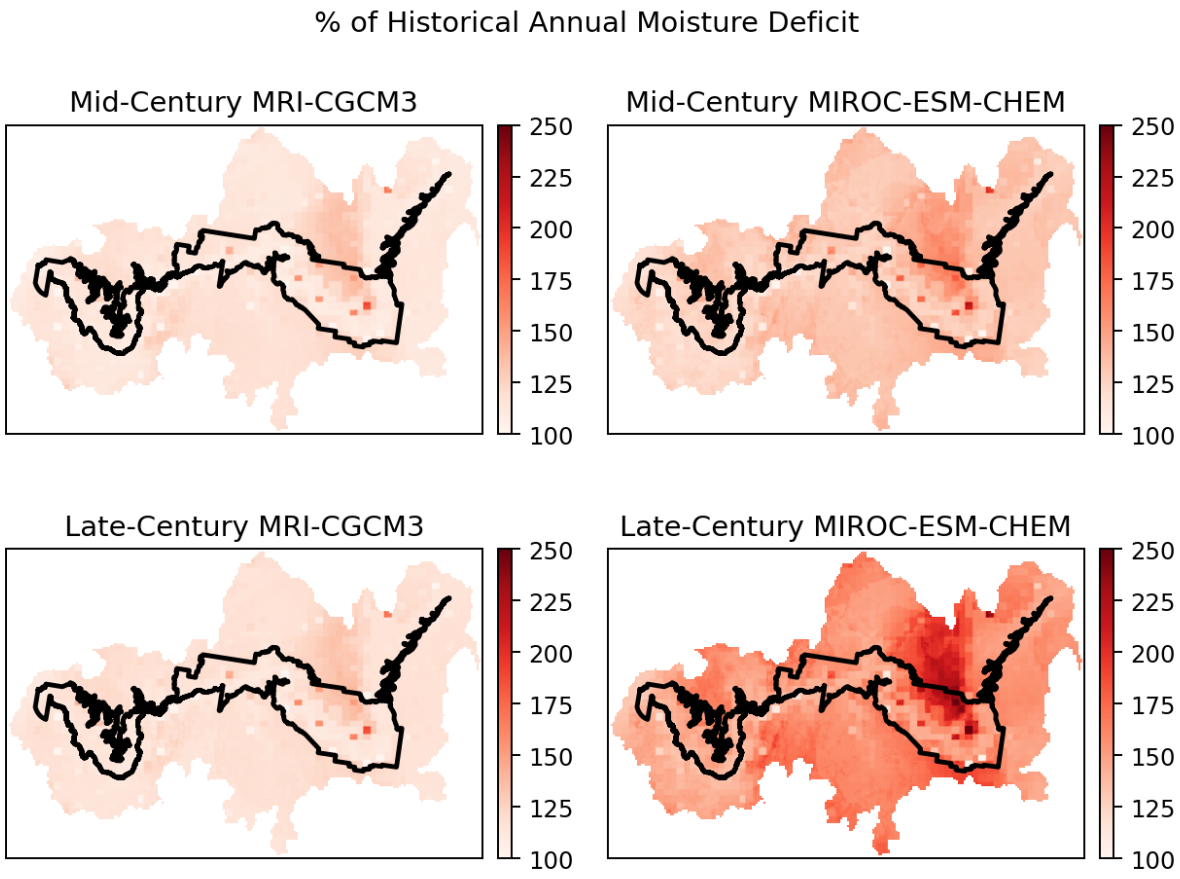

Figure 20. Percent of the historical annual moisture deficit (1981–2010) for the GGCL during the mid- and late-century for the MRI and MIROC climate futures. Deficit (PET-AET), indicates the amount of water plants would use if it were available, and provides a measure of landscape dryness.

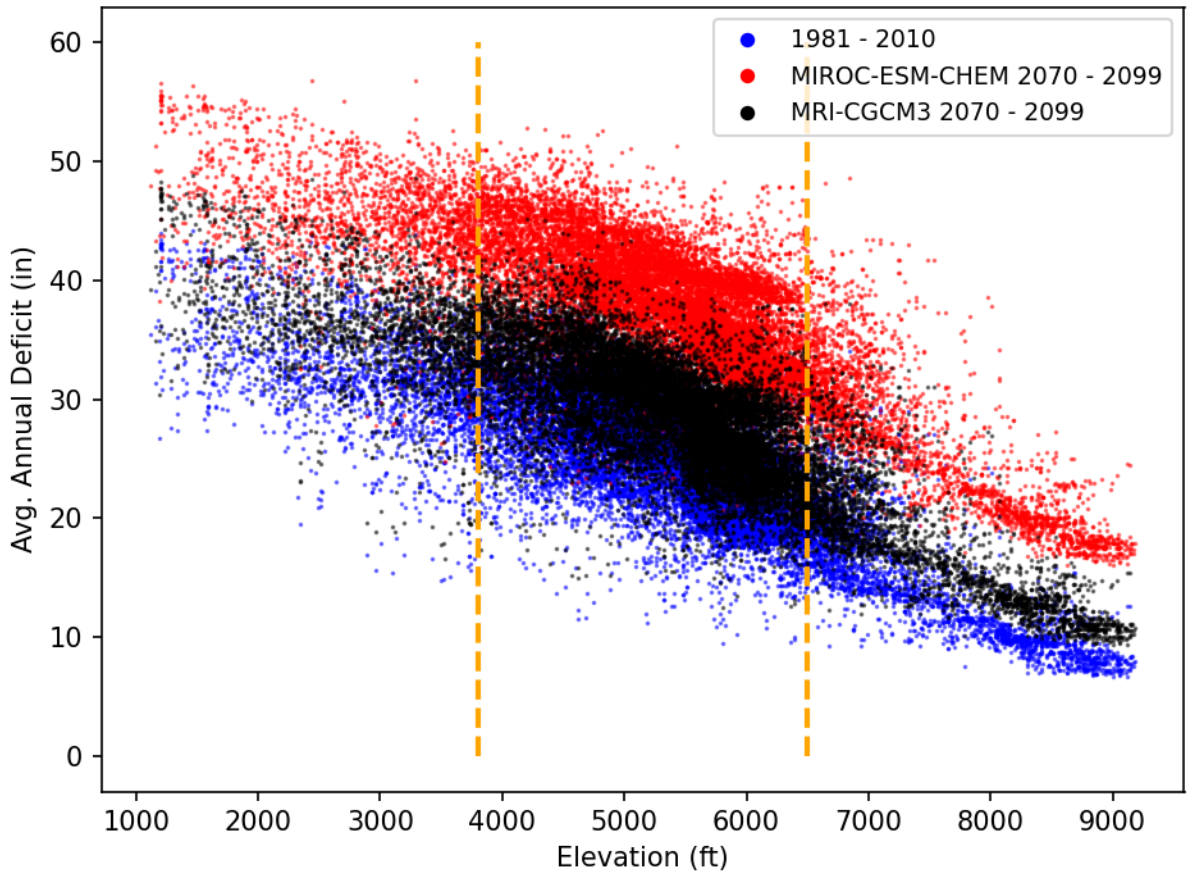

Figure 21. Average annual deficit by elevation across the GGCL for the historical reference period (1981–2010) and the late century period (2070–2099) for the MRI and MIROC climate futures. Vertical lines demarcate the elevation bands used throughout the report.

Cooler temperatures and greater precipitation at higher elevations result in less historical annual deficit with increasing elevation (Figure 21). By late-century both MRI and MIROC climate futures project an increase in annual deficit, with the hotter climate future (MIROC) indicating a greater deficit increase. Note that even though the annual precipitation is projected to increase under the MRI climate future, the annual deficit still increases as a result of increasing evapotranspiration associated with increasing temperatures (Figure 21). These results match a recent study of the Grand Canyon region that used similar methods (downscaling of CMIP5 models) and projected declining groundwater infiltration through the end of the 21st century despite no clear trend in projected annual precipitation (Tillman et al., 2020).

Absolute and relative annual and seasonal changes in deficit are provided across low, medium, and high elevation bands in Supplemental Figure A10 and Figure A11. Deficit increases in all seasons at all elevations and under both climate futures. The highest relative increases in deficit are projected for the MIROC climate future in winter and spring.

Figure 22 shows the relationship between annual deficit, the number of days with snow per year, and landscape elevation, historically and projected by late-century under the MRI and MIROC climate futures. By late-century there is a large contraction in the number of snow days per year under both climate futures. The increased deficit observed at mid to high elevations by late-century, especially under the MIROC climate future, may result because a longer snow free season results in more days per year where evaporation can occur, and evaporation itself is increased by increasing temperatures.

Spatial patterns of deficit by season are depicted in Supplemental Figures A12-A19, which show the historical deficit across the landscape and deficit projected under the MRI and MIROC climate future for a given season. Future projections of spring and winter deficit, measured as percent of the historical moisture deficit, increase most relative to the historical condition.

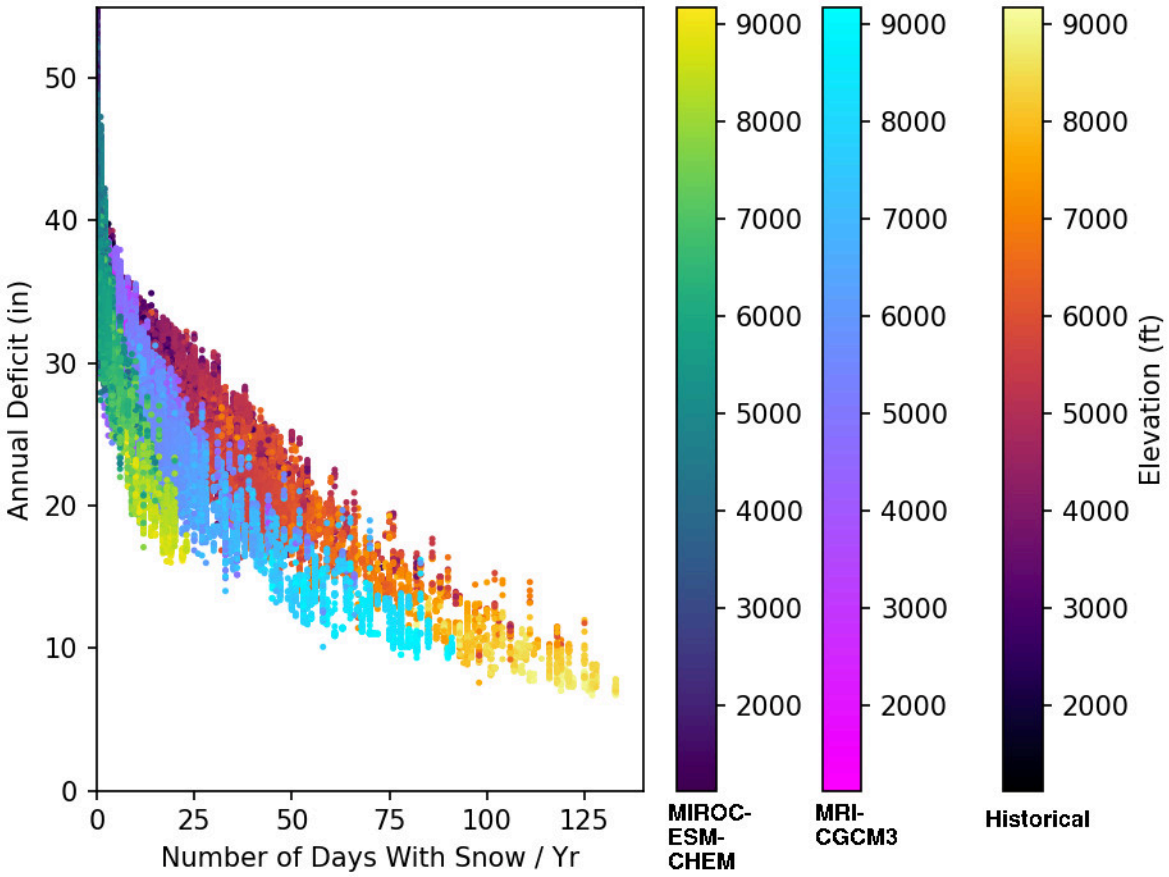

Figure 22. Annual deficit across the GGCL in relation to the number of days with snow per year and landscape elevation historically, and for late century MRI and MIROC climate futures.

Drought dynamics

The Standardized Precipitation Evaporation Index (SPEI) provides another metric to assess changing drought conditions (see methods for detailed explanation). Historical SPEI at the North Rim Campground is provided in Figure 23, showing drought characteristics (duration, return interval,

intensity, and severity) at this site from 1981–2020. Drought conditions for the North Rim Campground get progressively worse under the MIROC climate future as anthropogenic climate change causes aridification across the landscape (Figure 24). By mid-century, drought duration, intensity, and severity increase under the hotter MIROC climate future, while the average drought-free interval decreases. Under the wetter MRI climate future, drought duration and severity decrease relative to the historical period (1981–2010), while the average drought-free interval increases (indicating longer periods between droughts) (Figure 24).

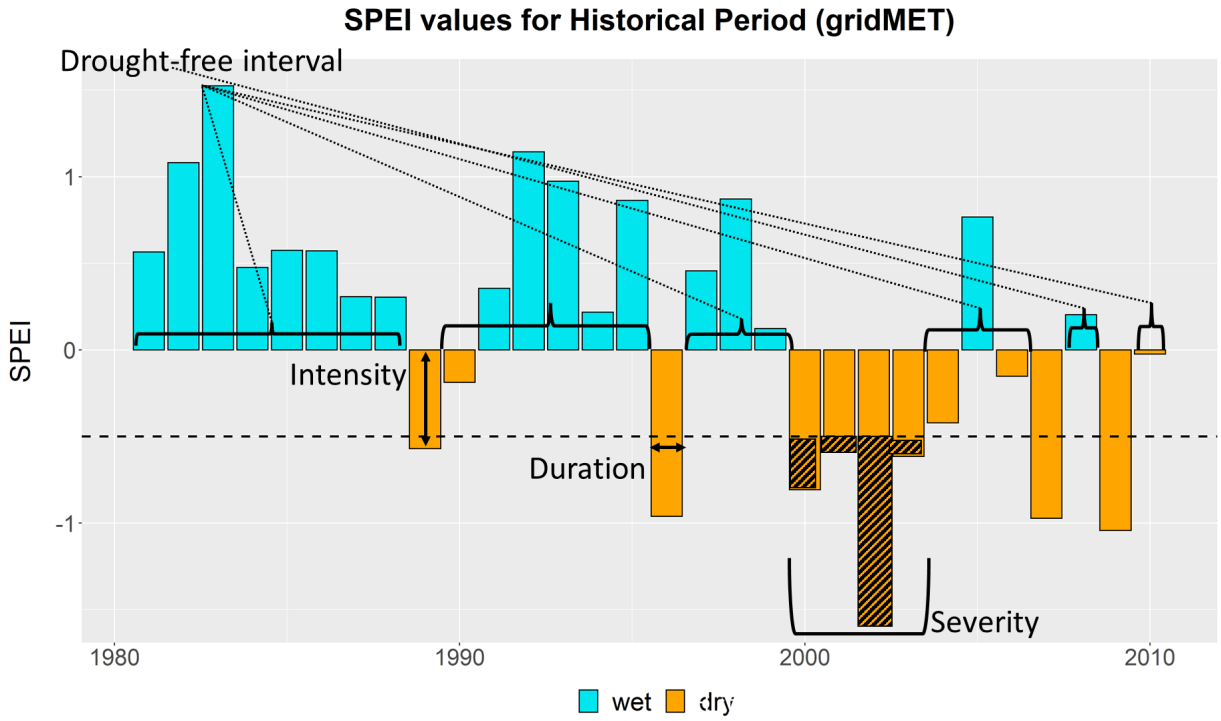

Figure 23. Four drought characteristics (duration, drought-free interval, intensity, and severity) were calculated at the North Rim Campground for the historical period 1981–2010. Drought events were defined as years when SPEI-6 fell below a threshold of −0.5. These characteristics are illustrated using observed, historical climate data (gridMET; Abatzoglou, 2013).

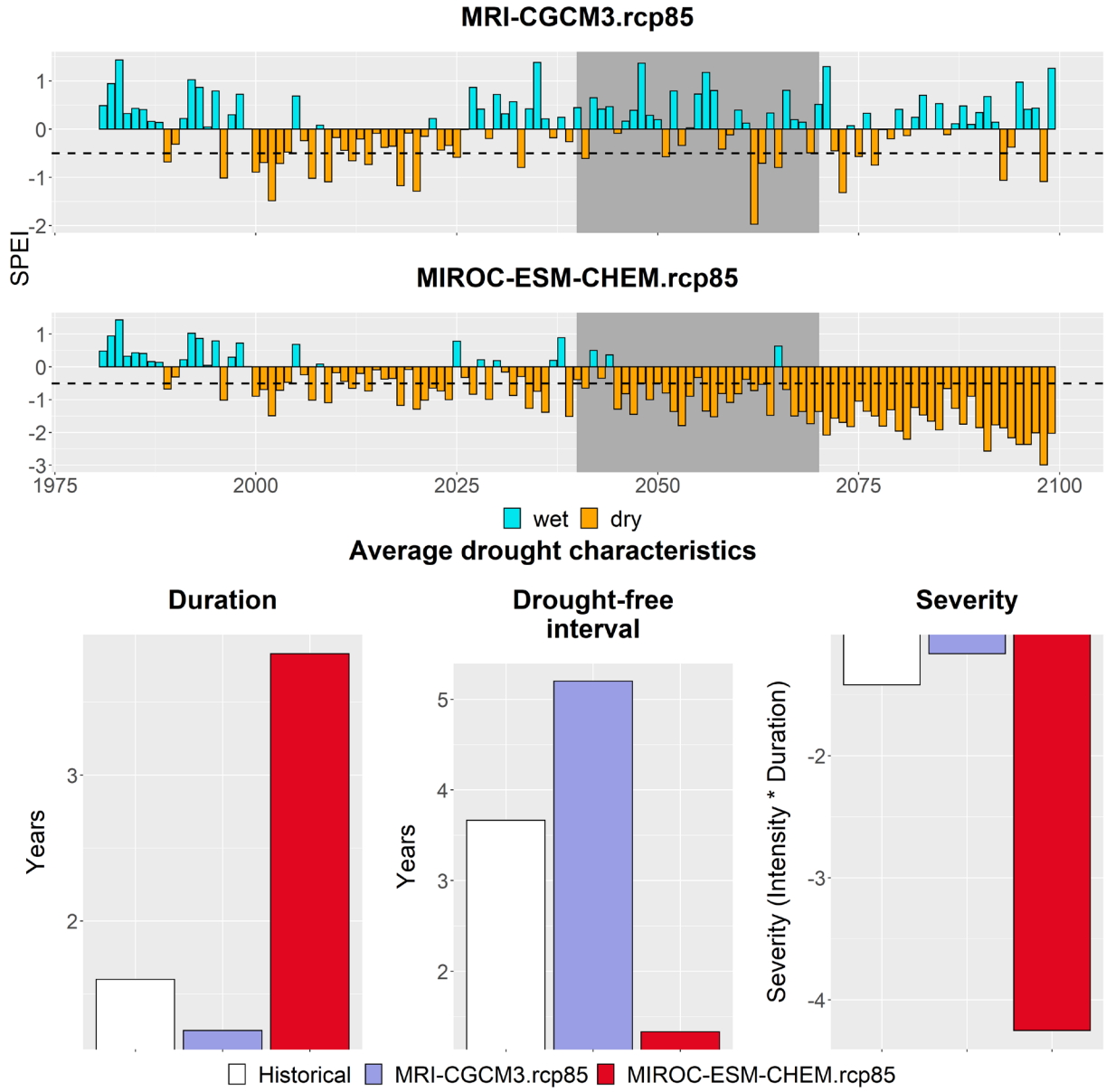

Figure 24. Top and middle panels: Drought index (SPEI-6) time series at the North Rim Campground for the MRI and MIROC climate futures. Data for the period prior to 2020 is gridMet (Abatzoglou, 2013) and after is MACA (Abatzoglou and Brown, 2012). The mid-century projection period (2055; 2040–2069) is highlighted in grey. Bottom left: Average drought duration historically and during mid-century under two climate futures, defined as the average number of years drought events last. Bottom middle: Average drought-free interval, or the number of years between the end of one drought event and the start of the next drought event historically and during mid-century under two climate futures. Bottom right: Average 'severity' of drought events, calculated as the duration multiplied by the intensity (minimum SPEI values for drought events) for the extent of the drought event historically and during mid-century under two climate futures. The historical period for all lower panel plots is 1981–2012 and was calculated using gridMet data.

Runoff

Future water runoff of the GGCL may increase or decrease depending on the climate future (Figure 25, Supplemental Figure A20). At the North Rim Campground both mid- and late-century projections indicate increasing runoff (relative to historical conditions) under the MRI climate future, whereas runoff declines significantly for the MIROC climate future. Runoff is projected to occur earlier under both climate futures and is projected to exhibit an episodic pattern. This contrasts the historical period with a long runoff season that did not have these breaks.

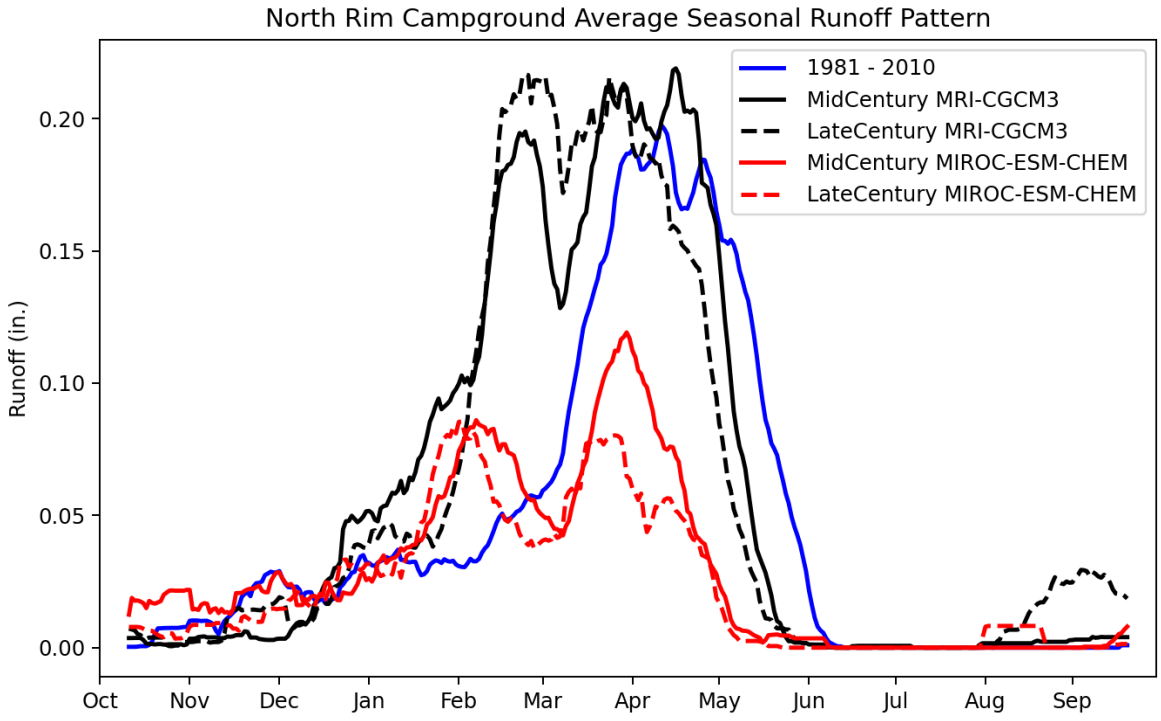

Figure 25. The seasonal runoff pattern (inches) at the North Rim Campground for the historical reference period and mid- and late-century MRI and MIROC climate futures.

The largest increases in runoff relative to the historical period under the MRI climate future are projected to occur at the highest elevation during the winter (Supplemental Figure A20). Runoff changes were small for this climate future during spring, summer and fall at mid-century, and during spring (low and medium elevations) and fall (all elevations) at late-century. The MIROC climate future projects the largest relative declines in runoff at the highest elevation during the spring and winter seasons of the mid- and late-century period (Supplemental Figure A20). Relatively little runoff change is projected for the summer and fall under the MIROC climate future at either the mid- or late-century period.

The karst nature of the high plateaus around the Grand Canyon causes most runoff to quickly infiltrate into the aquifers (with the exception of high-intensity summer thunderstorms). Depending on the regional geology, this water can be quickly discharged from springs after a few days (e.g., Kaibab Plateau; Jones et al., 2018; Tobin et al., 2018) or stored for centuries or millennia in the karst

aquifers (e.g., most of the Coconino Platform; Beisner et al., 2017). This variability in aquifer plumbing results in a wide variety of seasonal flow regimes for streams in the Grand Canyon. Springs and streams fed by aquifers with short residence times (e.g., Cheyava Falls) have strong seasonal variability, which is likely to shift in step with climate change. On the other hand, springs and streams sourced from aquifers with much longer residence times (e.g., Havasu and Blue Springs) will likely be buffered from the described climate changes for years to come.

Projected future risks

Continued climate change without carbon emissions reductions could increase temperatures by up to 9.3° F by mid-century (range 4.0–9.3° F) and 14.8° F by late-century (range 6.5 – 14.8° F; see Figure A5 from Appendix A). Emissions reductions could limit temperature increases by 66% (by 2100, RCP 2.6 versus RCP 8.5; Gonzalez et al., 2018). The projected physical and ecological changes listed below are based on those found in the scientific literature for Grand Canyon National Park and the surrounding region. This is not a comprehensive list of projected future risks and does not incorporate the extensive network of biotic and abiotic features of the park that are of critical value to Grand Canyon's 11 associated tribes. Additional work with tribal partners to identify and discuss ethnographic resources affected by climate change will be necessary to steward these culturally significant features of the park and mitigate ongoing threats to traditional ways of life (NFWPCAN, 2021). Recognition and understanding of indigenous knowledges will be a key focus area to inform and determine what projects and resources are prioritized within Grand Canyon in collaboration with ongoing work by tribal partners.

Drought

Climate change is already increasing, and will continue to increase, drought risk across North America. Under the highest emissions scenario, climate change could increase soil aridity in the Grand Canyon region in the period 2050–2099 to the 1% driest conditions experienced in the period 1931–1990 (Cook et al., 2015). For the southwestern U.S. as a whole, under the highest emissions scenario (RCP8.5), the severity of drought by 2100 A.D. could increase to the most severe level since 1000 A.D. (Cook et al., 2015).

Colorado River flow

Continued climate change could reduce Colorado River flow 10% to 45% by 2055 (BOR, 2016; Dettinger et al., 2015; Prein et al., 2016; Vano et al., 2014). The reduced flow derives from projected decreases of snowfall of 10% to 20% in the upper Colorado River basin (Lute et al., 2015) and increased evapotranspiration (BOR, 2016; Dettinger et al., 2015; Prein et al., 2016; Vano et al., 2014). Declining reservoir storage may limit management options for Colorado River flows designed to support the ecosystem (Bruckerhoff et al., 2022).

Hydrology changes

Under the range of emissions scenarios, from reduced emissions to highest emissions, projected temperature increases and changes in precipitation could reduce groundwater infiltration during three-fourths of the period 2020–2099, compared to the period 1951–2015 (Tillman et al., 2020). Battaglin et al. (2020) estimated spatially averaged change in runoff (mm/month) for Grand Canyon National Park (and contributing hydrologic response units) for 2060 (2051–2069) based on 214 climate projections using a monthly water balance model. The 50th percentile of all projections (i.e., the median) indicates runoff decreases in the 2060s during spring (April, May, June), summer (July, August, September), and fall months (October, November, December), and increases in runoff for the winter (January, February, March) from a 1981–1999 baseline.

Wildfire

In the western U.S., climate change under the highest emissions scenario could increase the number of large fires (area >50 km^2) by 300% by 2070 (2041–2070 average compared to 1971–2000 average) (Barbero et al., 2015). Carbon dioxide fertilization and increased temperature under climate change could increase invasive grasses in Mojave Desert ecosystems west of the park, providing more fuel for wildfire (Horn and St. Clair, 2017; Klinger and Brooks, 2017). Projected increases of wildfire could exacerbate post-fire erosion and increase sediment in Grand Canyon watersheds 10% to 100% in the period 2041–2050, compared to the period 2001–2010 (Sankey et al., 2017). Post-fire erosion could also extirpate native fish from tributaries that are now isolated from the mainstem due to Colorado River regulation (Healy et al., 2022).

Tree mortality

With continued climate change under the highest emissions scenario, northern Arizona forests would be highly vulnerable to drought-induced tree mortality by 2050 (Buotte et al., 2019). Continued climate change under the highest emissions scenario could cause up to twelve more episodes of drought-induced mortality of piñon pine (*Pinus edulis*) in the Grand Canyon region by 2100 (McDowell et al., 2016). The high drought-induced mortality of piñon pine and Utah juniper (*Juniperus osteosperma*) in Grand Canyon National Park since 1935 (Vankat, 2017) indicates a future sensitivity under continued climate change. In the Coconino National Forest, south of Grand Canyon National Park, mortality of two-thirds of trees, particularly ponderosa pine (*Pinus ponderosa*) and quaking aspen (*Populus tremuloides*), in the 15 years after the Leroux Fire indicates the risk of future drought-induced post-fire tree mortality under climate change (Stoddard et al., 2018).

Vegetation change

With continued climate change under the highest emissions scenario, projected increases of high-severity wildfire increase the risk of fire-driven conversion of ~4% of Colorado Plateau forest to non-forest by 2050 (Parks et al., 2019). The Grand Canyon region is highly vulnerable to biome shifts – upslope shifts of the elevational zones of pinyon-juniper woodland, ponderosa pine forest, and spruce-fir forest – due to continued climate change (Gonzalez et al., 2010) and the combination of climate change and land use change (Eigenbrod et al., 2015). Modeling of vegetation on the Kaibab Plateau, north of the park, projects potential upslope shifts equivalent to one vegetation zone, a doubling or more of non-forest area, and substantial aboveground biomass declines by 2090 under the highest climate change emissions scenario (Flatley and Fulé, 2016; O'Donnell et al., 2018).

Riparian vegetation and sediment

Riparian vegetation density depends on human control of water flow by the Glen Canyon Dam, upstream of the park, with woody vegetation colonizing river sediment deposits when water flows are low (Kasprak et al., 2018; Kasprak et al., 2021; Sankey et al., 2015). Field measurements along the upper 360 km of the Colorado River in Grand Canyon National Park indicate that increasing temperatures and drought under climate change could reduce the abundance of riparian vegetation that tolerates water inundation (Butterfield et al., 2018).

Invasive plant increase

Climate change can favor invasive (non-native) plants, including cheatgrass (*Bromus tectorum*), red brome (*Bromus rubens*), and yellow starthistle (*Centaurea solstitialis*), for three main reasons. (1) Carbon dioxide (CO2) enrichment—invasive plants generally exploit atmospheric CO2 more efficiently than native species, generating higher growth rates and increases in seed production (Davidson et al., 2011; Liu et al., 2017). (2) Warmth and moisture—increasing warmth and moisture due to climate change can increase the suitability of temperate zone ecosystems to plants from tropical zones (Hellmann et al., 2008; Theoharides and Dukes, 2007). Any future conditions of increasing aridity, however, would be unfavorable to invasive plants that thrive in moister conditions. Increased frequency of extreme storms could lead to episodes of higher moisture. (3) Disturbance—invasive plants often proliferate in sites disturbed by physical vegetation removal or by wildfire (Hellmann et al., 2008; Theoharides and Dukes, 2007). In the western U.S., anthropogenic climate change causes two disturbances, biome shifts (Gonzalez et al., 2010) and increased wildfire (Abatzoglou and Williams, 2016), that tend to increase the risk of invasive species establishment (Early et al., 2016). The combination of these climate change factors and the introduction and transportation of invasive species seeds by people causes a high risk of invasive species under climate change in northern Arizona (Early et al., 2016).

Desert bighorn sheep

While climate change increases the risk of habitat loss for desert bighorn sheep (*Ovis canadensis nelsoni*) at low elevations and genetic isolation at high elevations in southern California, Nevada, and northern Arizona (Creech et al., 2020; Epps et al., 2006; Epps et al., 2007), vulnerability in Grand Canyon National Park remains low because of the extensiveness of intact habitat, as well as high genetic and geographic connectivity (Creech et al., 2020). As heatwave intensity and length increase, sheep may have to make tradeoffs between good escape terrain, foraging areas, and access to water for improved thermoregulation (Gedir et al., 2020).

Birds

Climate change could continue to shift the ranges of bird species northward across the U.S. (Langham et al., 2015). Modeling of suitable climate for bird species in 2050 indicates that, under the highest emissions scenario, the park may gain suitable climate for 36 bird species not currently present in winter and 17 species not currently present in summer but lose suitable climate for 46 species in the summer and 16 species in winter (Wu et al., 2018). A potential colonizer is the bronzed cowbird (*Molothrus aeneus*). Species vulnerable to extirpation include the red-breasted nuthatch (*Sitta canadensis*), and the pine siskin (*Spinus pinus*) (Wu et al., 2018). According to van Ripper et al.'s (2014) analysis of the southwestern US, black-throated sparrow (*Amphispiza bilineata*) and gray vireo (*Vireo vicinior*) are projected to experience major gains in breeding habitat, while pinyon jay (*Gymnorhinus cyanocephalus*), pygmy nuthatch (*Sitta pygmaea*), sage thrasher (*Oreoscoptes montanus*), and Williamson's sapsucker (*Sphyrapicus thyroideus*) are projected to experience large losses in breeding habitat.

Reptiles

van Ripper et al. (2014) assessed future projections of five reptiles of the southwestern US, and found that 80% of these species (4 out of 5) are projected to experience loss of one-third of their distributional range by 2099 due to climate change. The only exception to this pattern was the Sonoran desert tortoise (*Gopherus morafkai*), whose distribution either increases (assuming unlimited dispersal) or does not change.

Amphibians

American bullfrogs (*Lithobates catesbeianus*) will likely have impacts to native amphibians (namely lowland leopard frogs, *Lithobates yavapaiensis*, in western Grand Canyon National Park) from direct predation and diseases (*Batrachochytrium dendrobatidis*, ranaviruses) if established. Warmer waters and lower flows will likely exacerbate their expansion from Lake Mead (Renner and Day, 2022).

Fish

Increases in river temperatures, due to a combination of climate change and overallocation of Colorado River flows, could favor warm water non-native fish species, including channel catfish (*Ictalurus punctatus*), red shiner (*Cyprinella lutrensis*), and smallmouth bass (*Micropterus dolomieu*) over native fishes, including Colorado pikeminnow (*Ptychocheilus lucius*), humpback chub (*Gila cypha*), and razorback sucker (*Xyrauchen texanus*) (Dibble et al., 2021). Tributaries of the GGCL are essential for native fish reproduction, and fish recruitment (both native and non-native) within these tributaries is strongly influenced by variability in annual streamflow (Healy et al., 2022; Healy et al., 2023). Therefore, shifts in the timing, magnitude, and duration of tributary runoff regimes are likely to influence population dynamics of native and introduced fishes. Further, if previously permanent tributaries to the Colorado River become intermittent it may create barriers to fish migration (Jaeger et al., 2014).

Crayfish

Non-native crayfish, including *Faxonius virilis* and *Procambrus clarkii*, have been documented in the upper and lower reach, respectively, of the Colorado River in Grand Canyon National Park. Non-native crayfish have been reported to impact native fishes and amphibians through direct and indirect interactions at multiple trophic levels and may expand as a result of climate change (Martinez, 2012).

Pollinators

A drier climate is anticipated to impact pollinators by shifting growing and blooming seasons, which weakens the plant-pollinator connection. Community science observations of recent butterfly declines in drought-affected areas of the southwestern U.S. indicate risks of substantial declines under projected aridity increases under climate change (Forister et al., 2021). Further, a broad investigation of butterfly abundance and biodiversity trends by Crossley et al. (2021) found that populations generally decline at increasing hot and dry sites (but increase at relatively cool and wet sites). Soroye et al. (2020) found an increasing frequency of unusually hot days is increasing local extinction rates of bumble bees, reducing their colonization and site occupancy, and decreasing species richness within a region, independent of land-use change and condition.

Visitation

Visitation is strongly correlated with air temperature in Grand Canyon National Park (Fisichelli et al., 2015). Thus, as temperatures increase, all else being equal, visitation is expected to increase. Under two scenarios of climate change, Fisichelli et al. (2015) project a 7–22% increase in annual visitation by mid-century (2041–2060). They also project a 4–11% increase in peak season visitation, a 10–22% increase in shoulder season visitation, a 16–57% increase in low season visitation, and a 11 to 36 day expansion of the visitation season by mid-century (Fisichelli et al., 2015).

Cultural resources

Potential impacts to archeological resources include exacerbation of existing threats, such as gullying and erosion associated with both natural events and controlled releases from Glen Canyon Dam that impact site deterioration and artifact transport (Collins et al., 2009; Pederson et al., 2006), as well as emergent vulnerabilities from increased frequency of extreme storms, wildfire, and vegetation loss (Cassar, 2005; Morgan et al., 2016; Ryan et al., 2012). Similarly, threats and impacts already identified for the park's cultural landscapes, including general exposure to elements, structural deterioration, improper drainage, flooding, and vegetation/invasive plants, could be intensified or accelerated by vegetation shifts, drought, and extreme storms (John Milner Associates, 2005; John Milner Associates, 2007; Morgan et al., 2016). Mechanical degradation, thermoclasticism, material erosion, and fire risks to the envelope and interiors of historic structures should also be considered (Sabbioni et al., 2008; Sesana et al., 2021).

View of the Colorado River from Plateau Point off the Bright Angel Trail. NPS photo/M.Quinn

Conclusions

Anthropogenic climate change is one of the greatest threats to resources in protected areas globally. This report examines climate change occurring across the Greater Grand Canyon Landscape, including Grand Canyon National Park. We use historical climate datasets to demonstrate that the GGCL has already warmed significantly over the period 1895–2020, with a greater rate of temperature increase over the period 1970–2020. Annual average precipitation across the GGCL and within Grand Canyon National Park did not change significantly over either time period examined (1895–2020; 1970–2020). We review the physical and ecological changes detected in the region and attributed to anthropogenic climate change, based on the published scientific literature, including change to drought dynamics, Colorado River flow, wildfire, tree regeneration, tree mortality, bird ranges, and insect changes.

Two 'climate futures' (i.e., descriptions of the physical attributes of plausible future climates) were evaluated for the GGCL, characterized for mid-century (2040–2069) and late-century (2070–2099). These climate futures were derived from the MRI and MIROC projections (global climate models run under the representative concentration pathway 8.5), and were chosen to provide contrasting, but plausible, climate futures for the region. Managers can examine contrasting climate futures to understand the range of how the climate may change and plan around that range, establishing climate-informed goals and strategies to achieve those goals robust to these climate futures. The climate futures described here include projections of change in air temperature, precipitation, snow, moisture deficit, drought, and runoff. Projections of change in fire regime were beyond the scope of this report, but some inference is available based on changes in moisture deficit (which is often positively correlated with conditions conducive to fire).

Both climate futures examined project increasing temperature across the GGCL. The milder MRI climate future projects mean temperature increases ranging from 4.0–4.2° F by mid-century and 6.5–6.6° F by late century, whereas the hotter MIROC climate future projects increases of 8.8–9.3° F by mid-century and 14.2–14.8° F by late-century. Under both climate futures extremely warm days increase and the days below freezing decline, varying in intensity based on the climate future examined. Annual precipitation increases under the MRI climate future, with relatively little change in annual precipitation for the MIROC climate future. The MRI and MIROC climate futures indicate an increase in extreme precipitation events at the North Rim Campground for all seasons, relative to the historical period for both the mid- and late-century periods. The number of days with snow per year declines under both climate futures examined, with progressively increasing declines from mid- to late-century. Moisture deficit, an indicator of landscape dryness, and correlate with plant stress and conditions conducive to fire, increases under both climate futures examined, including the wetter MRI (due to increased evapotranspiration associated with warming temperatures). Projections of drought conditions depend on the climate future considered. Droughts become longer, more severe, and occur at more frequent intervals under the MIROC climate future. Under the wetter MRI climate future the interval between droughts increases, and their duration and severity declines relative to the historical reference period. Future water runoff increases under the MRI climate future (relative to historical conditions), whereas runoff declines significantly for the MIROC climate future.

Future projections of changes resulting from climate change for Grand Canyon National Park and the surrounding region from the scientific literature are provided, including descriptions of change in drought conditions, Colorado River flow, hydrology, wildfire, tree mortality, vegetation change, riparian vegetation and sediment, invasive plants, mammals, birds, fish, insects, as well as changes in visitation and vulnerability of cultural resources.

One goal of this work is to support the Resource Stewardship Strategy (RSS) process that Grand Canyon plans to undertake in the future. We anticipate connecting the climate changes described here to the climate sensitivities of resources within the park in a participatory process with park partners and associated tribes, to inform goal setting and strategy development that is part of the RSS process, as well as proactively adapting to anticipated changes.

Deer Creek in Grand Canyon National Park. NPS photo/E.Whittaker

Literature Cited

Abatzoglou JT. 2013. Development of gridded surface meteorological data for ecological applications and modelling. International Journal of Climatology 33:121–131.

Abatzoglou JT, and TJ Brown. 2012. A comparison of statistical downscaling methods suited for wildfire applications. International Journal of Climatology 32:772–780.

Abatzoglou JT, and AP Williams. 2016. Impact of anthropogenic climate change on wildfire across western US forests. Proceedings of the National Academy of Sciences 113:11770–11775.

Barbero R, JT Abatzoglou, NK Larkin, CA Kolden, and B Stocks. 2015. Climate change presents increased potential for very large fires in the contiguous United States. International Journal of Wildland Fire 24:892–899.

Barsugli JJ, G Guentchev, RM Horton, A Wood, LO Mearns, X-Z Liang, . . . C Ammann. 2013. The Practitioner's Dilemma: How to Assess the Credibility of Downscaled Climate Projections. Eos, Transactions American Geophysical Union 94:424–425.

Battaglin W, L Hay, DJ Lawrence, G McCabe, and P Norton. 2020. Baseline conditions and projected future hydro-climatic change in national parks in the conterminous United States. Water 12:1704.

Beisner KR, FD Tillman, JR Anderson, RC Antweiler, and DJ Bills. 2017. Geochemical characterization of groundwater discharging from springs north of the Grand Canyon, Arizona, 2009–2016. Scientific Investigations Report, Reston, VA.

BOR. 2016. West-Wide Climate Risk Assessments: Hydroclimate Projections. Technical Memorandum No. 86-68210-2016-01. U.S. Bureau of Reclamation, Denver, CO.

BOR. 2023. March 24-month study. Date: March 15th 2023. https://www.usbr.gov/uc/water/crsp/studies/24Month_03_ucb.pdf.

Bruckerhoff LA, K Wheeler, KL Dibble, BA Mihalevich, BT Neilson, J Wang, . . . JC Schmidt. 2022. Water Storage Decisions and Consumptive Use May Constrain Ecosystem Management under Severe Sustained Drought. JAWRA Journal of the American Water Resources Association 58:654–672.

Buotte PC, S Levis, BE Law, TW Hudiburg, DE Rupp, and JJ Kent. 2019. Near-future forest vulnerability to drought and fire varies across the western United States. Global Change Biology 25:290–303.

Butterfield BJ, E Palmquist, and B Ralston. 2018. Hydrological regime and climate interactively shape riparian vegetation composition along the Colorado River, Grand Canyon. Applied Vegetation Science 21:572–583.

Cassar M. 2005. Climate Change and the Historic Environment. London: Centre for Sustainable Heritage, University College London.

Collins BD, D Minasian, and R Kayen. 2009. Topographic Change Detection at Select Archeological Sites in Grand Canyon National Park, Arizona, 2006–2007: U.S. Geological Survey Scientific Investigations Report 2009-5116, 58 p. [http://pubs.usgs.gov/sir/2009/5116/].

Cook BI, TR Ault, and JE Smerdon. 2015. Unprecedented 21st century drought risk in the American Southwest and Central Plains. Science Advances 1.

Creech TG, CW Epps, JD Wehausen, RS Crowhurst, JR Jaeger, K Longshore, . . . RJ Monello. 2020. Genetic and Environmental Indicators of Climate Change Vulnerability for Desert Bighorn Sheep. Frontiers in Ecology and Evolution 8.

Crossley MS, OM Smith, LL Berry, R Phillips-Cosio, J Glassberg, KM Holman, . . . WE Snyder. 2021. Recent climate change is creating hotspots of butterfly increase and decline across North America. Global Change Biology 27:2702–2714.

Cuarón AD, K Helgen, F Reid, J Pino, and JF González-Maya. 2016. Nasua narica. The IUCN Red List of Threatened Species 2016.

Davidson AM, M Jennions, and AB Nicotra. 2011. Do invasive species show higher phenotypic plasticity than native species and, if so, is it adaptive? A meta-analysis. Ecol Lett 14:419–431.

Davis KT, SZ Dobrowski, PE Higuera, ZA Holden, TT Veblen, MT Rother, . . . MP Maneta. 2019. Wildfires and climate change push low-elevation forests across a critical climate threshold for tree regeneration. Proceedings of the National Academy of Sciences:201815107.

Delworth TL, F Zeng, A Rosati, GA Vecchi, and AT Wittenberg. 2015. A Link between the Hiatus in Global Warming and North American Drought. Journal of Climate 28:3834–3845.

Dettinger M, B Udall, and A Georgakakos. 2015. Western water and climate change. Ecological Applications 25:2069–2093.

Dibble KL, CB Yackulic, TA Kennedy, KR Bestgen, and JC Schmidt. 2021. Water storage decisions will determine the distribution and persistence of imperiled river fishes. Ecological Applications 31:e02279.

Dixon KW, JR Lanzante, MJ Nath, K Hayhoe, A Stoner, A Radhakrishnan, . . . CF Gaitán. 2016. Evaluating the stationarity assumption in statistically downscaled climate projections: is past performance an indicator of future results? Climatic Change 135:395–408.

Early R, BA Bradley, JS Dukes, JJ Lawler, JD Olden, DM Blumenthal, . . . AJ Tatem. 2016. Global threats from invasive alien species in the twenty-first century and national response capacities. Nat Commun 7:12485.

Eigenbrod F, P Gonzalez, J Dash, and I Steyl. 2015. Vulnerability of ecosystems to climate change moderated by habitat intactness. Global Change Biology 21:275–286.

Epps CW, PJ Palsbøll, JD Wehausen, GK Roderick, and DR McCullough. 2006. Elevation and connectivity define genetic refugia for mountain sheep as climate warms. Molecular Ecology 15:4295–4302.

Epps CW, JD Wehausen, VC Bleich, SG Torres, and JS Brashares. 2007. Optimizing dispersal and corridor models using landscape genetics. Journal of Applied Ecology 44:714–724.

Fisichelli NA, GW Schuurman, WB Monahan, and PS Ziesler. 2015. Protected Area Tourism in a Changing Climate: Will Visitation at US National Parks Warm Up or Overheat? PLOS ONE 10:13.

Flatley WT, and PZ Fulé. 2016. Are historical fire regimes compatible with future climate? Implications for forest restoration. Ecosphere 7:e01471.

Forister ML, CA Halsch, CC Nice, JA Fordyce, TE Dilts, JC Oliver, . . . J Glassberg. 2021. Fewer butterflies seen by community scientists across the warming and drying landscapes of the American West. Science 371:1042–1045.

Gedir JV, JW Cain, TL Swetnam, PR Krausman, and JR Morgart. 2020. Extreme drought and adaptive resource selection by a desert mammal. Ecosphere 11.

Gonzalez P, RP Neilson, JM Lenihan, and RJ Drapek. 2010. Global patterns in the vulnerability of ecosystems to vegetation shifts due to climate change. Global Ecology and Biogeography 19:755–768.

Gonzalez P, F Wang, M Notaro, DJ Vimont, and JW Williams. 2018. Disproportionate magnitude of climate change in United States national parks. Environmental Research Letters 13:104001.

Healy BD, P Budy, MM Conner, and EC Omana Smith. 2022. Life and death in a dynamic environment: Invasive trout, floods, and intra-specific drivers of translocated populations. Ecological Applications n/a:e2635.

Healy BD, P Budy, CB Yackulic, BP Murphy, RC Schelly, and MC McKinstry. 2023. Exploring metapopulation-scale suppression alternatives for a global invader in a river network experiencing climate change. Conserv Biol 37:e13993.

Hellmann JJ, JE Byers, BG Bierwagen, and JS Dukes. 2008. Five potential consequences of climate change for invasive species. Conserv Biol 22:534–543.

Hoerling M, J Barsugli, B Livneh, J Eischeid, X Quan, and A Badger. 2019. Causes for the Century-Long Decline in Colorado River Flow. Journal of Climate 32:8181–8203.

Holden ZA, A Swanson, CH Luce, WM Jolly, M Maneta, JW Oyler, . . . D Affleck. 2018. Decreasing fire season precipitation increased recent western US forest wildfire activity. Proceedings of the National Academy of Sciences.

Holton B, T Theimer, and K Ironside. 2021. First records and possible range extension of the American Hog-nosed Skunk into Grand Canyon National Park, U.S.A. Small Carnivore Conservation 59: e59001.

Horn KJ, and SB St. Clair. 2017. Wildfire and exotic grass invasion alter plant productivity in response to climate variability in the Mojave Desert. Landscape Ecology 32:635–646.

Iknayan KJ, and SR Beissinger. 2018. Collapse of a desert bird community over the past century driven by climate change. Proceedings of the National Academy of Sciences 115:8597–8602.

IPCC. 2014a. Climate Change 2014: Impacts, Adaptation, and Vulnerability. Part A: Global and Sectoral Aspects. Contribution of Working Group II to the Fifth Assessment Report of the Intergovernmental Panel on Climate Change [Field, C.B., V.R. Barros, D.J. Dokken, K.J. Mach, M.D. Mastrandrea, T.E. Bilir, M. Chatterjee, K.L. Ebi, Y.O. Estrada, R.C. Genova, B. Girma, E.S. Kissel, A.N. Levy, S. MacCracken, P.R. Mastrandrea, and L.L. White (eds.)]. Cambridge University Press, Cambridge, United Kingdom and New York, NY, USA, 1132 pp. https://www.ipcc.ch/site/assets/uploads/2018/02/WGIIAR5-PartA_FINAL.pdf.

IPCC. 2014b. Climate Change 2014: Synthesis Report. Contribution of Working Groups I, II and III to the Fifth Assessment Report of the Intergovernmental Panel on Climate Change [Core Writing Team, R.K. Pachauri and L.A. Meyer (eds.)]. IPCC, Geneva, Switzerland, 151 pp.

IPCC. 2021. Climate Change 2021: The Physical Science. IPCC, Geneva, Switzerland.

Jaeger KL, JD Olden, and NA Pelland. 2014. Climate change poised to threaten hydrologic connectivity and endemic fishes in dryland streams. Proceedings of the National Academy of Sciences 111:13894–13899.

John Milner Associates I. 2005. Indian Garden, Grand Canyon National Park, Cultural Landscape Report, Contract No. 1443-C2000020300.

John Milner Associates I. 2007. Grand Canyon Village, Grand Canyon National Park, Cultural Landscape Inventory.

Jones CJR, AE Springer, BW Tobin, SJ Zappitello, NA Jones, M Parise, . . . N Ravbar. 2018. Characterization and hydraulic behaviour of the complex karst of the Kaibab Plateau and Grand Canyon National Park, USA. Page 0 Advances in Karst Research: Theory, Fieldwork and Applications. Geological Society of London.

Kasprak A, JB Sankey, D Buscombe, J Caster, AE East, and PE Grams. 2018. Quantifying and forecasting changes in the areal extent of river valley sediment in response to altered hydrology and land cover. Progress in Physical Geography: Earth and Environment 42:739–764.

Kasprak A, JB Sankey, and BJ Butterfield. 2021. Future regulated flows of the Colorado River in Grand Canyon foretell decreased areal extent of sediment and increases in riparian vegetation. Environmental Research Letters 16:014029.

Klinger R, and M Brooks. 2017. Alternative pathways to landscape transformation: invasive grasses, burn severity and fire frequency in arid ecosystems. Journal of Ecology 105:1521–1533.

La Sorte FA, and FR Thompson. 2007. Poleward Shifts in Winter Ranges of North American Birds. Ecology 88:1803–1812.

Langham GM, JG Schuetz, T Distler, CU Soykan, and C Wilsey. 2015. Conservation Status of North American Birds in the Face of Future Climate Change. PLOS ONE 10:e0135350.

Lawrence DJ, AN Runyon, JE Gross, GW Schuurman, and BW Miller. 2021. Divergent, plausible, and relevant climate futures for near- and long-term resource planning. Climatic Change 167:38.

Lehner F, C Deser, IR Simpson, and L Terray. 2018. Attributing the U.S. Southwest's Recent Shift Into Drier Conditions. Geophysical Research Letters 45:6251–6261.

Liu Y, AMO Oduor, Z Zhang, A Manea, IM Tooth, MR Leishman, . . . M van Kleunen. 2017. Do invasive alien plants benefit more from global environmental change than native plants? Global Change Biology 23:3363–3370.

Lute AC, JT Abatzoglou, and KC Hegewisch. 2015. Projected changes in snowfall extremes and interannual variability of snowfall in the western United States. Water Resources Research 51:960–972.

Mansuy N, C Miller, M-A Parisien, SA Parks, E Batllori, and MA Moritz. 2019. Contrasting human influences and macro-environmental factors on fire activity inside and outside protected areas of North America. Environmental Research Letters 14:064007.

Martinez PJ. 2012. Invasive crayfish in a high desert river: Implications of concurrent invaders and climate change. Aquatic Invasions 7:219–234.

McDowell NG, AP Williams, C Xu, WT Pockman, LT Dickman, S Sevanto, . . . C Koven. 2016. Multi-scale predictions of massive conifer mortality due to chronic temperature rise. Nature Climate Change 6:295–300.

Milly PCD, and KA Dunne. 2020. Colorado River flow dwindles as warming-driven loss of reflective snow energizes evaporation. Science 367:1252–1255.

Morgan M, M Rockman, C Smith, and A Meadow. 2016. Climate Change Impacts on Cultural Resources. Cultural Resources, Partnerships, and Science. Washington, DC: National Park Service.

NFWPCAN. 2021. National Fish, Wildlife, and Plants Climate Adaptation Network. Advancing the national fish, wildlife, and plants climate adaptation strategy into a new decade. Association of Fish and Wildlife Agencies, Washington, DC.

NPS. 2021. Planning for a Changing Climate: Climate-Smart Planning and Management in the National Park Service. National Park Service. Fort Collins, CO. Available at: https://irma.nps.gov/DataStore/Reference/Profile/2279647 (accessed 7 February 2020).

O'Donnell FC, WT Flatley, AE Springer, and PZ Fulé. 2018. Forest restoration as a strategy to mitigate climate impacts on wildfire, vegetation, and water in semiarid forests. Ecological Applications 28:1459–1472.

Paprocki N, JA Heath, and SJ Novak. 2014. Regional Distribution Shifts Help Explain Local Changes in Wintering Raptor Abundance: Implications for Interpreting Population Trends. PLOS ONE 9:e86814.

Parks SA, SZ Dobrowski, JD Shaw, and C Miller. 2019. Living on the edge: trailing edge forests at risk of fire-facilitated conversion to non-forest. Ecosphere 10:e02651.

Pascale S, LMV Carvalho, DK Adams, CL Castro, and IFA Cavalcanti. 2019. Current and Future Variations of the Monsoons of the Americas in a Warming Climate. Current Climate Change Reports 5:125–144.

Pederson JL, PA Petersen, and JL Dierker. 2006. Gullying and erosion control at archaeological sites in Grand Canyon, Arizona. Earth Surface Processes and Landforms 31:507–525.

Prein AF, GJ Holland, RM Rasmussen, MP Clark, and MR Tye. 2016. Running dry: The U.S. Southwest's drift into a drier climate state. Geophysical Research Letters 43:1272–1279.

Raffa KF, BH Aukema, BJ Bentz, AL Carroll, JA Hicke, MG Turner, and WH Romme. 2008. Cross-scale Drivers of Natural Disturbances Prone to Anthropogenic Amplification: The Dynamics of Bark Beetle Eruptions. Bioscience 58:501–517.

Renner J, and JL Day. 2022. Checklist of aquatic non-native and invasive species in lakes Mead and Mohave. BioInvasions Records 11:136–148.

Rodman KC, JE Crouse, JJ Donager, DW Huffman, and AJ Sánchez Meador. 2022. Patterns and drivers of recent land cover change on two trailing-edge forest landscapes. Forest Ecology and Management 521:120449.

Runyon AN, GW Schuurman, BW Miller, AJ Symstad, and AR Hardy. 2021. Climate change scenario planning for resource stewardship at Wind Cave National Park: Climate change scenario planning summary. Natural Resource Report. NPS/NRSS/NRR—2021/2274. National Park Service. Fort Collins, Colorado. https://doi.org/10.369.

Ryan KC, A Trinkle Jones, CL Koerner, and KM Lee (eds.) 2012. Wildland Fire in Ecosystems: Effects of Fire on Cultural Resources and Archeology. General Technical Report RMRS-GTR-42 volume 3. Fort Collins: Forest Service.

Sabbioni C, M Cassar, P Brimblecombe, and RA Lefevre. 2008. Vulnerability of cultural heritage to climate change. Strasbourg. Retrieved from https://www.coe.int/t/dg4/majorhazards/activites/2009/Ravello15-16may09/Ravello_APCAT2008_44_Sabbioni-Jan09_EN.pdf.

Sankey JB, J Kreitler, TJ Hawbaker, JL McVay, ME Miller, ER Mueller, . . . TT Sankey. 2017. Climate, wildfire, and erosion ensemble foretells more sediment in western USA watersheds. Geophysical Research Letters 44:8884–8892.

Sankey JB, BE Ralston, PE Grams, JC Schmidt, and LE Cagney. 2015. Riparian vegetation, Colorado River, and climate: Five decades of spatiotemporal dynamics in the Grand Canyon with river regulation. Journal of Geophysical Research: Biogeosciences 120:1532–1547.

Schuurman GW, DN Cole, AE Cravens, S Covington, SD Crausbay, CH Hoffman, . . . R O'Malley. 2022. Navigating Ecological Transformation: Resist–Accept–Direct as a Path to a New Resource Management Paradigm. Bioscience 72:16–29.

Sesana E, AS Gagnon, C Ciantelli, JA Cassar, and JJ Hughes. 2021. Climate change impacts on cultural heritage: A literature review. WIREs Climate Change 12:e710.

Shriver RK, CB Yackulic, DM Bell, and JB Bradford. 2022. Dry forest decline is driven by both declining recruitment and increasing mortality in response to warm, dry conditions. Global Ecology and Biogeography 31:2259–2269.

Soroye P, T Newbold, and J Kerr. 2020. Climate change contributes to widespread declines among bumble bees across continents. Science 367:685–688.

Star J, EL Rowland, ME Black, CAF Enquist, G Garfin, CHH Hoffman, . . . AM Waple. 2016. Supporting adaptation decisions through scenario planning: enabling the effective use of multiple methods. Climate Risk Management 13:88–94.

Stoddard MT, DW Huffman, PZ Fulé, JE Crouse, and AJ Sánchez Meador. 2018. Forest structure and regeneration responses 15 years after wildfire in a ponderosa pine and mixed-conifer ecotone, Arizona, USA. Fire Ecology 14:12.

Stortz SD, CE Aslan, TD Sisk, TA Chaudhry, JM Rundall, J Palumbo, . . . B Dickson. 2018. Natural resource condition assessment: Greater Grand Canyon landscape assessment. Natural Resource Report NPS/GRCA/NRR—2018/1645. National Park Service, Fort Collins, Colorado.

Taylor KE, RJ Stouffer, and GA Meehl. 2012. An overview of CMIP5 and the experiment design. Bulletin of the American Meteorological Society 93:485–498.

Tercek MT, D Thoma, JE Gross, K Sherrill, S Kagone, and G Senay. 2021. Historical changes in plant water use and need in the continental United States. PLOS ONE 16:e0256586.

Theoharides KA, and JS Dukes. 2007. Plant invasion across space and time: factors affecting nonindigenous species success during four stages of invasion. New Phytologist 176:256–273.

Thoma DP, MT Tercek, EW Schweiger, SM Munson, JE Gross, and ST Olliff. 2020. Water balance as an indicator of natural resource condition: Case studies from Great Sand Dunes National Park and Preserve. Global Ecology and Conservation 24.

Tillman FD, S Gangopadhyay, and T Pruitt. 2020. Recent and projected precipitation and temperature changes in the Grand Canyon area with implications for groundwater resources. Sci Rep 10:19740.

Tobin BW, AE Springer, DK Kreamer, and E Schenk. 2018. Review: The distribution, flow, and quality of Grand Canyon Springs, Arizona (USA). Hydrogeology Journal 26:721–732.

Udall B, and J Overpeck. 2017. The twenty-first century Colorado River hot drought and implications for the future. Water Resources Research 53:2404–2418.

van Mantgem PJ, NL Stephenson, JC Byrne, LD Daniels, JF Franklin, PZ Fulé, . . . TT Veblen. 2009. Widespread Increase of Tree Mortality Rates in the Western United States. Science 323:521–524.

van Riper iii C, JR Hatten, JT Giermakowski, D Mattson, JA Holmes, MJ Johnson, . . . CR Schwalbe. 2014. Projecting climate effects on birds and reptiles of the Southwestern United States. Open-File Report, Reston, VA.

Vankat JL. 2017. Post-1935 changes in Pinyon-Juniper persistent woodland on the South Rim of Grand Canyon National Park, Arizona, USA. Forest Ecology and Management 394:73–85.

Vano JA, B Udall, DR Cayan, JT Overpeck, LD Brekke, T Das, . . . DP Lettenmaier. 2014. Understanding Uncertainties in Future Colorado River Streamflow. Bulletin of the American Meteorological Society 95:59–78.

Vicente-Serrano SM, S Beguería, and JI López-Moreno. 2010. A Multiscalar Drought Index Sensitive to Global Warming: The Standardized Precipitation Evapotranspiration Index. Journal of Climate 23:1696–1718.

Vose RS, S Applequist, M Squires, I Durre, MJ Menne, CNJ Williams, . . . D Arndt. 2014. NOAA Monthly U.S. Climate Gridded Dataset (NClimGrid), Version 1. NOAA National Centers for Environmental Information. DOI:10.7289/V5SX6B56. Accessed September 1, 2021.

Wheeler KG, B Udall, J Wang, E Kuhn, H Salehabadi, and JC Schmidt. 2022. What will it take to stabilize the Colorado River? Science 377:373–375.

Williams AP, ER Cook, JE Smerdon, BI Cook, JT Abatzoglou, K Bolles, . . . B Livneh. 2020. Large contribution from anthropogenic warming to an emerging North American megadrought. Science 368:314–318.

Woodhouse CA, and GT Pederson. 2018. Investigating Runoff Efficiency in Upper Colorado River Streamflow Over Past Centuries. Water Resources Research 54:286–300.

Wu JX, CB Wilsey, L Taylor, and GW Schuurman. 2018. Projected avifaunal responses to climate change across the U.S. National Park System. PLOS ONE 13:e0190557.

Xiao M, B Udall, and DP Lettenmaier. 2018. On the Causes of Declining Colorado River Streamflows. Water Resources Research 54:6739–6756.

Appendix A

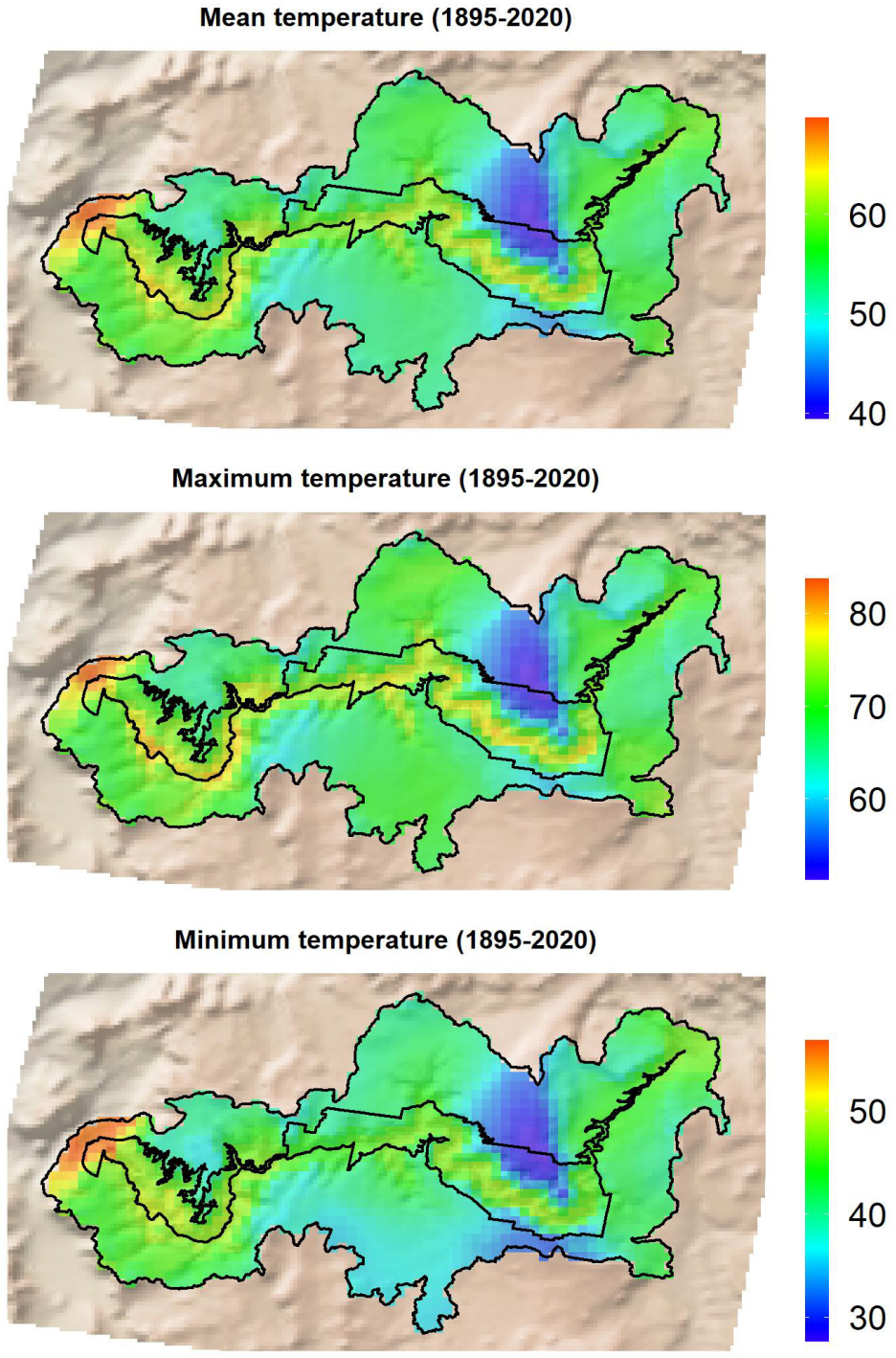

Figure A1. Average annual mean, maximum, and minimum temperature (°F) in 5 km-by-5 km cells from 1895–2020 across the GGCL. Data is derived from the NOAA nClimGrid data set.

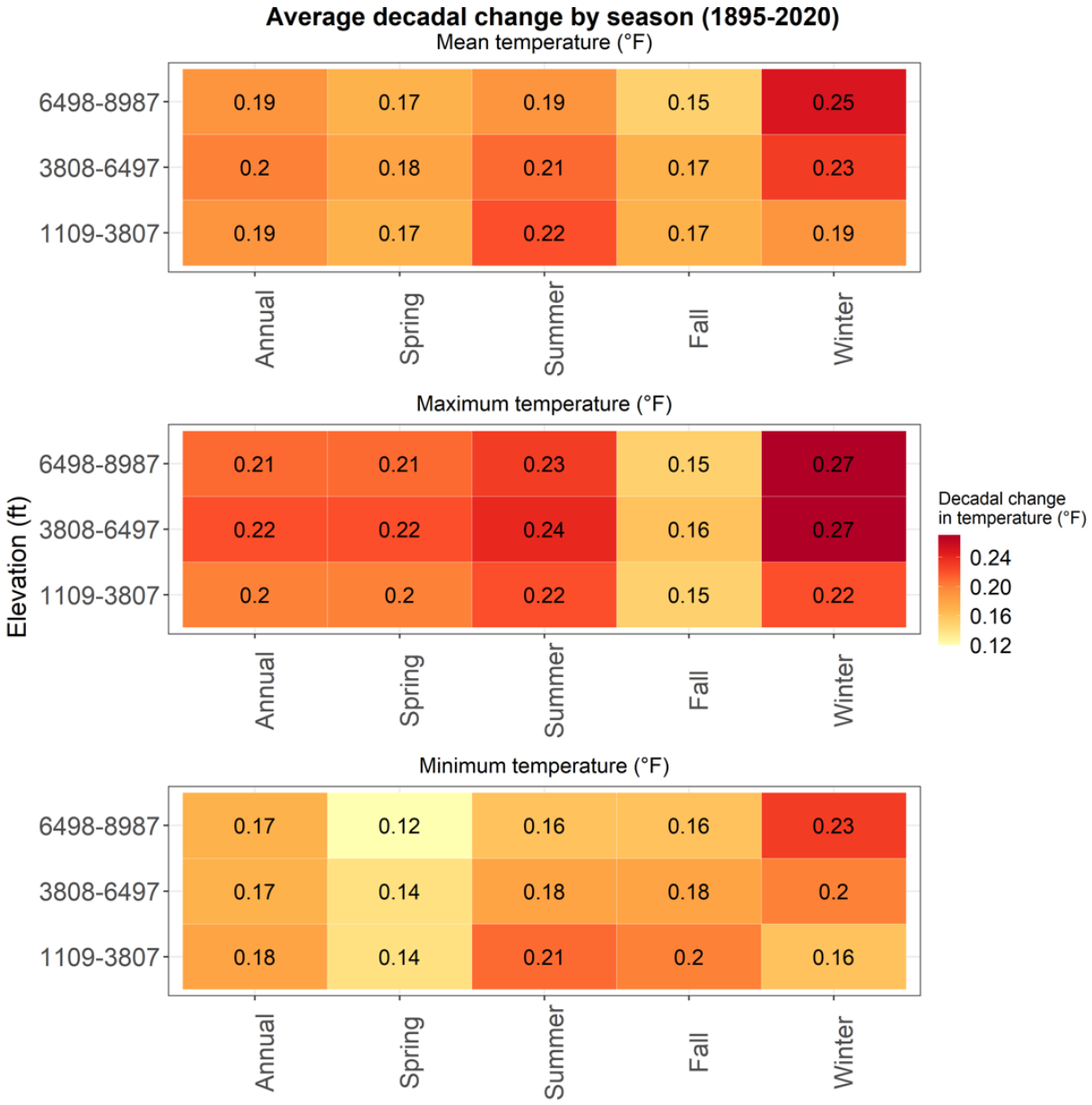

Figure A2. Average warming per decade in mean (top), maximum (middle), and minimum (bottom) temperature (°F) from 1895–2020 across the GGCL, by season. Derived from the NOAA nClimGrid dataset (Vose et al., 2014). Table B1 is a more accessible version of this information presented in a format that is designed specifically to be read by screen-reading software.

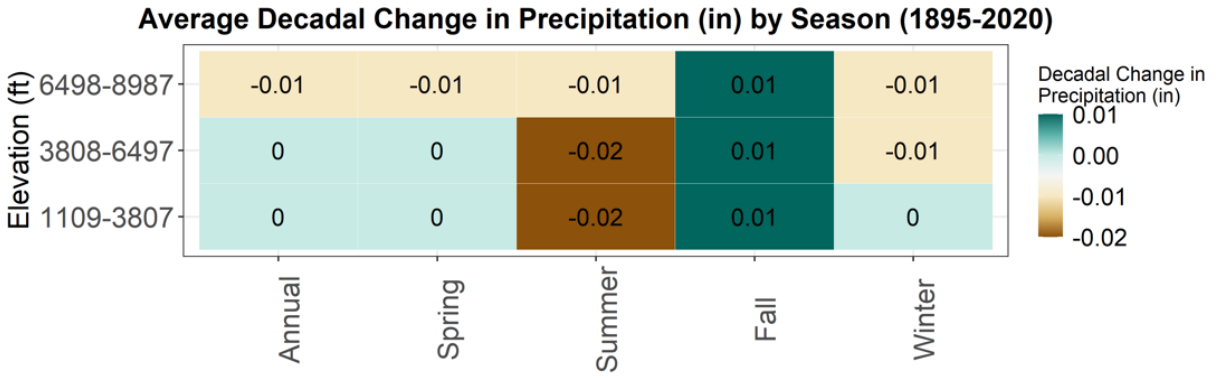

Figure A3. Average change per decade in precipitation (inches) from 1895–2020 by season across the GGCL. Data are derived from the NOAA nClimGrid dataset. Table B2 is a more accessible version of this information presented in a format that is designed specifically to be read by screen-reading software.

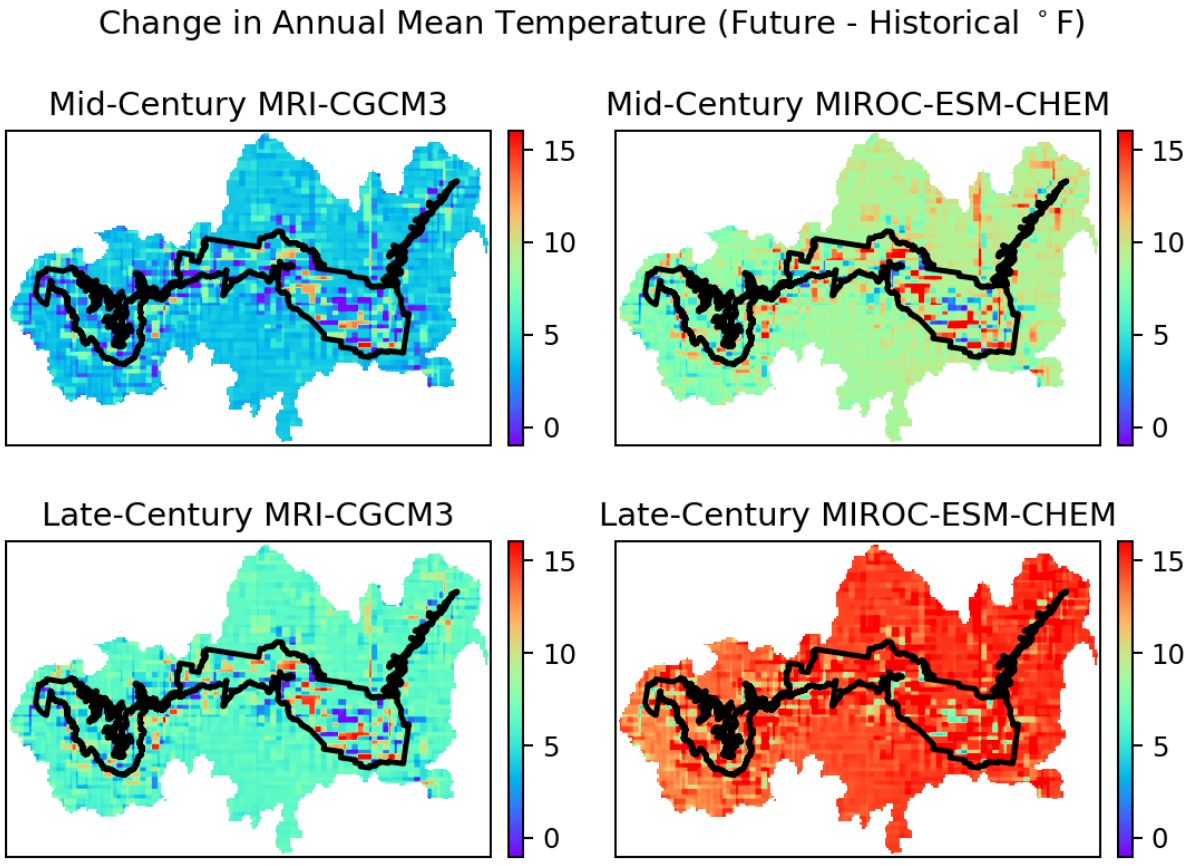

Figure A4. Change in annual mean temperature for mid-(2055) and late-century (2085) MRI and MIROC climate futures relative to the historical period (1981–2010) across the GGCL.

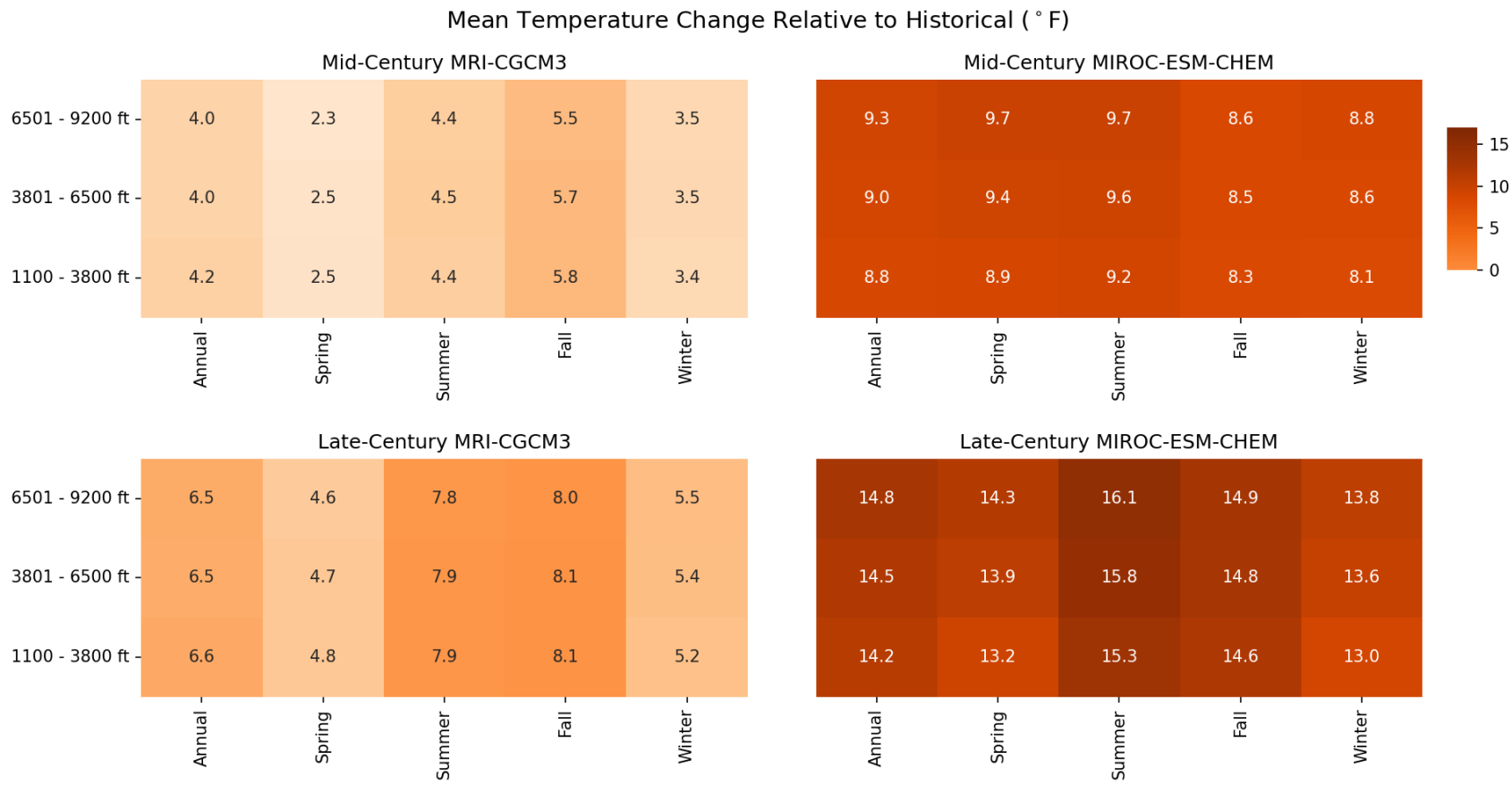

Figure A5. Mean temperature change for mid-(2055) and late-century (2085) MRI and MIROC climate futures relative to historical temperatures (1981–2010) at low, medium, and high elevations of the GGCL, annually and divided into seasons (spring, summer, fall, winter). Table B3 is a more accessible version of this information presented in a format that is designed specifically to be read by screen-reading software.

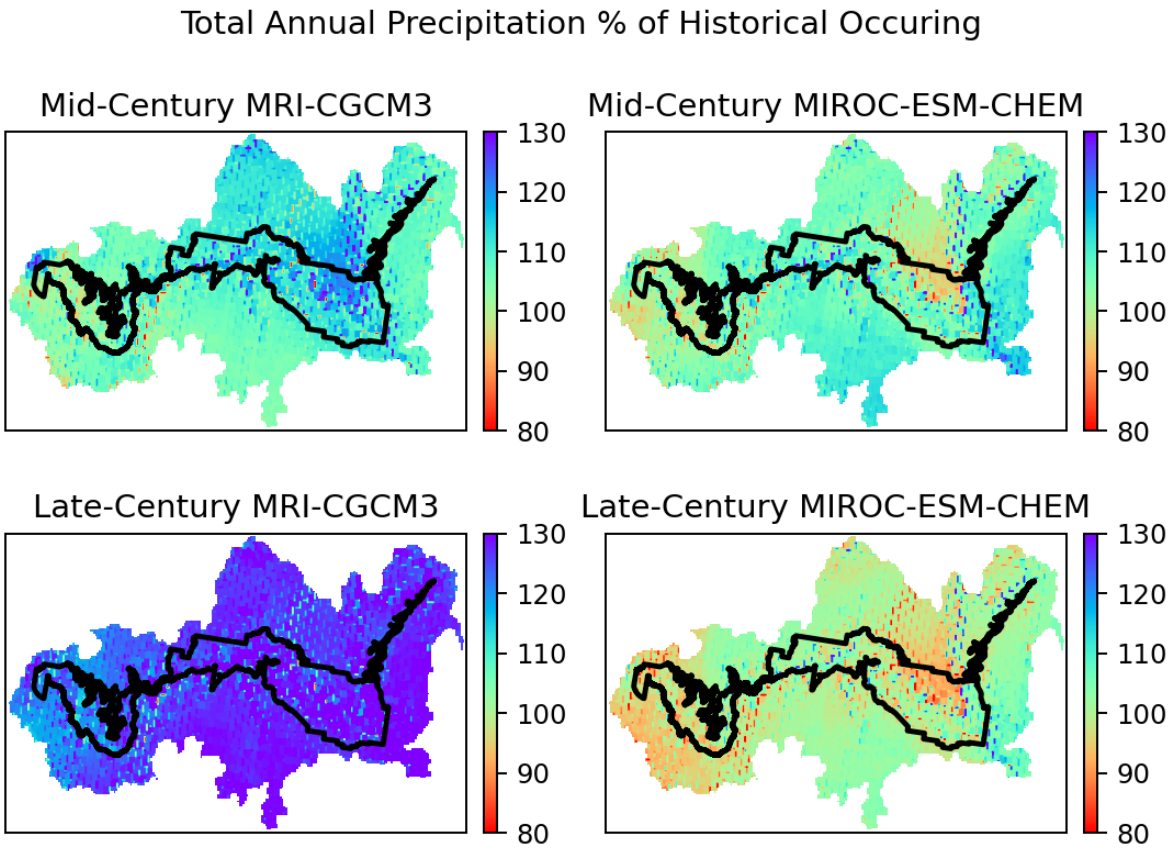

Figure A6. Change in total annual precipitation for mid-(2055) and late-century (2085) MRI and MIROC climate futures relative to the historical period (1981–2010) across the GGCL.

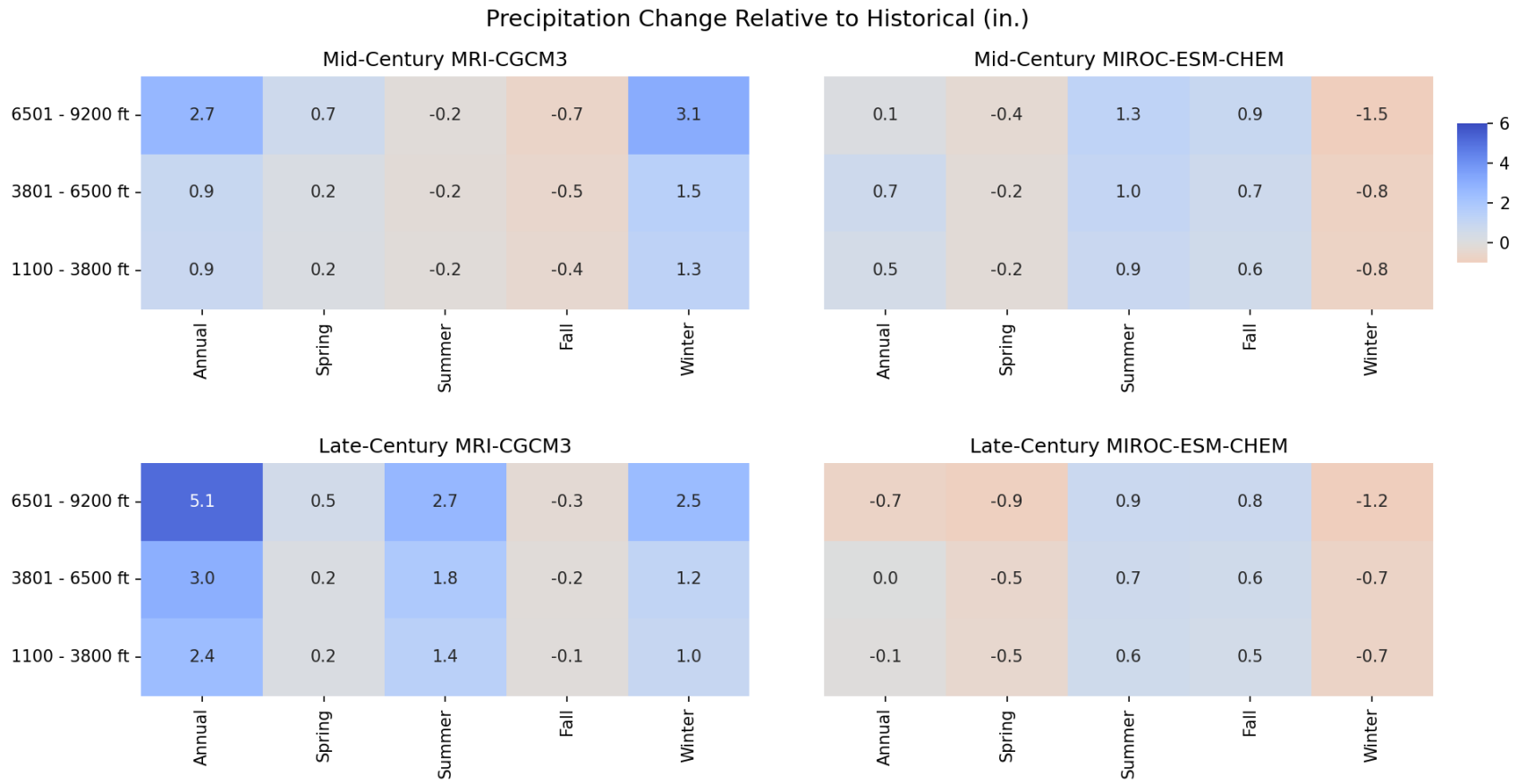

Figure A7. Precipitation change (inches) for mid-(2055) and late-century (2085) under MRI and MIROC climate futures relative to historical precipitation (1981–2010) at low, medium, and high elevations of the GGCL, annually and divided into seasons (spring, summer, fall, winter). Table B4 is a more accessible version of this information presented in a format that is designed specifically to be read by screen-reading software.

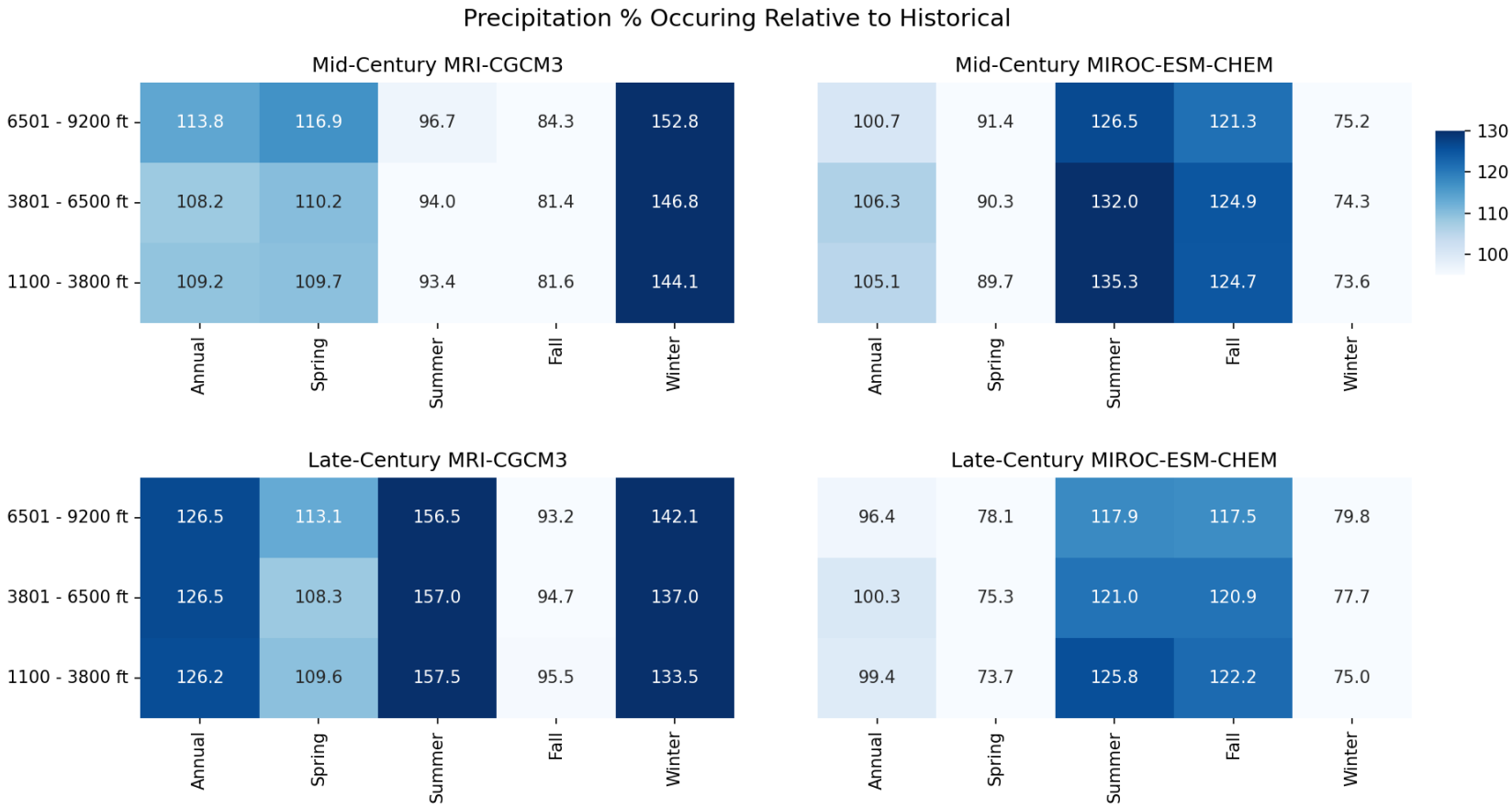

Figure A8. Percent of historical (1981–2010) average total annual precipitation under mid- and late-century MRI and MIROC climate futures at low, medium, and high elevations of the GGCL, annually and divided into seasons (spring, summer, fall, winter). Table B5 is a more accessible version of this information presented in a format that is designed specifically to be read by screen-reading software.

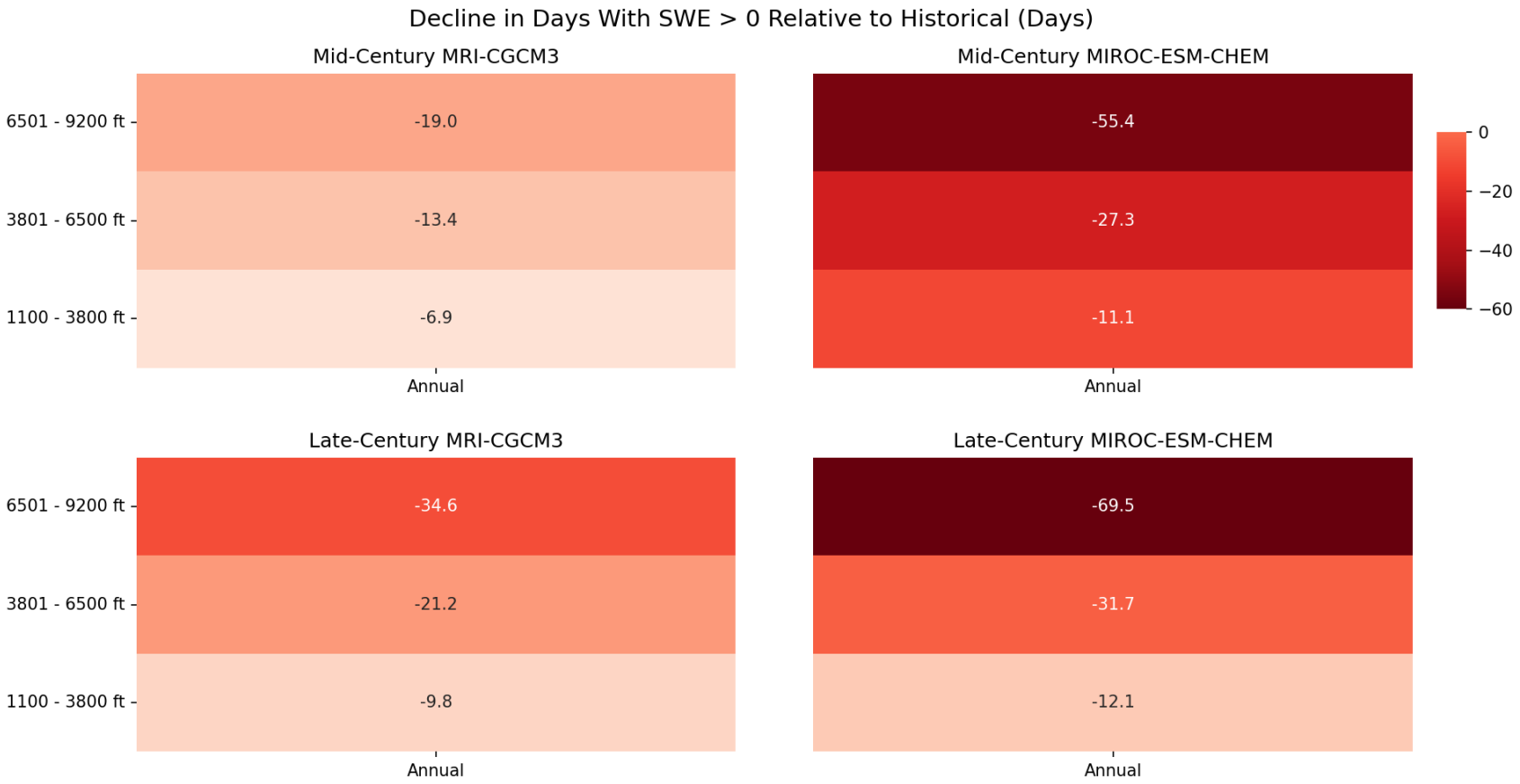

Figure A9. Declines in the number of days with snow water equivalent greater than 0 relative to the historical period during the mid- and late-century for the MRI and MIROC climate futures at low, medium, and high elevations of the GGCL. Historically elevations received the following snow water equivalent greater than 0 totals: 6501–9200 ft – 77.7 days; 3801–6500 ft – 33.1 days; 1100–3800 ft – 12.3 days. Table B6 is a more accessible version of this information presented in a format that is designed specifically to be read by screen-reading software.

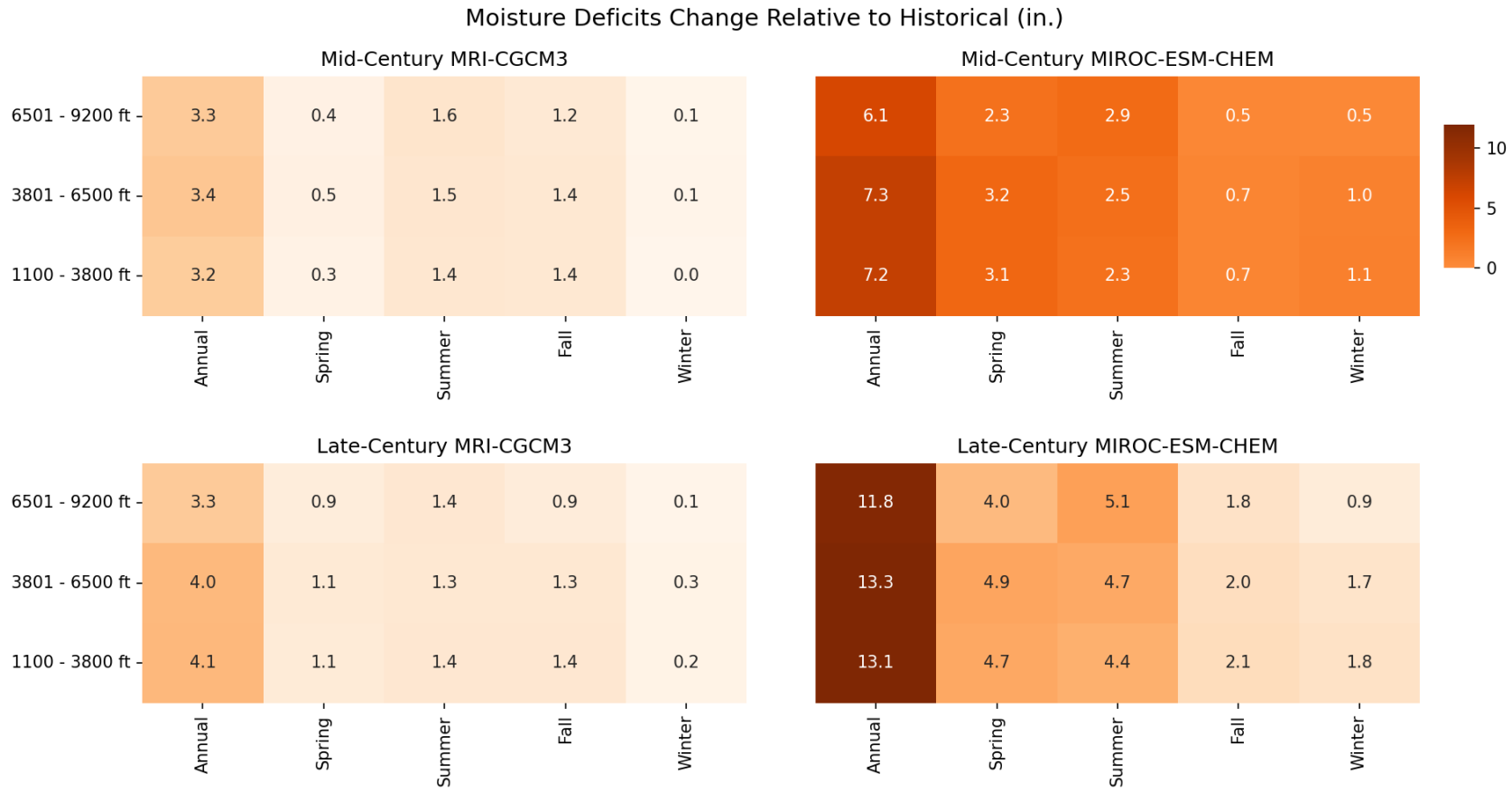

Figure A10. Absolute change in moisture deficit relative to historical deficit annually and seasonally for the GGCL at low, medium, and high elevations during the mid- and late-century for the MRI and MIROC climate futures. Table B7 is a more accessible version of this information presented in a format that is designed specifically to be read by screen-reading software.

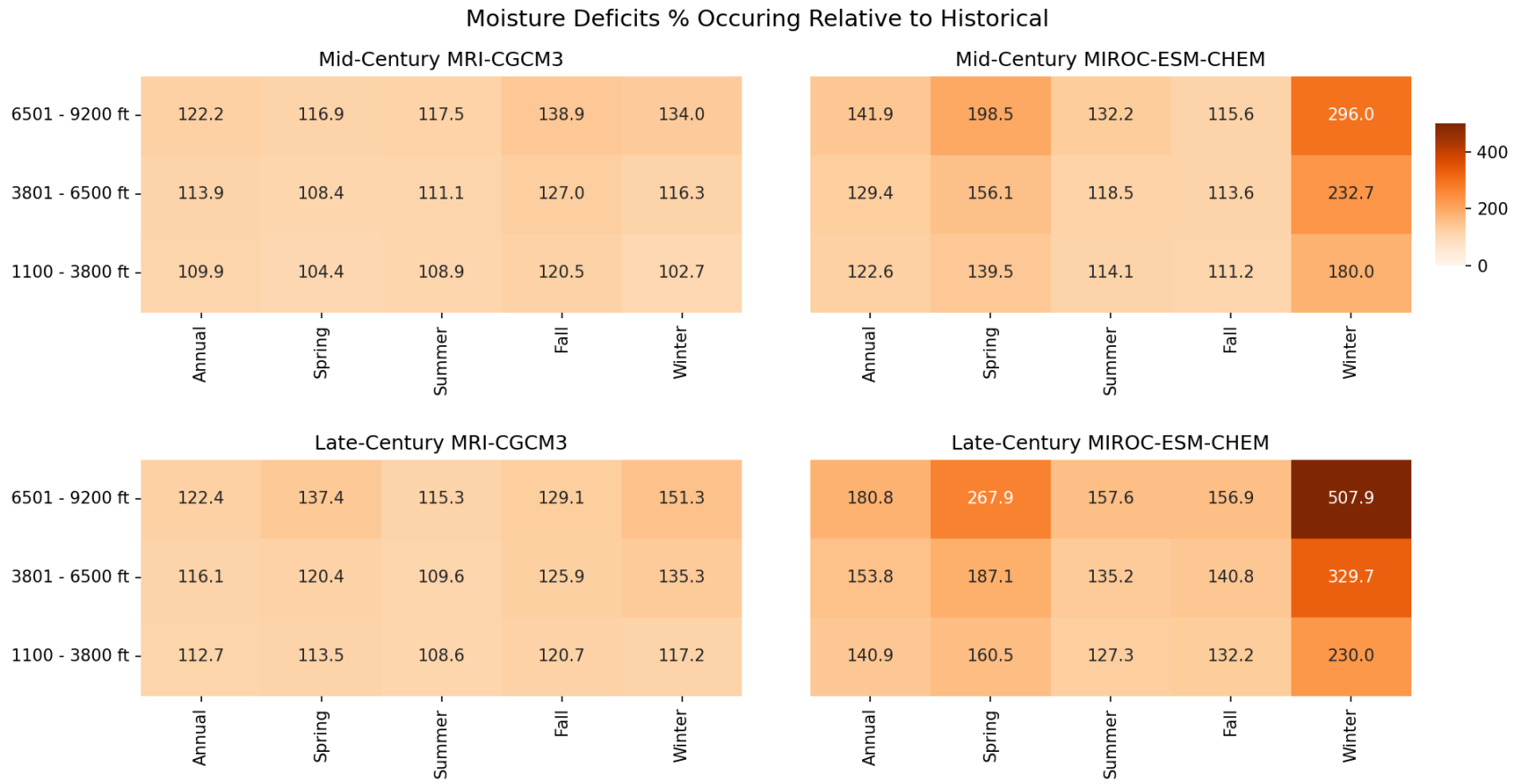

Figure A11. Percent of the historical moisture deficit (1981–2010) annually and seasonally for the GGCL at low, medium, and high elevations during the mid- and late-century for the MRI and MIROC climate futures. Table B8 is a more accessible version of this information presented in a format that is designed specifically to be read by screen-reading software.

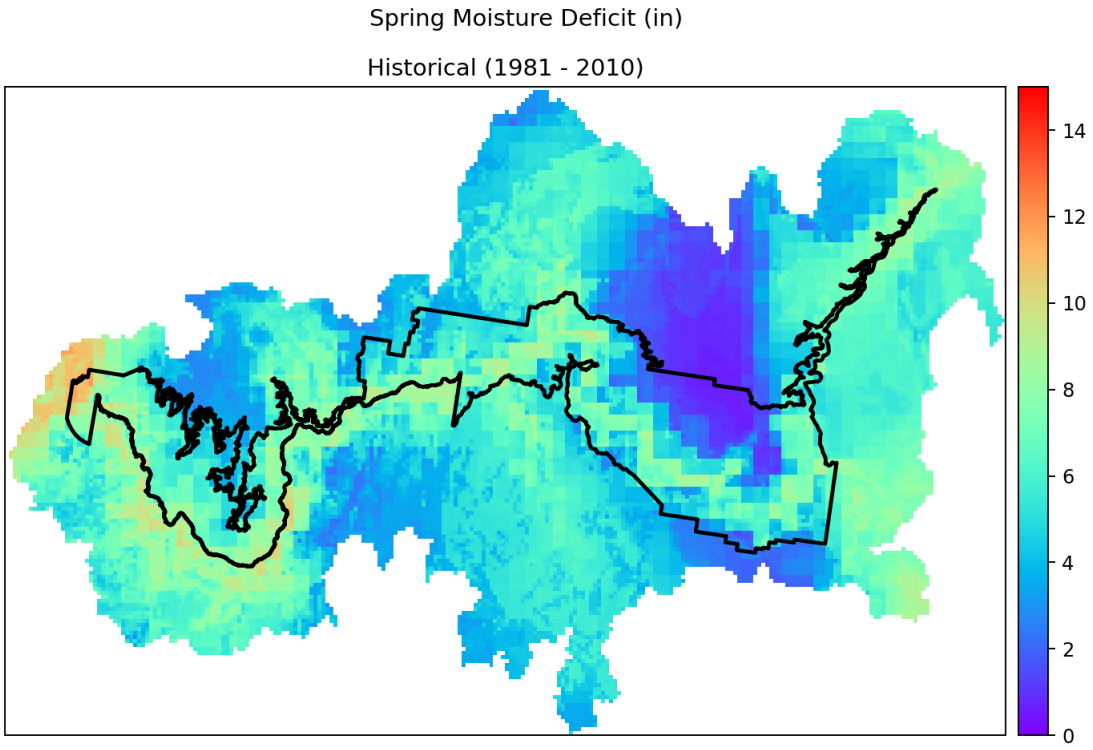

Figure A12. Historical spring moisture deficit (inches) for the GGCL. Deficit (PET-AET), indicates the amount of additional water plants would use if it were available, and provides a measure of landscape dryness.

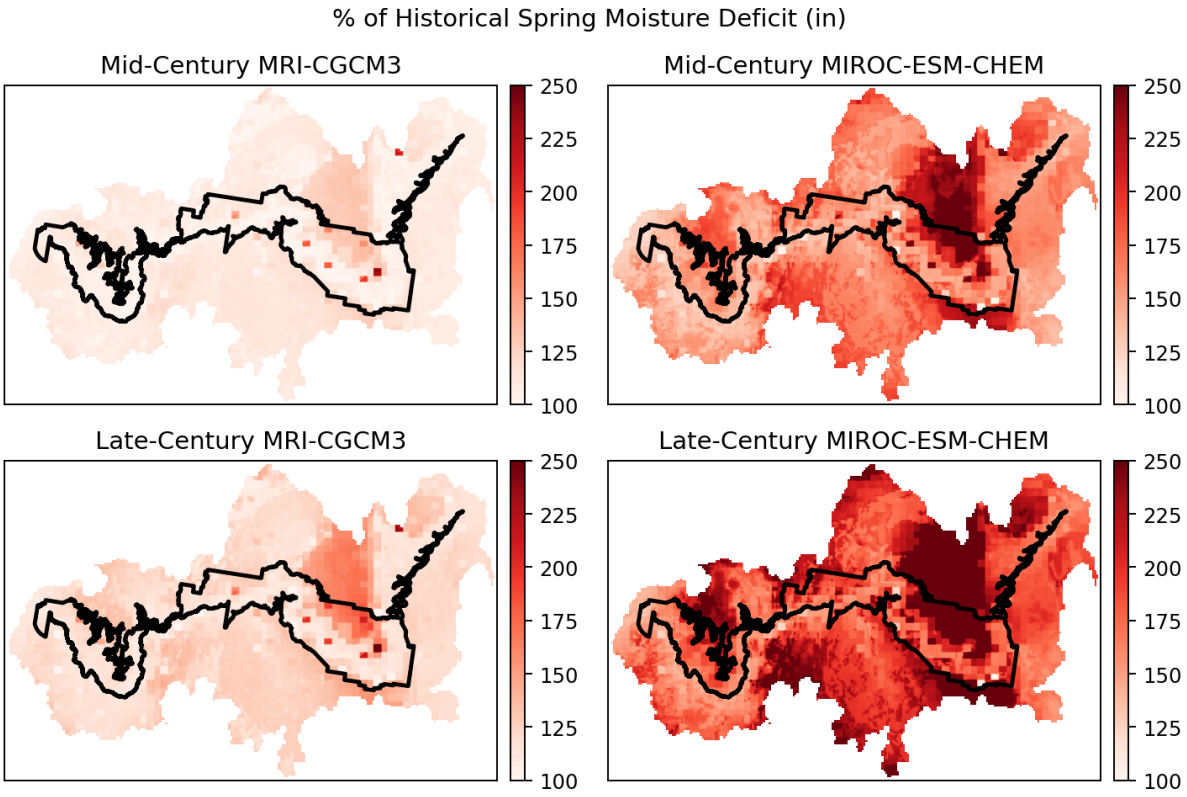

Figure A13. Percent of historical spring moisture deficit (1981–2010) for the GGCL during the mid- and late-century for the MRI and MIROC climate futures. Deficit (PET-AET), indicates the amount of additional water plants would use if it were available, and provides a measure of landscape dryness.

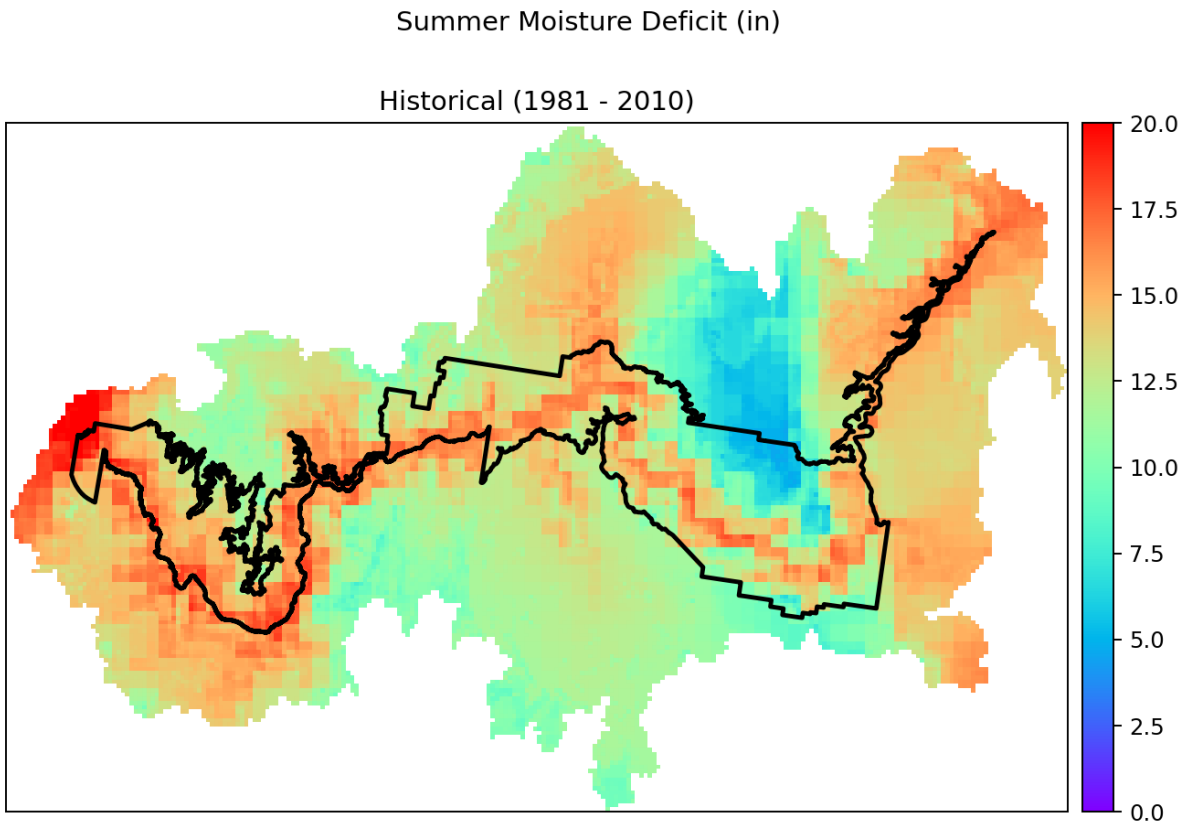

Figure A14. Historical summer moisture deficit (inches) for the GGCL. Deficit (PET-AET), indicates the amount of additional water plants would use if it were available, and provides a measure of landscape dryness.

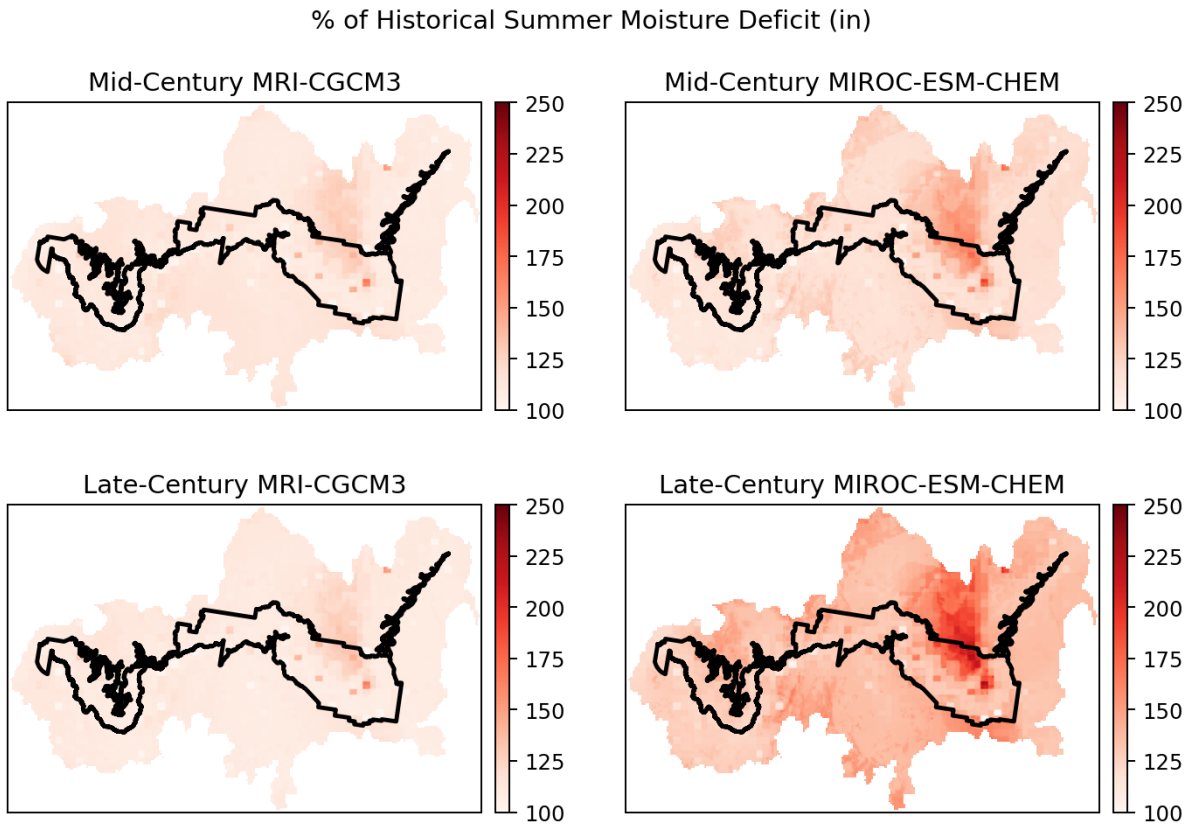

Figure A15. Percent of historical summer moisture deficit (1981–2010) for the GGCL during the mid- and late-century for the MRI and MIROC climate futures. Deficit (PET-AET), indicates the amount of additional water plants would use if it were available, and provides a measure of landscape dryness.

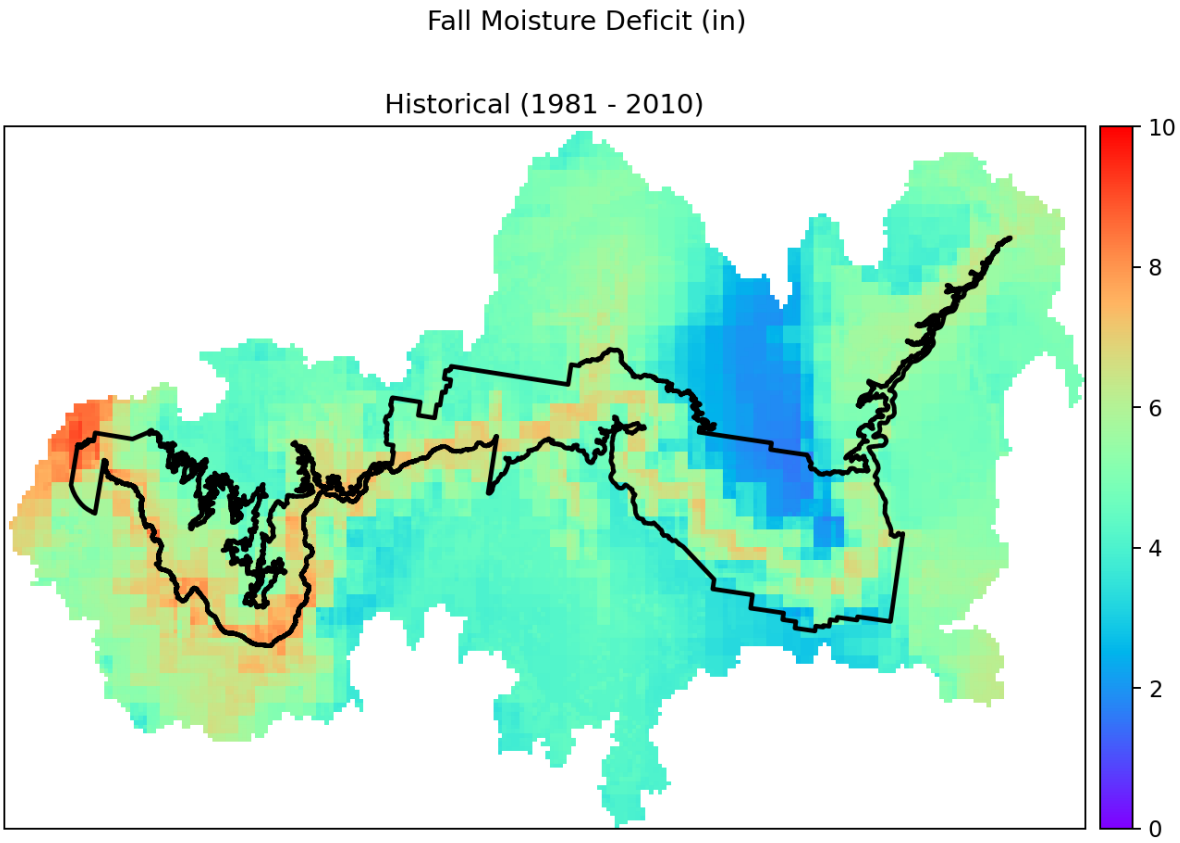

Figure A16. Historical fall moisture deficit (inches) for the GGCL. Deficit (PET-AET), indicates the amount of additional water plants would use if it were available, and provides a measure of landscape dryness.

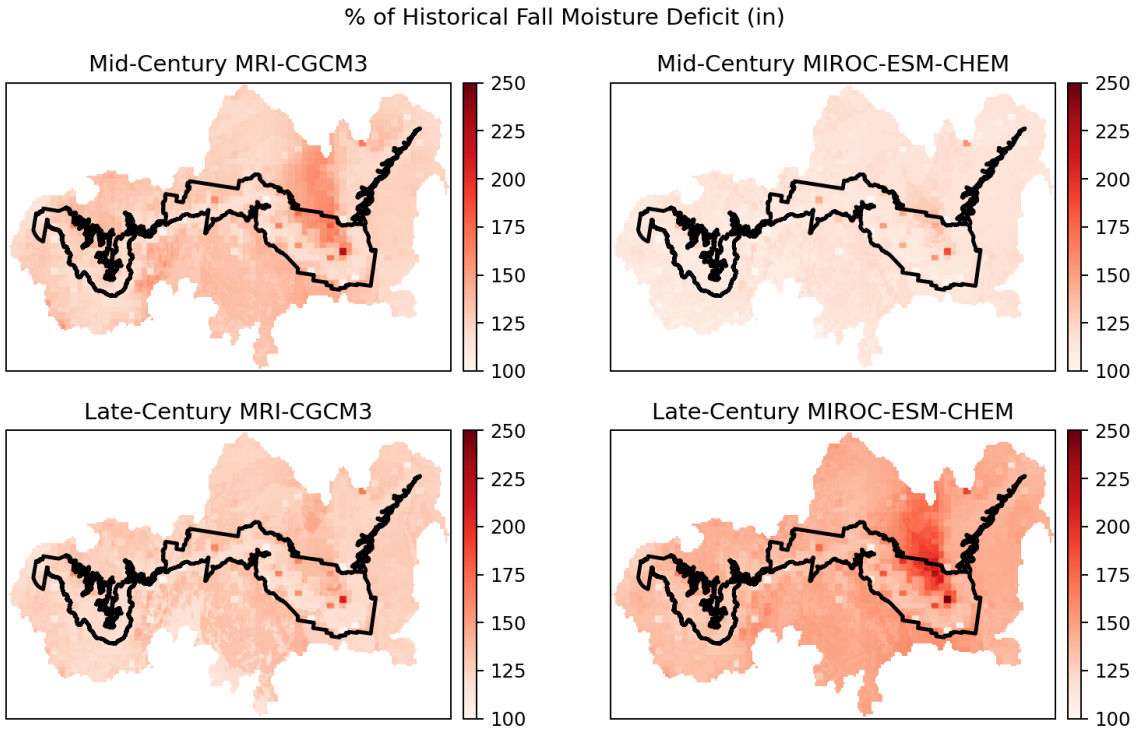

Figure A17. Percent of historical fall moisture deficit (1981–2010) for the GGCL during the mid- and late-century for the MRI and MIROC climate futures. Deficit (PET-AET), indicates the amount of additional water plants would use if it were available, and provides a measure of landscape dryness.

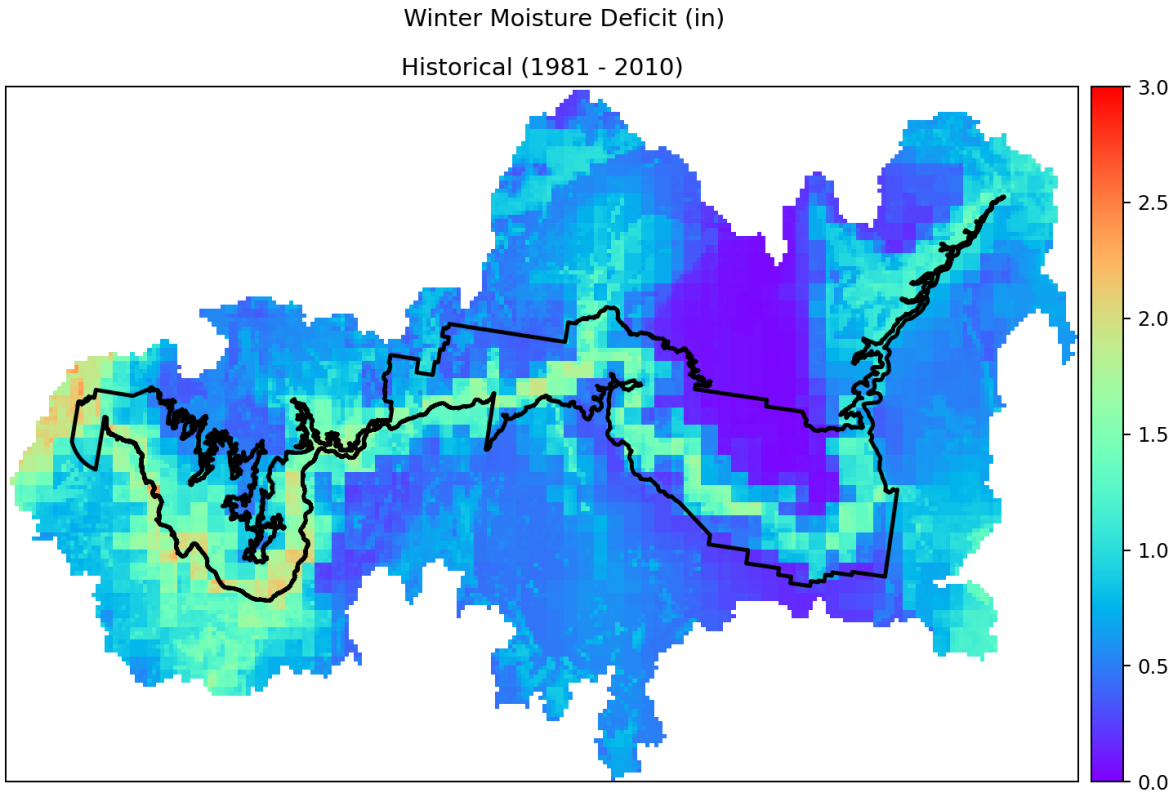

Figure A18. Historical winter moisture deficit (inches) for the GGCL. Deficit (PET-AET), indicates the amount of additional water plants would use if it were available, and provides a measure of landscape dryness.

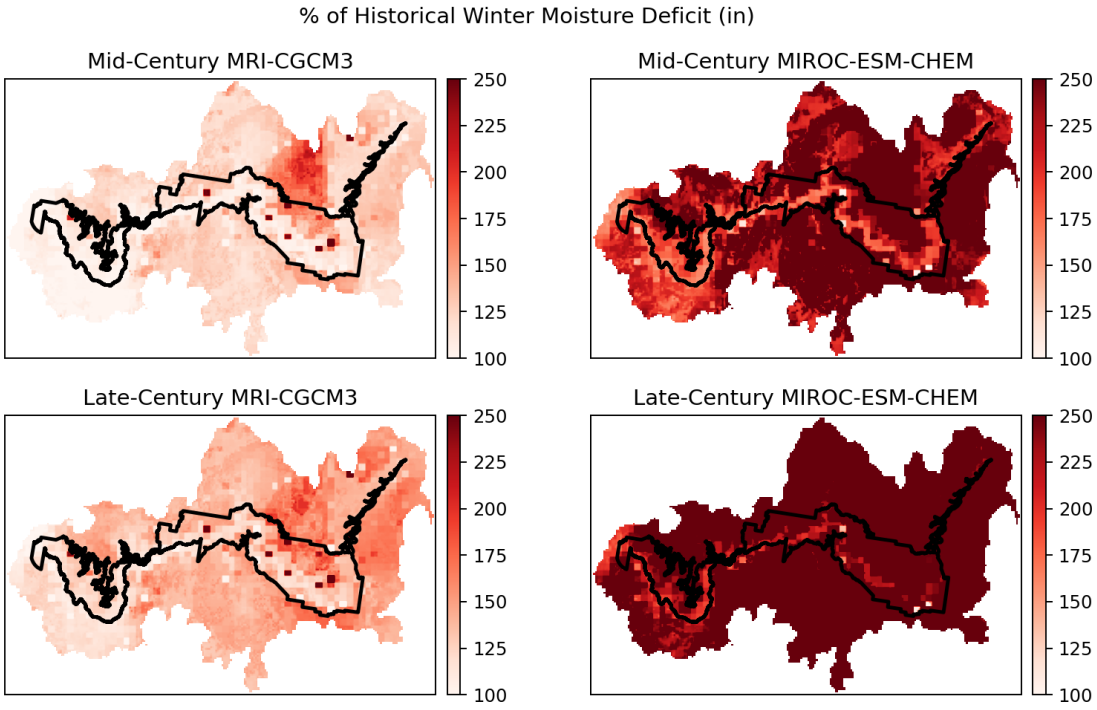

Figure A19. Percent of historical winter moisture deficit (1981–2010) for the GGCL during the mid- and late-century for the MRI and MIROC climate futures. Deficit (PET-AET), indicates the amount of additional water plants would use if it were available, and provides a measure of landscape dryness.

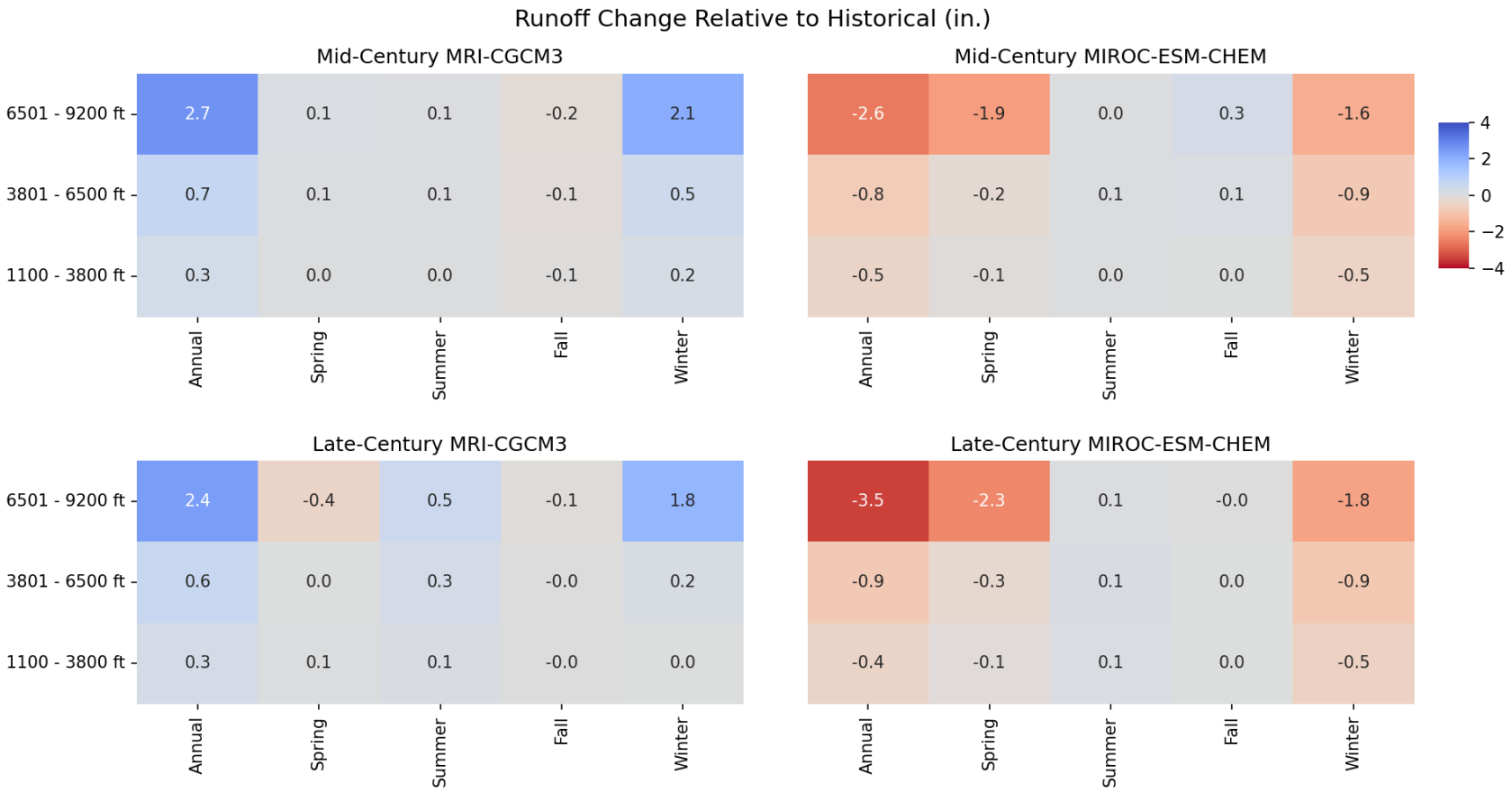

Figure A20. Change in runoff relative to historical runoff annually and seasonally for the GGCL at low, medium, and high elevations during the mid- and late-century for the MRI and MIROC climate futures. Table B9 is a more accessible version of this information presented in a format that is designed specifically to be read by screen-reading software.

Appendix B

Table B1. This table presents Figure A2 information in an accessible tabular format that can be read by screen-reading software. Average warming per decade in mean, maximum, and minimum temperature (°F) from 1895–2020 across the GGCL, by season. Derived from the NOAA nClimGrid dataset (Vose et al., 2014).

Temperature	Elevation level (ft)	Annual decadal temperature change (F)	Spring decadal temperature change (F)	Summer decadal temperature change (F)	Fall decadal temperature change (F)	Winter decadal temperature change (F)
Mean	6501–9200	0.19	0.17	0.19	0.15	0.25
	3801–6500	0.2	0.18	0.21	0.17	0.23
	1100–3800	0.19	0.17	0.22	0.17	0.19
Maximum	6501–9200	0.21	0.21	0.23	0.15	0.27
	3801–6500	0.22	0.22	0.24	0.16	0.27
	1100–3800	0.2	0.2	0.22	0.15	0.22
Minimum	6501–9200	0.17	0.12	0.16	0.16	0.23
	3801–6500	0.17	0.14	0.18	0.18	0.2
	1100–3800	0.18	0.14	0.21	0.2	0.16

Table B2. This table presents Figure A3 information in an accessible tabular format that can be read by screen-reading software. Average change per decade in precipitation (inches) from 1895–2020 by season across the GGCL. Data are derived from the NOAA nClimGrid dataset.

Elevation level (ft)	Annual decadal temperature change (F)	Spring decadal temperature change (F)	Summer decadal temperature change (F)	Fall decadal temperature change (F)	Winter decadal temperature change (F)
6501–9200	−0.01	−0.01	−0.01	0.01	−0.01
3801–6500	0	0	−0.02	0.01	−0.01
1100–3800	0	0	−0.02	0.01	0

Table B3. This table presents Figure A5 information in an accessible tabular format that can be read by screen-reading software. Mean temperature change for mid-(2055) and late-century (2085) MRI and MIROC climate futures relative to historical temperatures (1981–2010) at low, medium, and high elevations of the GGCL, annually and divided into seasons (spring, summer, fall, winter).

Time period	Global climate model	Elevation level (ft)	Annual mean temperature change relative to historical (F)	Spring mean temperature change relative to historical (F)	Summer mean temperature change relative to historical (F)	Fall mean temperature change relative to historical (F)	Winter mean temperature change relative to historical (F)
Mid-century	MRI-CGCM3	6501–9200	4.0	2.3	4.4	5.5	3.5
	MRI-CGCM3	3801–6500	4.0	2.5	4.5	5.7	3.5
	MRI-CGCM3	1100–3800	4.2	2.5	4.4	5.8	3.4
	MIROC-ESM-CHEM	6501–9200	9.3	9.7	9.7	8.6	8.8
	MIROC-ESM-CHEM	3801–6500	9.0	9.4	9.6	8.5	8.6
	MIROC-ESM-CHEM	1100–3800	8.8	8.9	9.2	8.3	8.1
Late-century	MRI-CGCM3	6501–9200	6.5	4.6	7.8	8.0	5.5
	MRI-CGCM3	3801–6500	6.5	4.7	7.9	8.1	5.4
	MRI-CGCM3	1100–3800	6.6	4.8	7.9	8.1	5.2
	MIROC-ESM-CHEM	6501–9200	14.8	14.3	16.1	14.9	13.8
	MIROC-ESM-CHEM	3801–6500	14.5	13.9	15.8	14.8	13.6
	MIROC-ESM-CHEM	1100–3800	14.2	13.2	15.3	14.6	13.0

Table B4. This table presents Figure A7 information in an accessible tabular format that can be read by screen-reading software. Precipitation change (inches) for mid-(2055) and late-century (2085) under MRI and MIROC climate futures relative to historical precipitation (1981–2010) at low, medium, and high elevations of the GGCL, annually and divided into seasons (spring, summer, fall, winter).

Time period	Global climate model	Elevation level (ft)	Annual mean precipitation change relative to historical (in)	Spring mean precipitation change relative to historical (in)	Summer mean precipitation change relative to historical (in)	Fall mean precipitation change relative to historical (in)	Winter mean precipitation change relative to historical (in)
Mid-century	MRI-CGCM3	6501–9200	2.7	0.7	−0.2	−0.7	3.1
	MRI-CGCM3	3801–6500	0.9	0.2	−0.2	−0.5	1.5
	MRI-CGCM3	1100–3800	0.9	0.2	−0.2	−0.4	1.3
	MIROC-ESM-CHEM	6501–9200	0.1	−0.4	1.3	0.9	−1.5
	MIROC-ESM-CHEM	3801–6500	0.7	−0.2	1.0	0.7	−0.8
	MIROC-ESM-CHEM	1100–3800	0.5	−0.2	0.9	0.6	−0.8
Late-century	MRI-CGCM3	6501–9200	5.1	0.5	2.7	−0.3	2.5
	MRI-CGCM3	3801–6500	3.0	0.2	1.8	−0.2	1.2
	MRI-CGCM3	1100–3800	2.4	0.2	1.4	−0.1	1.0
	MIROC-ESM-CHEM	6501–9200	−0.7	−0.9	0.9	0.8	−1.2
	MIROC-ESM-CHEM	3801–6500	0.0	−0.5	0.7	0.6	−0.7
	MIROC-ESM-CHEM	1100–3800	−0.1	−0.5	0.6	0.5	−0.7

Table B5. This table presents Figure A8 information in an accessible tabular format that can be read by screen-reading software. Percent of historical (1981–2010) average total annual precipitation under mid- and late-century MRI and MIROC climate futures at low, medium, and high elevations of the GGCL, annually and divided into seasons (spring, summer, fall, winter).

Time period	Global climate model	Elevation level (ft)	Annual mean precipitation percent relative to historical	Spring mean precipitation percent relative to historical	Summer mean precipitation percent relative to historical	Fall mean precipitation percent relative to historical	Winter mean precipitation percent relative to historical
Mid-century	MRI-CGCM3	6501–9200	113.8	116.9	96.7	84.3	152.8
	MRI-CGCM3	3801–6500	108.2	110.2	94.0	81.4	146.8
	MRI-CGCM3	1100–3800	109.2	109.7	93.4	81.6	144.1
	MIROC-ESM-CHEM	6501–9200	100.7	91.4	126.5	121.3	75.2
	MIROC-ESM-CHEM	3801–6500	106.3	90.3	132.0	124.9	74.3
	MIROC-ESM-CHEM	1100–3800	105.1	89.7	135.3	124.7	73.6
Late-century	MRI-CGCM3	6501–9200	126.5	113.1	156.5	93.2	142.1
	MRI-CGCM3	3801–6500	126.5	108.3	157.0	94.7	137.0
	MRI-CGCM3	1100–3800	126.2	109.6	157.5	95.5	133.5
	MIROC-ESM-CHEM	6501–9200	96.4	78.1	117.9	117.5	79.8
	MIROC-ESM-CHEM	3801–6500	100.3	75.3	121.0	120.9	77.7
	MIROC-ESM-CHEM	1100–3800	99.4	73.7	125.8	122.2	75.0

Table B6. This table presents Figure A9 information in an accessible tabular format that can be read by screen-reading software. Declines in the number of days with snow water equivalent greater than 0 relative to the historical period during the mid- and late-century for the MRI and MIROC climate futures at low, medium, and high elevations of the GGCL. Historically elevations received the following snow water equivalent greater than 0 totals: 6501–9200 ft – 77.7 days; 3801–6500 ft – 33.1 days; 1100–3800 ft – 12.3 days.

Time period	Global climate model	Elevation level (ft)	Annual mean decline in days with SWE > 0 relative to historical
Mid-century	MRI-CGCM3	6501–9200	−19.0
	MRI-CGCM3	3801–6500	−13.4
	MRI-CGCM3	1100–3800	−6.9
	MIROC-ESM-CHEM	6501–9200	−55.4
	MIROC-ESM-CHEM	3801–6500	−27.3
	MIROC-ESM-CHEM	1100–3800	−11.1
Late-century	MRI-CGCM3	6501–9200	−34.6
	MRI-CGCM3	3801–6500	−21.2
	MRI-CGCM3	1100–3800	−9.8
	MIROC-ESM-CHEM	6501–9200	−69.5
	MIROC-ESM-CHEM	3801–6500	−31.7
	MIROC-ESM-CHEM	1100–3800	−12.1

Table B7. This table presents Figure A10 information in an accessible tabular format that can be read by screen-reading software. Absolute change in moisture deficit relative to historical deficit annually and seasonally for the GGCL at low, medium, and high elevations during the mid- and late-century for the MRI and MIROC climate futures.

Time period	Global climate model	Elevation level (ft)	Annual mean moisture deficits change relative to historical (in)	Spring mean moisture deficits change relative to historical (in)	Summer mean moisture deficits change relative to historical (in)	Fall mean moisture deficits change relative to historical (in)	Winter mean moisture deficits change relative to historical (in)
Mid-century	MRI-CGCM3	6501–9200	3.3	0.4	1.6	1.2	0.1
	MRI-CGCM3	3801–6500	3.4	0.5	1.5	1.4	0.1
	MRI-CGCM3	1100–3800	3.2	0.3	1.4	1.4	0.0
	MIROC-ESM-CHEM	6501–9200	6.1	2.3	2.9	0.5	0.5
	MIROC-ESM-CHEM	3801–6500	7.3	3.2	2.5	0.7	1.0
	MIROC-ESM-CHEM	1100–3800	7.2	3.1	2.3	0.7	1.1
Late-century	MRI-CGCM3	6501–9200	3.3	0.9	1.4	0.9	0.1
	MRI-CGCM3	3801–6500	4.0	1.1	1.3	1.3	0.3
	MRI-CGCM3	1100–3800	4.1	1.1	1.4	1.4	0.2
	MIROC-ESM-CHEM	6501–9200	11.8	4.0	5.1	1.8	0.9
	MIROC-ESM-CHEM	3801–6500	13.3	4.9	4.7	2.0	1.7
	MIROC-ESM-CHEM	1100–3800	13.1	4.7	4.4	2.1	1.8

Table B8. This table presents Figure A11 information in an accessible tabular format that can be read by screen-reading software. Percent of the historical moisture deficit (1981–2010) annually and seasonally for the GGCL at low, medium, and high elevations during the mid- and late-century for the MRI and MIROC climate futures.

Time period	Global climate model	Elevation level (ft)	Annual mean moisture deficits percent relative to historical	Spring mean moisture deficits percent relative to historical	Summer mean moisture deficits percent relative to historical	Fall mean moisture deficits percent relative to historical	Winter mean moisture deficits percent relative to historical
Mid-century	MRI-CGCM3	6501–9200	122.2	116.9	117.5	138.9	134.0
	MRI-CGCM3	3801–6500	113.9	108.4	111.1	127.0	116.3
	MRI-CGCM3	1100–3800	109.9	104.4	108.9	120.5	102.7
	MIROC-ESM-CHEM	6501–9200	141.9	198.5	132.2	115.6	296.0
	MIROC-ESM-CHEM	3801–6500	129.4	156.1	118.5	113.6	232.7
	MIROC-ESM-CHEM	1100–3800	122.6	139.5	114.1	111.2	180.0
Late-century	MRI-CGCM3	6501–9200	122.4	137.4	115.3	129.1	151.3
	MRI-CGCM3	3801–6500	116.1	120.4	109.6	125.9	135.3
	MRI-CGCM3	1100–3800	112.7	113.5	108.6	120.7	117.2
	MIROC-ESM-CHEM	6501–9200	180.8	267.9	157.6	156.9	507.9
	MIROC-ESM-CHEM	3801–6500	153.8	187.1	135.2	140.8	329.7
	MIROC-ESM-CHEM	1100–3800	140.9	160.5	127.3	132.2	230.0

Table B9. This table presents Figure A20 information in an accessible tabular format that can be read by screen-reading software. Change in runoff relative to historical runoff annually and seasonally for the GGCL at low, medium, and high elevations during the mid- and late-century for the MRI and MIROC climate futures.

Time period	Global climate model	Elevation level (ft)	Annual mean runoff change relative to historical (in)	Spring mean runoff change relative to historical (in)	Summer mean runoff change relative to historical (in)	Fall mean runoff change relative to historical (in)	Winter mean runoff change relative to historical (in)
Mid-century	MRI-CGCM3	6501–9200	2.7	0.1	0.1	−0.2	2.1
	MRI-CGCM3	3801–6500	0.7	0.1	0.1	−0.1	0.5
	MRI-CGCM3	1100–3800	0.3	0.0	0.0	−0.1	0.2
	MIROC-ESM-CHEM	6501–9200	−2.6	−1.9	0.0	0.3	−1.6
	MIROC-ESM-CHEM	3801–6500	−0.8	−0.2	0.1	0.1	−0.9
	MIROC-ESM-CHEM	1100–3800	−0.5	−0.1	0.0	0.0	−0.5
Late-century	MRI-CGCM3	6501–9200	2.4	−0.4	0.5	−0.1	1.8
	MRI-CGCM3	3801–6500	0.6	0.0	0.3	0.0	0.2
	MRI-CGCM3	1100–3800	0.3	0.1	0.1	0.0	0.0
	MIROC-ESM-CHEM	6501–9200	−3.5	−2.3	0.1	0.0	−1.8
	MIROC-ESM-CHEM	3801–6500	−0.9	−0.3	0.1	0.0	−0.9
	MIROC-ESM-CHEM	1100–3800	−0.4	−0.1	0.1	0.0	−0.5

The Department of the Interior protects and manages the nation's natural resources and cultural heritage; provides scientific and other information about those resources; and honors its special responsibilities to American Indians, Alaska Natives, and affiliated Island Communities.

NPS 113/192072, January 2024

National Park Service
U.S. Department of the Interior

Natural Resource Stewardship and Science
1201 Oakridge Drive, Suite 150
Fort Collins, CO 80525